A study of membrane swelling and transport mechanisms in solvent-resistant nanofiltration

A STUDY OF MEMBRANE SWELLING AND TRANSPORT MECHANISMS IN SOLVENT RESISTANT NANOFILTRATION

by

Kevin Terry Cliff

A Doctoral Thesis submitted in partial fulfilment of the requirements for the award of Doctor of Philosophy of Loughborough University

June 2011

Abstract

Recently a large amount of interest has developed around separating out impurities of small size; pertinent examples are found within fuel and solvent processing. For such applications a leading candidate process is nanofiltration. This thesis focuses on SRNF (solvent resistant nanofiltration) composite membranes consisting of a dense polymer active layer bonded to a stronger, but ultimately more porous, support layer. The composite membranes that have been produced during the course of this work consist of a PDMS (polymdimethylsiloxane) active layer bonded to a commercially available support layer of PAN (polyacrylonitrile). To create the membrane a monomer was spread over the support layer and then polymerised to form the matrix which was responsible for separation. Commercially, either heat or radiation is often applied to cause polymerisation, however the membranes in the current work have been formed by the used of a homogeneous catalyst. This thesis investigates the transport and separation dynamics of the produced membranes for a series of fuel simulants composed of organometallics and poly-nuclear aromatic solutes dissolved in aromatic and alkane solvents.

Membrane composition and the extent of polymer swelling were found to be the two key factors which had the greatest influence on solvent flux and solute rejection. By increasing catalyst concentration it was found that the dual effects of increased rejection and reduced flux occurred, with the converse also being true. The effective pore size of the membrane could also be controlled by varying the catalyst amount during manufacture as this directly affected the limit of crosslinking which formed. Polymer swelling was the most pronounced using solvents with a solubility parameter close to that of the polymer. The membrane transport mechanism was most accurately forecast by the solution diffusion model for flux predictions and the convection diffusion model for rejection predictions, however all the models tried were in close agreement. This was postulated to be due to the swelled polymer matrix which allows for both convective and diffusive transport to occur.

Keywords: PDMS, nanofiltration, membrane swelling, dense membrane, catalyst, polymer slab.

Acknowledgments

I would like to thank my supervisor, Dr. Steve Tarleton for his invaluable support and guidance throughout the duration of the project. In particular, I would like to express my gratitude for the time taken to read this thesis, and for providing continued support throughout the project.

I would also like to give credit to the various people who have contributed to the success of the project, the staff at Loughborough University. Particular mention is given to Sean Creedon, Mark Barron, Steve Bowler, Jim Muddimer, Terry Neale, Dave Smith, Graham Moody, Kim Robertshaw, Monika Pietrzak, Adrian Broster and Steve Horner for my experimental work.

Furthermore, I would like to thank my friends and family for their support during the course of this project. Jian Shen Low and Khai Siang Lee for their help as sounding boards during the initial stages of this project. Charlotte Zommers, Ann Zommers and my parents Christine and Terry for the time they took to read this thesis before submission.

Table of Contents

List of Figures

List of Tables

Acronyms

The following list of acronyms has been used throughout the thesis.

910	9,10-Diphenylanthracene
AD	Area degree
CD	Convection diffusion
DBT	Dibutyl dilurate
HD	Height degree
Hep	Heptane
I3A	Iron (III) acetylacetonate
I3N	Iron (III) naphthenate
KK	Keden Katchalsky
MD	Swelling degree
MWCO	Molecular weight cut off
Oct	Octane
PAN	Polyacrylonitrile
PD	Pure diffusion
PDMS	Polydimethylsiloxane
PF	Pore flow
ppm	Parts per million
PMCC	Product moment correlation coefficient
RO	Reverse osmosis
SD	Solution diffusion
SDI	Solution diffusion with imperfections
SEM	Scanning electron microscope
SK	Spiegler Kedem
SRNF	Solvent resistant nanofiltration
UV/VIS	Ultra violet / visible light
VDB	van der Bruggen
VOC	Volatile organic compound
Xyl	Xylene

1. Introduction

The broad area of this research is nanofiltration and more specifically an investigation into solvent resistant nanofiltration (SRNF) membranes. SRNF membranes, like all nanofiltration membranes, operate at a very small scale and are used to separate out dissolved species from a feed stream; with generally only fluids and ions passing through unhindered. SRNF is a largely emerging technology. Membranes of this type are used for a variety of different applications from fuel processing to the purification of pharmaceutical intermediates, making this technology critical to modern life.

Nanofiltration is a filtration process regime which exists between ultrafiltration and reverse osmosis (RO). RO is the finest liquid filtration process typically removing all but the smallest dissolved ions and water. As such RO membranes do not even have pores to filter with in the classical sense of the word but rather separate by diffusion. The permeate diffuses through the membrane material where the retentate can not fit through the transport regions (essentially the tiny spaces between the polymer chains which make up the membrane). Ultrafiltration by comparison typically works by separating out chemical species by a size exclusion process, the smaller species can pass through the membrane pores whilst the larger species cannot. As nanofiltration falls between these two different processes a great amount of interest has arisen recently over this process and whether or not pores exits within its structure.

As a technology, non-aqueous membrane separation is not as developed as aqueous separation due to the inherent problems with membrane stability when processing organic solvents (Scarpello *et al*, 2002). Polymeric membranes characteristically swell in the presence of organic solvents which affect the arrangement of the individual polymer chains. This swelling, at best, alters the filtration properties of the membrane and at worst causes the membranes to lose integrity and fail completely. Similar problems do not occur when filtering aqueous solutions. However, with the development of SRNF membranes, non-aqueous filtration by polymeric membranes has become an attractive alternative, initiating the development of new technologies and processes, in several different industries. The different industrial uses of membrane technology are briefly described below with detailed discussions on specific work occurring in Chapter two.

Fuel Processing

Most fuel processing stages (distillation, cracking, coaking) use heat as a key separation tool, which typically causes the release of VOC's into the vapour phase. This contaminated gas stream needs to be purified before it can be released into the atmosphere, a process for which membranes can be used. Membrane based vapour permeation has been used by Gales *et al* (2002) to produce a cleaned up retentate fit for direct venting to atmosphere.

Historically one limitation to fuel refining is the azeotropic point reached when distilling binary mixtures. Standard distillation works by creating a compositional difference between counter current streams of liquid and gas within a tower, however when distilling certain binary mixtures there comes a point when the composition of both phases is identical and so no further separation can be achieved. Polymer membranes can be used either as an additional or an alternative processing step to circumvent this problem.

Pharmaceutical Processing

The size of the pharmaceutical industry is such that every separation technique possible is utilised – membrane separations have found uses in both catalyst and solvent recovery. In general the synthesis of active pharmaceutical ingredients employs transition metal catalysts which are both highly expensive and environmentally hazardous. Prior to membrane separation the removal of these catalysts required the use of energy intensive and waste generating downstream processing (Jodicke *et al*, 1999), which either reduced the effectiveness of or simply inactivated the catalysts completely. With the application of membrane separation these catalysts could be recovered in a useable state leading to a more environmentally sound process as well as generating significant cost savings (Scarpello *et al*, 2002).

Membranes have also been successfully integrated into solvent recovery processes. A counter current membrane cascade can be used to recover 'used' solvents from process streams returning just over 75 % of the total solvent in a three stage system (Lin and Livingston, 2007). This solvent can then be reused leading to both environmental and cost savings as a result. By reusing components in this way the potential savings outweigh the initial cost of membrane unit operations.

Water Processing

Similarly to solvent recovery in the pharmaceutical sector, membrane separations can be applied to the reclamation of wastewater. For example, dyeing of clothes in the textile industries in India produce between 80 and 200 tonnes of contaminated

wastewater for every tonne of clothes produced (Ranganathan *et al*, 2007) which, in a country with insufficient drinking water to begin with, is a major problem. A multi stage membrane process has been developed which can purify the contaminated water for less than the price of purchasing 'fresh' water, drastically reducing the demand for industrial needs. Additionally some of the dyes removed are in a useable state, leading to a recycling of raw materials as well.

NF membranes can also be used as a replacement to existing ultrafiltration membrane systems. Endocrine disrupting compounds and pharmaceutical products can be present in wastewater effluents. These compounds have been detected in drinking water supplies around the world for years but these chemicals have recently been linked to health risks in both humans and animals (Yoon *et al*, 2007). Therefore a need to removed or at least reduce the levels present has been created. Both ultrafiltration and nanofiltration processes are capable of partial removal of these chemicals with nanofiltration removing around 30 % more than ultrafiltration due to the smaller solute size nanofiltration can filter.

During operation SRNF membranes often swell to an extent dependent on the type of chemical species passing through. For filtration to occur, 'space' needs to be present inside the membrane structure to allow for the passage of permeants. To achieve this, it is postulated by the author that the polymer chains move further apart and as a result the overall volume of the membrane increases. Such swelling causes problems as the transport properties are altered by this rearrangement, making predictions about the way a specific membrane will behave difficult to evaluate.

1.1. Novelty of the Research

The PDMS/PAN composite has been reported in numerous journals and is a well known nanofiltration membrane (Dijkstra *et al*, 2006, Ebert *et al,* 2006, Low 2009, Robinson *et al,* 2004, Tarleton *et al,* 2005). What is not well known, however, is the mechanism by which chemical species pass through or get rejected by the membrane. Part of the novelty of this project comes from the attempt to deduce this mechanism. Novel aspects will be achieved both by the use of several different testing rigs each designed to exploit one aspect of transportation, and the variance that can be achieved in the membrane itself. By producing the membranes 'in house' aspects of their structure are better known and can be tailored to investigate different effects from

active layer thickness to crosslinking concentration. By such an approach it is envisioned that a deeper understanding of the mechanics behind the phenomenon can be achieved.

1.2. Aims of the Project

There are a total of four different aims to this work.

- Production of composite membranes
  The purpose of this aim was to obtain PAN backed cellulose sheets, and bond these to a selective layer of PDMS to create the composite membrane. The PDMS was made from a two part kit which uses a homogeneous catalyst as the crosslinking agent rather than raised temperature or radiation. This kit has previously been used by Gevers *et al* (2006) as a source of PDMS for nanofiltration membranes. An investigation was conducted into the effect of different degrees of crosslinking and the effects of selective layer thickness. The data from these tests was used to see if there was any effect on the transport rates of solvent and solutes, and ultimately used to see if these changes have any effect on the validity of the standard transport models.

- Characterisation of PDMS
  Once the polymer had been produced, tests had to be conducted to check the physical properties of the matrix. These tests were essential to ensure that the polymer behaves in a similar way to the PDMS reported in pre-existing literature. This comparison was achieved by measuring swelling data against known values and also from physical tests done to bars cast from PDMS.

- Identification of transport mechanism
  The overall aim was to deduce the transport mechanism in action across this type of membrane, for example does the pore flow or solution diffusion model best describe the experimental data. As detailed in Chapter five, pore flow models tend to fit well for operations carried out at the ultrafiltration scale, and solution diffusion models were more appropriate for reverse osmosis. However, the range of nanofiltration falls squarely in the region between the two models resulting in some situations were pore flow was valid and others where solution

diffusion was the better choice. As the membranes covered in this work were produced with varying crosslinking densities it was hoped that it would be possible to produce more dense membranes that behave in a solution diffusion manner and less dense membranes that behave in a pore flow manner.

- Determination of effective pore size
  This parameter is an important factor in the selection of membranes for industrial applications and so the determination of the effective pore size within the produced membranes was determined during the characterisation. Using experimental data this value was deduced using analytical modelling.

To achieve these aims several different consecutive tasks were completed. Initially a source for the support layer had to be found which then had to be tested for applicability to form composite membranes. Concurrently pure PDMS polymer slabs were produced and the swelling characteristics were confirmed for a range of different solvents. Additionally the Young's modulus of slabs created with different catalyst amounts was deduced. The production of composite membranes occurred next with several different methods considered, before the chosen method was refined. Selection of the support layer brand occurred in this stage. Finally the flux and rejection characteristics of the produced membranes were assessed by a series of crossflow experiments (detailed in Section 4.1) separating out different poly-nuclear aromatic and organometallic solutes from a range of different alkane and aromatic solvents. From the data produced it was possible to plot a chart similar to the sketch shown as Figure 1.1, which was used to deduce trends with solubility parameter and swelling extent. The data produced were then compared to the predictions from seven different established filtration models to find the most accurate model for this process.

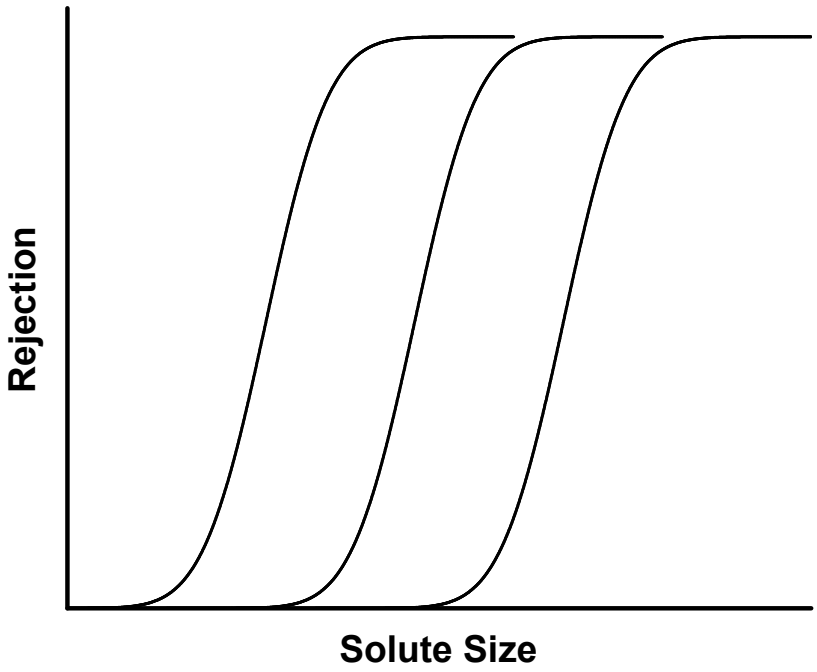

Figure 1.1 – Possible data trends from nanofiltration experiments.

1.3. Structure of the Thesis

This thesis is arranged into distinct chapters that each cover a different aspect of the work completed. Chapter two contains a critical assessment of some of the relevant work published by other authors and serves to increase the reader's background knowledge in the subject area. Chapter three contains the work conducted on the polymer, including polymer slab manufacture and swelling, and composite membrane production, refinement and characterisation. Filtration performance and analysis of the produced membranes is covered in Chapter four which details the experiments conducted using a crossflow apparatus and a series of test solutions. Chapter five is where the filtration performance of the membranes is compared to predictions from seven existing filtration models. Chapter six contains the overall conclusions drawn from this work and Chapter seven contains suggestions for future work. References and nomenclature, where applicable, are found at the end of each chapter.

1.4. References

Dijkstra M.F.J., Bach S., Ebert K., 2006. A transport model for organophilic nanofiltration. *J. Membrane Science*, **286**, 60-68.

Ebert K., Koll J., Dijkstra M.F.J., Eggers M., 2006. Fundamental studies on the performance of a hydrophobic solvent stable membrane in non-aqueous solutions, *J. Membrane Science*, **285**, 75-80.

Gales L., Mendes A., Costa C., 2002, Removal of acetone, ethyl acetate and ethanol vapours form air using a hollow fibre PDMS membrane module, *J. Membrane Science*, **197**, 211-222.

Gevers L.E.M., Vankelecom I.F.J., Jacobs P.A., 2006. Solvent-resistant nanofiltration with filled polydimethylsiloxane (PDMS) membranes, *J. Membrane Science*, **278**, 199-204.

Jodicke G., Zenklusen O., Weidenhaupt A., Hungerbuhler K., 1999, Developing environmentally-sound processes in the chemical industry: a case study on pharmaceutical intermediates, *J. Cleaner Prod.*, **7**, 159–166.

Lin J.C.T., Livingston A.G., 2007, Nanofiltration membrane cascade for continuois solvent exchange, *Chemical Engineering Science*, **62**, 2728-2736.

Low J.S., 2004, A Study of Organic Solvent Nanofiltration, PhD thesis, Loughborough University.

Ranganathan K., Karunagaran K., Sharma D.C., 2007, Recycling of wastewaters of textile dyeing industries using advanced treatment technology and cost analysis – Case studies, *Resources Conservation & Recycling*, **50**, 306-318.

Robinson J.P., Tarleton E.S., Millington C.R., Nijmeijer A., 2004. Solvent flux through dense polymeric nanofiltration membranes, *J. Membrane Science*, **230**, 29-37.

Scarpello J.T., Nair, D., Freitas dos Santos L.M., White L.S., Livingston A.G., 2002, The separation of homogeneous organometallic catalysts using solvent resistant nanofiltration, *J. Membrane Science*, **203**, 71-85.

Tarleton E.S., Robinson J.P., Smith S.J., Na J.J.W., 2005. New experimental measurments of solvent induced swelling in nanofiltration membranes, *J. Membrane Science*, **261**, 129-135.

Yoon Y, Westerhoff P., Snyder S.A., Wert E.C., Yoon Y., 2007, Removal of endocrine disrupting compounds and pharmaceuticals by nanofiltration and ultrafiltration membranes, *Desalination*, **202**, 16-23.

2. Literature Survey

This chapter presents a discussion on published work in the same general area as the experimental work presented in later chapters. It begins by considering the history of membrane separation, moving through nanofiltration developments and ending with a discussion on specific recently published work. In an effort to predict the filtration properties of different membrane types several different models have been produced and subsequently applied by different authors (Ahmad *et al*, 2004, Darvishmanesh *et al,* 2009, Dijkstra *et al*, 2006, Robinson, 2004, Santos *et al*, 2007, Sherwood *et al*, 1967, Szymczky *et al*, 2003, Tarleton *et al*, 2005, Wang *et al*, 1997, Yaroshchuk, 1995). The discussion pertaining to these models has been included in Chapter five rather than here as it is integral to the structure of that chapter.

Over the past two centuries the prevalence of membrane applications has increased from minor laboratory scale experiments to a fully fledged industry. The main reason for this growth was due to the physical behaviour of membranes especially with regard to component flux. Membranes will allow different species through at different rates and so, can be used to separate a solution into its more constituent species. Membrane separation does not require high operating temperatures, only moderate operating pressures and few specialist units making the process economically attractive compared to energy intensive operations such as distillation or evaporation (White, 2006). “The growing interest has forced the development of both polymeric and inorganic membranes significantly” (Ebert *et al*, 2004). Membrane separation is somewhat dependant on surface charge with certain ionic species and those with significant surface charge being repelled by the membrane; highly viscous solutions cannot be processed due to the viability of time constraints.

2.1. Developments in Membrane Technology

The records of experiments using membranes date back to the 18th century. In one of the earliest records Abbe Nolet defined the word ‘osmosis’ as the permeation of water through a membrane (diaphragm) in 1748. All of this early work applied membranes as tools for determining physicochemical properties of specific chemicals rather than as a viable separation technique. This continued to be the status quo throughout the nineteenth and early twentieth centuries until a crucial development in the 1960’s made

large scale processing possible. By 1960 modern science had been developed and the world had seen significant progress and rapid growth in almost every field after decades of stagnation. Membrane science however had not progressed for four main reasons;

1. Unreliability

Early membranes were constructed from whatever natural diaphragms were available; the bladders of cattle, intestines of pigs and the like were commonly used. As these membranes came from once living animals, variation between individual membranes was to be expected. Synthetic membranes had not been developed at this point.

2. Low permeation rate

To preserve the mechanical strength of the membranes, they had to be used as obtained i.e. they could not be made thinner. This meant that initial membranes were relatively thick and so permeation rates were low. Large scale processing was not viable due to this constraint.

3. Poor selectivity

The selectivity of the initial membranes was quite poor as they were not designed for artificial separations.

4. High cost

The costs in obtaining the raw materials and then cleaning without damaging the membranes were quite high.

The above points changed in the early 1960's with the development of the Loeb-Sourirajan process for making defect-free, high-flux, anisotropic reverse osmosis membranes (Loeb and Sourirajan, 1963). These membranes were formed from two layers; a selective surface layer (normally around 20 μm thick) bonded to a much thicker but significantly more permeable microporous support which provided the mechanical strength. The flux of the first Loeb-Sourirajan reverse osmosis membrane was ten times greater than that of any membrane then available and made reverse osmosis a potentially practical method of desalting water (Baker, 2004). This technology, plus funding from the US government, led to the commercialisation of reverse osmosis which in turn branched out to the fields of ultrafiltration and microfiltration. Simultaneous with this development were significant advances in the fields of medicine and healthcare using membrane separation. Kolf produced the first

working artificial kidney in 1944 (Kolf and Berk, 1944), which subsequently took him a further 20 years to perfect, in line with the discoveries of Loeb and Sourirajan. The healthcare markets demand for membranes has increased to the point where it currently exceeds the total industrial membrane separation market (Baker, 2004).

From these beginnings membrane technology progressed quickly in the twenty years from 1960 to 1980. The original Loeb-Sourirajan technology was extended to create several other membrane formation methods, including polymerisation and composite casting, making high performance membranes easier to manufacture. This technology led to a reduction in the minimum thickness of the selective layer. Specialised forms were also incorporated into this upgrade with spiral wound, plate and frame, hollow fibre and capillary modules now becoming standard types. Since the 1980's the new development has been gas membrane separation plants, whilst the established methods have been further refined. This increase can be seen by the number of papers published about nanofiltration which rose from 20 in 1992, to more than 200 in 2002 (Schafer *et al,* 2005) and to more than 1100 in 2011.

2.1.1. Isotropic and Anisotropic Membranes

Membranes can be broadly thought to belong to one of two mutually exclusive categories; isotropic or anisotropic, see Figure 2.1. Isotropic membranes are uniform in porosity and a cross-section taken along any conceivable plane will result in similar morphology. Anisotropic membranes are not uniform and show differences in porosity throughout the membrane. All dense polymers, including PDMS, are by definition isotropic as they are uniform, however the membranes covered in this study are turned anisotropic by the addition of the support layer which is of different morphology to the PDMS layer. Similarly all membranes produced by the Loeb-Sourirajan process are anisotropic due to the changes in porosity within the membrane that this process creates.

Figure 2.1 – Comparison of membrane types (Baker, 2004).

2.1.1.1. Isotropic Membranes

There are three main types of isotropic membranes each of which separate components by potentially different mechanisms (Baker, 2004).

- Microporous Membranes

  These membranes separate species based on molecular/particular size, surface charge and adsorption. The typical separation mechanism is pore flow, meaning that there are a range of different pore sizes in the structure rather than a single uniform size, thereby creating a pore size distribution. Molecules larger than the pores will be rejected; molecules smaller than the pores with pass through and molecules which fall inside the pore size distribution will be partially rejected.

- Nonporous Dense Membranes

  This is the category that polydimethylsiloxane (PDMS) belongs to, and the mechanism for separation is based on diffusion through the intermolecular spaces including sorption and desorption. Separation in this case is totally dependent on having a mixture with different component solubilities towards the membrane material. Any component with a high affinity for the membrane will pass through and any component with low affinity will be rejected. Components with neither high nor low affinities will be rejected to an intermediate extent.

- Charged Membranes

  The pore walls of this type of membrane are charged by the presence of fixed polarity ions. Anion exchange membranes employ positive ions and cation exchange membranes employ negative ions. The separation mechanism is based on this charge and is used to separate ionic components from a solution by repelling them from the membrane and ensuring that they cannot pass through.

2.1.1.2. Anisotropic Membranes

The time required for a given chemical species to cross a membrane is inversely proportional to the membranes thickness and as larger throughputs are normally required, this means that the membrane should be as thin as possible (Verhoef *et al,* 2008). However the thinner a membrane, is the less mechanical strength it has, so there is usually a trade-off between mechanical strength and throughput. Anisotropic membranes are a novel way of bypassing this trade off as they consist of one selective

layer and one (or more) backing layers sandwiched together. The advantage of this arrangement is that the selective layer can be an order of magnitude or two thinner than single layer membranes, which leads to an increase in throughput whilst the backing layer is strong enough to support the forces applied to the entire composite. As the backing layer is significantly more porous than the selective layer it does not hold up the permeate and the overall flux rate is determined by the flux solely across the selective layer. A practical issue with membranes of this type is delamination where the active layer peels from the support. An additional disadvantage of this arrangement is the difficulty of modelling separation characteristics beforehand, Albrecht *et al,* (2005) found that "if the separation layer of an asymmetric membrane is highly permeable, the support layer resistance can become significant. A highly asymmetric structure over the entire cross-section of a membrane is a prerequisite for the restriction of this resistance", which is a problem for most modelling trends which assume that the support layer plays no part in the separation.

2.2. Filtration Processes

2.2.1. Filtration Summary

Filtration can take many forms from macro-scale operations such as draining peas in a colander, to micro-scale operations such as water purification. The macro-applications are dependent on the size of the holes in the filter media and essentially separate based on relative size. The micro-applications, involve relative size separation, but are also influenced by other factors such as coupled transport and species charge. The micro-applications are split into four distinct processes based on the species they can segregate; a typical size grade chart for these is shown as Figure 2.2. At the centre of each of these operations is a membrane to provide the selective barrier for separation, which can be considered a semi-permeable material between two phases (Geens, 2006). Membranes transport one component more readily than others because of differences in physical and/or chemical properties between the membrane and the permeating species (Mulder, 2000). This work details research conducted on nanofiltration membranes, and as can be seen from Figure 2.2 this is the second finest filtration process. Nanofiltration will remove all dissolved solids and particulates in the feed stream allowing only liquids and ions to enter the permeate unhindered.

Nanofiltration is therefore ideally suited to the purification of fuel and pharmaceutical intermediates, as discussed in Chapter one.

Figure 2.2 – Differences in separation processes (Tarleton).

2.2.1.1. Experimental Configurations

The vast majority of filtration processes can be split into one of two categories based on the orientation of the filter media and feed flow. These configurations are called deadend and crossflow, schematics of each can be seen in Figure 2.3, which also shows the flux time relationships typically achieved with each process.

Figure 2.3 – Schematics of deadend filtration and crossflow filtration. (Ho and Sirkar, 1992)

In deadend filtration there is no retentate fraction as all of the feed either passes through the filter to form the permeate or builds up on or in the filter as a fouling layer. As the fouling layer increases in depth, the flux through the expanding media decreases and essentially makes deadend filtration a batch process. The driving force for this type of operation is derived from the pressure gradient over the filter caused by either, hydrostatic pressure from the head of liquid on the feed side or from mechanical intervention, a pump on the feed side or suction applied to the permeate side.

Crossflow filtration was designed to operate continuously and is, to an extent, self cleaning (Holdich, 2002). The main differences between crossflow and deadend are that crossflow is operated with the process stream tangential to the filter medium instead of perpendicular, and that there is a retentate stream, where one does not exist in deadend (although the build up formed in the fouling layer can be thought of as a stored retentate). As with deadend filtration, a fouling layer does form at the filter surface, but unlike deadend filtration this layer does not expand indefinitely and reaches an equilibrium depth dependent on the physical properties and process conditions of the system with the depth generally shear limited. As the fouling layer builds up it expands towards the centre of the channel where the fluid velocity is greater. The shear generated motivates the fallen particles and sweeps them along to be removed with the retentate. This process keeps the depth of the fouling layer low

ensuring that crossflow operations can usually be operated for longer before cleaning is required compared to dead end operations.

In homogeneous systems, such as the one detailed in Chapter 4, the fouling layer build up does not occur due to the lack of solids in the feed stream. As such the operational choice between dead end or crossflow is not predicated on the same concerns as are found in solid liquid separations. This brief overview has been acknowledged as it is an important distinction in the field of filtration rather than for any specific concern to this research.

2.2.1.2. Filtration Terminology

The following entries are general definitions of key filtration terminology, supplementary information is covered in the relevant sections.

Flux

The rate of flux is the volume of permeate collected over a period of time for a membrane of a given size. Solvent flux was calculated using Equation 2.1.

$$J = \frac{V}{A \cdot t} \tag{2.1}$$

Where J is solvent flux, V is permeate volume, A is membrane area and t is time.

Permeability

A measure of the ability of a fluid to pass through a porous material. A membrane with larger transport regions will have a higher permeability than one with smaller transport regions and as a membrane swells its permeability will increase. Permeability is required in the calculation of Darcy's law (See Section 4.3.1)

Rejection

The extent to which the desired components of a feed flow are reduced by filtration. Rejection extent is equal to the ratio of solute concentration in the permeate to solute concentration in the feed. See Section 4.1.2.3.

Size Exclusion

A surface rejection effect in which the solute does not pass through the membrane due to its size or complex shape. The solutes size, or shape, is such that it cannot pass through the transport regions within the membranes form.

Charge Exclusion

A surface rejection effect which the solute does not pass through the membrane due to its inherent charge. This effect is mostly attributed to solvent-membrane interactions caused by steric hindrance effects (Verliefde *et al*, 2008)

Concentration Polarisation

During operation rejected solute can accumulate at the membrane surface lowering the overall flux rate. This accumulation can lead to surface deposits which cause blocking of the membrane surface. Crossflow operation can alleviate this effect by motivating the solute by tangential shear forces.

Osmotic Pressure

Osmotic pressure has been calculated by Equation 2.2, which has been taken from Ho and Sirkar (1992).

$$\Pi = R \cdot T \cdot c \tag{2.2}$$

Where Π is osmotic pressure, R is gas constant and c is molarity. Osmotic pressure has been used in the solution to the SDi model (Section 5.2.5).

Stage Cut

The ratio of feed flow to permeate flow. In the filtration experiments in Chapter 4 a stage cut of 10% was used meaning that the experiment was stopped when 10% of the initial feed was collected as permeate.

2.2.2. The Effect of Solvent Type on Flux and Rejection

The flux of solvent through a membrane is one of the standard values reported in literature, and as such there is a significant amount of information available for this aspect of the review. Most of this can only be taken as work in the same general area due to the use of a different membrane material and/or different solvents, but the research that was found to be relevant throughout the course of this review is detailed below.

Robinson *et al,* (2004) presented a significant amount of data pertaining to flux rates through PDMS/PAN membranes with a selection of solvents over a range of pressures. The PDMS/PAN membranes used in his work were supplied by GKSS and used without further modification. The membranes were produced by radiation crosslinking, with an active layer thickness of 2 µm, however, it is stated that slight variance between 1.5 µm and 3 µm was observed. The flux-pressure relationship of nine different pure solvents were measured including representatives of aromatic, alkane and alcohol species to ensure an adequate range of testing materials for the membrane. The experimental rig used for this work was a deadend test cell which housed a 75 mm diameter circular membrane. The tests were conducted at seven different pressures over a range from 300 to 900 kPa, plotted and linearised. The equation of the straight line plotted through the data is shown as Table 2.1, reproduced from Robinson *et al* (2004).

Table 2.1 – Flux / pressure relationship data (Adapted from Robinson, 2004).

In addition to the relationships in Table 2.1, a sample of PAN backing without a PDMS selective layer was tested and produced flux values approximately two orders of magnitude higher than when PDMS was present confirming that PDMS had a significant effect on transportation rates. Methanol and ethanol rates could not be determined as the evaporation of the permeate was reported to be significant compared to the flux rate, which affected the results significantly.

Similar relationships for flux through PDMS membranes were reported by several authors. Ebert *et al,* (2006) produced PDMS/PAN membranes by first casting PAN on to a nonwoven support using the phase inversion technique. Once set, a 0.5 µm PDMS

layer was produced by dip coating of the composite. The PDMS was dissolved in n-octane and crosslinked by a mixture of catalyst interaction, thermal and radiation crosslinking. When tested the flux of these membranes produced a similar result to those of Robinson *et al, (*2004), with n-hexane producing a flux of 13.3 l $m^{-2}h^{-1}bar^{-1}$ and ethanol a value of 1.75 l $m^{-2}h^{-1}bar^{-1}$. The absolute value of flux was slightly higher for the membranes Ebert *et al* (2006) tested where values around 20 l $m^{-2}h^{-1}bar^{-1}$ were common, this was most likely due to the relatively thinner active layer of PDMS.

Gevers *et al,* (2006) also produced membranes but these were made of PDMS thermally crosslinked onto a support layer composed of polyimide on a nonwoven polypropylene support. In this paper the transport rates of various dyes were calculated with the result that the transport of dyes with a molar volume above 230 ml/mol was significantly lower than the transport rate of dyes with a molar volume below 230 ml/mol. In addition those dyes tested below this value were heavily dependent on the solvent they were dissolved in. Only one comparable result could be found to the reports above, which was the solvent flux for methanol. When the units are converted the methanol flux seems to be several orders of magnitude higher than the typical flux reported in journals for similar experimental arrangements. Again this could be due to differences in the support layer, and active layer. The measured flux seems to be highly dependent on the components involved (solvent and selective layer) and also dependent on the thickness of the active layer.

The flux and rejection characteristics of polymer nanofiltration membranes were altered by the use of different solvents. Vankelecom *et al* (2004) reported variances in both flux and rejection whilst using dead end filtration to separate dyes from a range of solvents. For a PDMS membrane the rejection of methylene blue dye was increased by 3% and the rejection of rose bengal dye was increased by 8% by using 2-propanol rather than methanol (all other operational conditions were maintained constant). Repeat tests using the commercially available MPF-50 membrane (Koch membrane systems) produced a 22% increase for methylene blue and a 3% increase for rose bengal for identical conditions. As the main impetus of the work was to compare the two membrane types no explanation of this effect was proffered. Vankelecom *et al* (2004) also reported effect of solvent type on flux with an approximately linear relationship between PDMS swelling extent and flux being apparent. In the paper several different charts of the data have been produced varying by x-axis alone – the MV/η parameter suggested by Bhanushali *et al* (2001) gave a regression coefficient of only $R^2 = 0.303$ and the 1/η parameter suggested by Machado *et al* (1999) was even worse at $R^2 =$

0.125. Relating the flux directly to PDMS swelling gave a better correlation of R^2 = 0.801 but this link did not adequately explain the differences between solvents with similar swelling extents but ultimately different swellings. A comparison based on the Hildebrand solubility parameter (See Section 2.2.5.1) of the specific solvent used is also noted to give similar correlation to the swelling regression coefficient (R^2 = 0.756), which support the link previously stated. The final regression coefficient, shown as Figure 2.4, swelling extent / solvent viscosity gave a regression coefficient of R^2 = 0.946 which means that both parameters seem to have an effect on the overall membrane permeability. Drawing an all encompassing conclusion from the results of six solvent tests is not prudent however the correlation is strong enough to indicate dependency. The authors conclude that a diffusion term is not required due to the highly porous polymer (PDMS) and the relatively small molecular size of the solvents.

Figure 2.4 – Permeability of different solvents through PDMS membrane (Vankelcom *et al*, 2004).

Tarleton *et al* (2006a) has reported a similar variance in rejection extent based on solvent choice. The study used PDMS/PAN composite membranes to remove oxygenate species from a xylene/oxygenate feed stream. The filtration was operated in crossflow with the retentate being continuously recycled back to the feed. The separation was operated at a 10% stage cut. The authors found rejections of upto 30% possible depending on initial feed composition. It was found that the highest rejection corresponded to the highest polarity oxygenate, a relationship which holds true for successively lower polarity species. The least polar of the oxygenates tested (MTBE) did not separate from xylene at all. Based on the relative size of the molecules the paper suggests that separation in this case has occurred due to polarity rather than size. Additionally the methanol and ethanol systems exhibited a maxima which is noted as a unique finding for SRNF membranes. Further work presented goes on to examine the effect of mixture viscosity. Typically increasing the component flux could be achieved by lowering the mixture viscosity however by adding methanol to the xylene base this effect was not noted. The supplied reason was that the effect of polymer swelling had “a significantly more pronounced effect on component flux than the viscosity of the mixture” Tarleton *et al* (2006a).

The flux rates of different solvents for the same experimental conditions were also covered by Machado *et al* (1999). MPF-50 silicone polymeric membranes were tested

in a dead end filtration cell to which compressed nitrogen was fed providing the pressure difference / driving force. A total of eight different solvents were permeated using this set up over a pressure range of 5 to 30 atmospheres. The three non-alcohol species tested demonstrated a linear relationship but the five alcohol species tested demonstrated non-linear behaviour – see Figure 2.5. The curved data exhibits a falling rate behaviour which is more prominent with higher molecular weight species. For the linear trend species the flux was equal to resistance multiplied by pressure where the resistance was a constant. For the non-linear trends however the resistance varies due to the membrane compression and so it increased at higher pressures leading to reduced flux. Membrane compression is discussed in the next section.

Figure 2.5 – Effect of pressure on solvent flux. a) linear trends; b) Non-linear trends (Machado *et al*, 1999).

Solvent based flux and rejection variances were also found in hybrid membranes. Kusakbe *et al* (1998) produced a range of hybrid membranes composed of a polyurethane and tetraethylorthosilicate mixture, coated upon a porous α-alumina support tube. Pervaporation experiments conducted using the membranes showed preferential transport of benzene over cyclohexane which was further altered by active layer composition. For a 3 to 1, polymer to silicate, mass ratio membrane the total permeation flux was recorded as 5.5 x 10^{-5} kg $m^{-2}s^{-1}$ and an approximate selectivity (inferred from chart) of 60% benzene to 40% cyclohexane was produced from an equal proportion feed composition. Further reductions in the polymer/silicate ratio had the dual effect of decreasing the total permeation flux and increasing the benzene/cyclohexane selectivity to 19 to 1. The authors also noted that reducing the proportion of polymer reduced the total swelling observed which was the reason for increased selectivity and reduced flux.

Three microporous composite ceramic membranes studied by Guizard *et al* (2002) reported flux variations with differing solvents. The three membranes coded AZ, SZ and ST (Aluminium oxide/zirconium oxide blend, silicon oxide/zirconium oxide blend and silicon oxide/titanium oxide blend respectively) where prepared by the sol-gel process and tested at pilot plant scale. The sol-gel process involves creating a colloidal solution which is gradually changed to gel by removal of the liquid phase, usually by sedimentation first, then heating. As the gel forms, a very even coating with an integrated network of polymer chains is formed. The flux performance of each

membrane was tested against three solvents. The normalised results are shown as Figure 2.6. In this case it was found that ethanol elicits the largest flux due to its polar nature and the fact that ceramic oxides can be considered as high energetic surfaces. The base chemistry of the membrane-solvent interaction results in the ethanol molecules being passed at a higher rate compared to the non-ionic solvents tested, which are being actively repelled by the charge difference caused at the membrane surface. Beyond that it was noted that the lower flux of toluene compared to heptane could be explained by "a long-range molecular ordering for toluene in the micropores which does not exist for heptane."

Figure 2.6 – Normalised flux results for ceramic membranes (Adapted from Guizard *et al*, 2002).

From this review it is clear that several key findings are as follows. Relative flux is inversely proportional to selective layer thickness. It has been shown that for similar membranes the thinner the selective layer of PDMS the larger the transport rate of solvents across the membrane. It has also been seen that testing the support layer alone produces flux rates a couple of orders of magnitude higher than comparable tests conducted with a 2 μm active layer membrane. This means that the characteristics of the active layer define the flux performance of the entire composite. Relative flux is also dependent on the solvent type with greater swelling solvents producing larger flux than poorer swelling solvents. The membrane swelling effect also affects rejection with a swelled membrane providing lower rejection than a non-swelled membrane of the same type. Combination of these two results means that membrane swelling both increases flux and lowers rejection. Polarity of the solute used has been shown to affect the extent of rejection with higher polarity species being rejected more than lower polarity species, however this effect is less pronounced than either effect of swelling or selective layer thickness.

Compaction of membranes

Membrane compaction is defined as compression of the membrane structure under the trans-membrane pressure, causing a decrease in membrane permeability (Gekas, 1988). The compressive forces placed on polymeric membranes during use cause compaction of the internal structure which affects the filtration properties. One of the main effects of compaction is a noticeable drop in permeability especially in the first

few operational hours of a fresh membrane. Vankelecom *et al* (2004) noted that an initial methanol flux of 39 l/m^{2}hr had declined to become constant after approximately one hour of operation to 26 l/m^{2}hr. This result was achieved using a MPF-50 membrane from Koch at 16 bar and 30°C. As 'pure' methanol was used the authors have discounted concentration polarisation and fouling effects so concluding that the observed flux reduction can only be attributed to compaction. Further testing confirmed that this compaction was partially reversible. Initially the membrane was relatively swollen but as pressure is applied the dense top layer is compacted slowly until an equilibrium was reached between the expansion effect of membrane swelling and the compaction effect of applied pressure. This equilibrium is reached at a certain constant flux. When the pressure was relieved the membrane could swell without restriction thus returning the membrane to its initial flux rate.

Similar flux decreases were found by Kallioinen *et al* (2007) who noted a 25% decrease in the flux of two UF membranes after 48 hours of operation. The first membrane (C30FM) was made from polyethylene terephtalate and the second (C2) was a blend of polypropylene and polyethylene. The membranes were first cleaned of any membrane preservation agents by immersion in RO water, subsequently polyethylene glycol (PEG) was passed through the membranes at 300 kPa for 23 hours then at 800 kPa for 25 hours. The performance of each membrane was checked against the initial performance with a 25% flux decrease for each membrane noted. When the same procedure was conduced using pure water rather than PEG the membrane flux decreased further still. Permanent damage to the membranes was assessed by confirming the pure water flux of used membranes and so was proved that PEG did not foul the membranes, indicating that the flux decrease was caused by membrane compaction. The higher flux value for PEG compared pure water was attributed to osmotic pressure and concentration polarisation effects reducing the trans-membrane pressure inherent in such testing.

Persson *et al* (1995) has presented a significant amount of work on the compression of membranes at different applied pressures. The compression of three different ultrafiltration membranes and a separate PET support layer was tested using a dial gauge connected to a hydraulic press. The pertinent results are shown in Table 2.2 where compression extent is defined as 'the final membrane thickness expressed as a percentage of the initial membrane thickness'. Despite having a significantly larger porosity the cellulose acetate membrane did not (relatively) compress any more than the porous support, whilst the polyamide and polysulfone membranes were shown to

compress more. Viscosity was put forward as reason for this result. After compression the water flux of the membranes was assessed and, apart from some instant relaxation, it was found that the membranes never recovered to match the initial flux values meaning that some permanent deformation must have occurred. The extent of flux reduction was found to mirror the compression extent with the higher compressed membrane eliciting the greatest flux loss. A similar result was found by Peterson *et al* (1998) who noted that cellulose acetate membranes do not recover their initial state after compression and that the extent of deformation was proportional to the initial porosity of otherwise identical membranes.

Table 2.2 – Physical membrane data (adapted from Persson *et al*, 1995).

Titanium dioxide can be used to retard compaction of polymer membranes. Ebert *et al* (2004) produced PVDF membranes both with and without TiO_2 filler. The membranes were pressurised to 40 bar for 4 hours. The pore volume of fresh and pressurised membranes was then determined by porometry. The addition of the filler greatly reduced the extent of compaction with an 83% decrease of pore volume recorded for the PVDF membrane compared to a 17% decrease for the PVDF/40wt% TiO_2 membrane. The greater resistance to compaction also produced a greater permeability when the nitrogen flux of each membrane was assessed at 30 bar – see Figure 2.7. The addition of the filler had little effect on the initial properties of the membrane with a flux of 290 $m^3\ m^{-2}h^{-1}bar^{-1}$ for the PDVF membrane compared to a flux of 289 m^3/m^2 h bar for the PDVF/TiO2 membrane. After 300 hours the flux of both membranes had settled to their equilibrium values, 70 $m^3\ m^{-2}h^{-1}bar^{-1}$ (24% of initial) for PDVF membrane and 143 $m^3\ m^{-2}h^{-1}bar^{-1}$ (49% of initial) for PDVF membrane. The PDVF/TiO_2 membranes were stable after heat treatment at 180°C, which is above the normal stability range for PVDF membranes. Using TiO_2 the membranes produced are stronger and have more favourable permeation rates. Unfortunately solute rejection experiments were outside the scope of that work so the effect of the addition of TiO_2 on rejection was not considered.

Figure 2.7 – Nitrogen permabilities of PVDF and PVDF/TiO2 membranes measured at 30 bar as a function of pressurising time (Ebert *et al*, 2004).

The term compaction has also been applied in a work by Szilasi *et al* (2011) with a different definition. The work addressed the extent of 'compaction' which was caused by proton beam irradiation during manufacture. PDMS was spun coated upon a glass substrate to create a layer thickness in the region of 95 microns, which was then baked to finish the sample. Each sample was then subjected to one of five different irradiation levels and one of three irradiation spacing schemes. The irradiation took the form of a 2MeV proton beam operating in parallel lines with variable line widths/periods. The term compaction in this work referred to the shrinkage of the polymer matrix when irradiated. When a polymer is subjected to a high energy ion the chain is broken and volatile products form – in the case of PDMS these are hydrogen, methane and ethane gasses. Figure 2.8 shows the results of the investigation. Different beam operations are shown in the form of beam widths / periods, i.e. the 15/30 result indicates a polymer that was subjected to 15 μm irradiation followed by 30 μm no irradiation in sequence. The study showed that increased irradiation dose and larger periods increased the degree of compaction which was attributed to an increase in ion energy and interference from non irradiated polymer chains causing increased stress within the bulk polymer respectively. Studies on the irradiation of PDMS have also been conducted by Hill *et al* (2001) who found similar molecular weight decreases. As Szilasi *et al* (2011) was the only reference found which used this definition of 'compaction', the definition initially proposed by Gekas and subsequently adopted by the vast majority of authors will be taken as the implied term when future instances of the term are present.

Figure 2.8 – The degree of compaction as a function of the irradiation influence in cases of different line widths/spacing. (Szilasi *et al*, 2011)

Membrane compaction is typically inferred from decreasing solvent flux during operation or from physical analysis (direct measurement/SEM photography) after use. These methods do not provide real time information as to the state of compaction only the compaction remaining after the applied pressure was removed. Any expansion realised by removing and analyzing the membranes could alter the reported compaction extent, thereby affecting any conclusions drawn. Reinsch *et al* (2000) developed a non-invasive technique utilising ultrasonic time-domain reflectrometry to produce real time measurements of the extent of compaction for gas separation processes. The process was similar to that already described by Peterson *et al* (1998). The process involves passing ultrasonic waves through the membrane cell and recording the time for the reflected wave to occur. The return time was relatable to the

current membrane thickness. Good correlation between compaction and permeability was found for asymmetric cellulose acetate membrane and nitrogen system. The main use of this technique was to aid model development.

2.2.3. Size Exclusion / Molecular Weight Cut Off

To date, little information is supplied by manufacturers when membranes are purchased, for confidentially issues. This leads to problems when trying to select the best membrane for a given process and comes down to a mixture of personal experience and specific testing in the lab. One value that is usually stated is the molecular weight cut off (MWCO), the theoretical size a molecule has to be so that it is retained by the membrane. This value is obtained by plotting the rejection of solutes versus their molecular weight, and interpolating this data to find the molecular weight corresponding to 90% rejection (See-Toh *et al,* 2007). However, this method is not standard and so inconsistencies can occur between different companies when describing functionally identical membranes. Yang *et al,* (2001), has reported that the stated MWCO values seem to only be valid for aqueous systems and bear little resemblance to the cut off produced from organic solvent based systems. Additionally separation in nanofiltration membranes primarily occurs due to steric hindrance and membrane solute interactions (Teixeira *et al,* 2005) See-Toh *et al,* (2007) has outlined a method for determining this value in the hope of creating an industry standard to allow easier membrane selection in the future, but presently it is too early to see if this takes root. MWCO is only one physical parameter, and one of limited usefulness, when considering SRNF membranes as the MWCO is not a fixed value due to swelling effects, but nevertheless this process of standardisation is still an important one.

2.2.4. Nanofiltration Developments

2.2.4.1. Developments in Silicon Based Nanofiltration

One of the most universal substances in solvent resistant nanofiltration is a class of silicon containing polymers called siloxanes. As a group siloxanes have a wide range of physical properties which allows them to be used in an entire range of applications from electronics to conformal coatings, encapsulants to adhesives (Song *et al,* 2007). Individual siloxanes can be viscous yet lubricating as liquids, while an apparently solid form can be either rigid or elastomeric (Polk, 2001). The many varied and useful

applications, for this material contribute to the growing size of the polymer market, and ensure that future research will be conduced leading to new applications for this material.

Siloxanes are monomer units which can be polymerised to form polysiloxanes which in turn can be crosslinked to increase the mechanical strength and resistance to chemical degradation. The generic structure of polysiloxanes is shown as Figure 2.9, where the backbone is composed of alternating oxygen and silicon molecules single bonded with two side branches on the silicon to fill the remaining valency of the +4 silicon ion; it should be noted that the two side branches need not be identical. Siloxane polymers are classed as inorganic regardless of the side groups attached. A polymer is defined as inorganic if the backbone contains less than 50% carbon atoms (Elias, 1997). The side branches are utilised as a way of altering the physical properties of the polymer from one polysiloxane to the next, and are controlled by altering the monomer source material used. By far the most common side branch is the methyl group, which creates PDMS; with over 1900 articles published which list this substance as a keyword. The reason why the simple methyl group is used is that as the proposed size of the side branch increases the energy required to establish a stable bond increases as well.

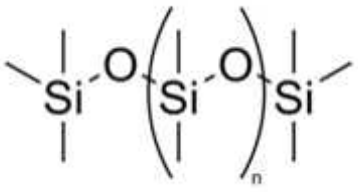

Figure 2.9 – General structure of a polysiloxane molecule.

2.2.4.2. Properties of Polydimethylsiloxane

The strength of a polymer is determined by the strength of its weakest link and the silicon oxygen backbone of siloxanes ensure that they are one of the strongest polymers. The Si-O bond has a bond energy of 107 kcal, which compares favourably to carbon based bonds which have values typically around 80 kcal (C-C is 83 kcal and C-O 85 kcal) (Ellis, 1984). This higher bond energy means that siloxane based polymers will be able to withstand harsh conditions such as temperature or chemical attacks which would break other organic based polymers.

Similarly to bond strength the bond angle of silicon containing pairings is also favourable to that of organics. The Si-O-Si bond is ~144° and O-Si-O is ~110°, while the C-Si-C bond is 111°. These bond angles allow relatively free rotation around the backbone and in the case of PDMS relatively free rotation around the methyl side groups leading to exceptional low temperature properties (Clarson & Semlyen, 1993), and a wide range of polymer chain arrangements. Thermal and oxidative stability is ensured by the nature of the siloxane backbone. When included as the selective layer in a composite membrane PDMS typically has a barrier thickness of less then 10 µm (Ulbricht *et al*, 2006) which as at the lower end for membranes meaning that high flux rates are possible. Table 2.3 lists properties of PDMS relevant to this project; a full list has been published by Clarson & Semlyen (1993).

Table 2.3 – Qualitative attributes of polydimethylsiloxane. (Clarson & Semlyen, 1993)

2.2.5. Concepts of Solvent Resistant Nanofiltration

Solvent resistant nanofiltration membranes by definition will not dissolve or degrade in the presence of solvents however they do swell in contact with such fluids. The extent to which SRNF membranes swell is the focus of extensive research, looking into the fundamental mechanics behind it, and establishing models to predict swelling behaviour. The purpose of this section is to outline the main factors of membrane swelling, some of the key parameters involved, and present relevant findings of other authors.

2.2.5.1. Solubility Parameter

To vaporise a liquid two forms of heat are required; normal heat to bring the liquid up to its boiling point and extra heat to overcome intermolecular Van der Waals forces to separate the liquid molecules and produce a phase change. The total of these two energies must be sufficient to overcome the molar cohesive energy, *-U* of that liquid. Equation (2.3) is one way of determining that amount of energy.

$$-U = {}_{l}\Delta_{g}H + {}_{g}\Delta_{\infty}H - RT + P_{s}V \qquad (2.3)$$

where ${}_l\Delta_g H$ *is* the molar vaporisation enthalpy, ${}_g\Delta_\infty H$ is enthalpy change on isothermally expanding 1 mol of saturated vapour to zero pressure, R is universal gas constant, T is temperature of the solution, P_s is saturation vapour pressure and V is molar volume of the liquid.

This equation can be derived, introducing the concepts of cohesive energy density and solubility parameter to slightly different form, which takes into account the effect of polarity, dispersion and hydrogen bonding, shown as Equation (2.4) (Tarleton *et al,* 2006a).

$$\delta = \sqrt{\delta_p^2 + \delta_d^2 + \delta_h^2} \tag{2.4}$$

The appliance of this concept is slightly different when considering polymer swelling as the polymer chains do not technically mix with the bulk solution but rather they absorb the solution into the structure, increasing in both size and mass. The solvent fills the inter-polymer spaces within the membrane and causes the polymer chains to move further apart, so a polymer slab swollen with solvent retains its isotropic tendencies simply with an altered bulk density.

2.2.5.2. Experimental Review

This section details work that has been published in the direct area of the research, namely solvent nanofiltration using PDMS/PAN membranes.

Solubility Parameter and Swelling

The relationship between swelling degree and solubility parameter is well established and has been reported by many authors (Bhanushali *et al* 2001, Robinson *et al,* 2004, Tarleton *et al*, 2004 and Yoo *et al*, 1999). The typical range of solvents used in these studies includes alkanes, aromatics and alcohols, with or without specific impurities such as heavy metals or organometallics. As such the solvents usually span a range of 10 to 30 $MPa^{0.5}$ for solubility parameter, and tend to produce a distinctive curve when plotted against overall swelling. A typical example for PDMS can be seen as Figure 2.10 (Tarleton *et al*, 2005), where a maximum expansion was attained at 15.5 $MPa^{0.5}$ before noting reduced expansion at the higher end of solubility parameter. The initial thickness of the PDMS layer in Figure 2.10 was 10 µm, and the maximum swelling was reported as 169% of its initial height when n-heptane was used. This swelling trend is similar to the underlying trend in the results previously discussed as Table 2.1. The solvents which elicit the biggest swelling effect (i.e. heptane and hexane) also elicit the largest flux rates for any given pressure, and the lowest swelling solvents correspond to the smaller flux rates. Combining these results implies that as the polymer swells the relative porosity increases which in turn increases the noted flux values.

Figure 2.10 – Typical swelling curve for PDMS (Tarleton *et al*, 2005).

The effect of solubility parameter on swelling so far discussed only covers the use of pure solvents rather than solvent mixtures. It has been reported that the application of solubility parameter to predict swelling of mixtures is not as appropriate as for pure solvents. Robinson *et al* (2004) has noted nonlinearity between swelling amounts and fractional composition of a cyclohexane/n-hexane mixture, implying that when more than one chemical species was involved, use of the solubility parameter alone to predict swelling was insufficient.

Similar nonlinearity was also reported by Yoo *et al* (1999) for mixtures of n-hexane/acetone and n-hexane/ethanol. The polymer used by Yoo *et al* (1999) was hydroxyl-terminated PDMS obtained from General Electric and crosslinked by the addition of a catalyst. The polymer slabs created were also subjected to two high temperature vulcanisation procedures at 142.5°C and 205.4°C, before being shaped into cuboids. The samples were then weighed and immersed in a chosen solvent mixture. When swelling had reached equilibrium the sample was weighed again and the resultant values allowed for a measurement of the swelling extent to be determined. This method for the preparation by Yoo *et al* (1999) was similar to the one carried out to produce the polymer slabs in the experimental section (Section 3.1.1.) of the main report. Yoo *et al* (1999) then presented an extensive matrix of test results for binary and ternary systems, where it was deduced that swelling for a binary solution was not linearly dependent on composition. The paper details a series of experiments where heptane/acetone mixtures (11 in total ranging from pure heptane to pure acetone in steps of 10%) were used to swell PDMS slabs. Figure 2.11 shows the results of the experiment with pure heptane eliciting the largest swelling extent and pure acetone the least.

Figure 2.11 – PDMS swelling ratios for hexane/acetone system (Yoo *et al*, 1999).

The swelling ratio of PDMS slabs immersed in a mixture of n-hexane/acetone was reported to show a maximum at 90% n-hexane 10% acetone which then trails off towards pure n-hexane, it was also stated that the equilibrium values past 50% could not be taken as constant as a certain amount of variation in the values was found. If the swelling extent was linearly affected by solution composition each of the lines in Figure 2.11 would be evenly spaced and the 90% maximum would not be present. Additional research has confirmed that a similar phenomenon was found when investigating n-hexane/ethanol binary solutions.

There was a distinct relationship between swelling of PDMS and the solubility parameter of solvent(s) in contact with the membrane. For single species contact the swelling seems to be dependent on the difference in solubility parameters, however this is not always the case as PDMS membranes have been produced by Twente which do not follow this trend (Tarleton *et al*, 2009). The Twente membranes when tested for swelling characteristics were found to posses a minimum rather than a maximum at a solubility parameter of 15.5 $MPa^{0.5}$. the purpose of the work was to

check swelling extents so no explanation for this effect was given. This means that for even single species systems the trend shown as Figure 2.10 is not definitive. Binary systems are even more complicated as they are non-proportional to the single species system.

Membrane Form

The versatility of PDMS means that even the shape of the membrane can be altered to maximise the separation achieved and so the material can be tailored to meet the exact process needs. The mainstream shape for these membranes is flat sheets, but other authors have conducted work characterising different shapes. Cocchini *et al* (2002a) has experimented with steel braided PDMS membranes and found that they can be advantageous in separating VOCs from water streams due to their high burst pressure. In the report steel wires were braded around a central cylindrical core of PDMS to restrain the overall swelling extent and provide a more uniform transport profile. This type of arrangement is good for certain extraction processes however for others (namely water based systems) it actually lowers the productivity by introducing another mass transfer resistance. In addition to the solid PDMS membrane, this work applied liquid membranes to increase the effectiveness of the solute transport. An extension to this work (Cocchini *et al* 2002b) used the same membrane configuration but focused heavily on the liquid membrane aspect of the rig by modelling contained liquid membrane transport.

Doig *et al* (1998) used a shell and tube exchanger for the determination of mass transfer rates, and found that the resistances in series model is adequate for the prediction of the process. Silicon tubing was used as the selective barrier in this work, its composition was 30 wt% fumed silica and 70 wt% PDMS, and due to its default shape; it was used as it was supplied. Change in membrane volume was used as the defining characteristic for swelling rather than the standard change by weight so the results do not directly compare with those stated above. The greatest swelling was found by toluene (72 % increase), 2-Octanone (57 % increase) and ethyldecanoate (54 % increase) which are all simple hydrocarbons. 2-Octanone and ethyldecanoate are both straight chain hydrocarbons each with a single double bonded oxygen as the only side chain, so it is no surprise that they function in a similar manner to other alkanes like n-heptane or i-octane. Toluene (syn. methylbenzene) does not have a straight chain arrangement due to the cyclic ring at its centre yet it has the greatest effect on

the tubing. This implies that toluene can diffuse through the non-swollen structure and, once inside, affect it more due to its inherent shape.

The specific form of a membrane has an effect on the separation properties of a process. Two membranes composed of the same materials can have different characteristics due to the manufacturing process. Robinson *et al* (2005) has extensively studied PDMS/PAN composite nanofiltration membranes that were manufactured differently. The effects of varying selective layer thickness and irradiation dose have been considered by testing different membranes from the same range. All membranes were tested using a crossflow nanofiltration apparatus which recycled the retentate back into the feed. The xylene flux of otherwise identical membranes with selective layer thicknesses of 1, 2 and 10 microns was determined to be 1.928×10^{-12} $m^2s^{-1}bar^{-1}$, 2.592×10^{-12} $m^2s^{-1}bar^{-1}$ and 1.820×10^{-12} $m^2s^{-1}bar^{-1}$ respectively. In each case the membranes were tested over the range 2 ~ 9 bar and flux/pressure relationships were linear throughout. As the flux results are in close agreement, no significance was attributed to the relative size of the xylene flux for different active layer thicknesses. Three membranes, of nominal selective layer thickness 2 microns, were manufactured with different levels of crosslinking by exposure to different levels of irradiation, namely 50 kGy, 100 kGy and 200 kGy. The xylene permeation was determined using the same procedure as for the different thickness membranes and is shown as Figure 2.12a. Linear flux/pressure relationships were produced for each membrane with the larger gradients being produced by the least irradiated membrane. This effect was explained by membrane swelling. It was postulated that a swelled membrane has an inherently higher solvent flux and as swelling is restricted by crosslinking extent, the smaller irradiation dose membranes will swell the most. The rejection of the irradiated membranes was checked by removing 9,10-diphenylanthracene from xylene over the pressure range 2 ~ 8 bar with the results shown as Figure 2.12b. For any given pressure the rejection extent is greater for a more crosslinked membrane. This was explained similarly to the effect on flux, as a membrane swells the transport regions within the selective layer increase as well, diminishing the size-exclusion effect and lowering rejection. As the selective layer is irradiated free radicals form which subsequently combine to create covalent crosslinking bonds up to a point, however membrane degradation also occurs. An optimum irradiation dose therefore exists, which was found to be around 150 kGy for these membranes. This finding is similar to the one found by Szilasi *et al* (2011), discussed in Section 2.2.2. Differently irradiated PDMS/PAN membranes have also been researched by Tarleton *et al* (2006b) who found almost identical swelling extents for 100 kGy and 200 kGy membranes, slightly

higher swelling for 50 kGy membranes and significantly higher swelling for 80 kGy irradiated membranes. This behaviour supports Robinson's hypothesis of membrane degradation at high irradiation doses.

Figure 2.12 – Performance of differently irradiated membranes. a) flux performance, b) rejection performance (Robinson *et al*, 2005)

Continuous Operation

The vast majority of work involving SRNF membranes involves batch type separations of known solvents; however some recent studies cover the applications of SRNF in a continuous arrangement for streamlining of pharmaceutical processes (Lin and Livingston, 2006). The report outlines significant advantages for using a cascade arrangement which culminates in an improved solvent exchange. Pharmaceutical processes generally involve large amounts of solvents which cost money to replace for each new batch of drugs produced, by the use of a cascade system these solvents can be recycled cutting down the raw material cost for any applicable process. Using the cascade system Lin and Livingston (2006) have experimentally shown that recoveries of 47.8%, 59.2%, and 75.3% are possible in the first, second and third stage of the rig. This was achieved by the use of a simulant mixture composed from toluene and methanol, so the efficiency of this process to other product streams has yet to be confirmed. However the potential savings make this process intriguing.

Active Layer Swelling

Geens *et al* (2004) has reported a series of membrane swelling experiments carried out on three commercially available polymeric nanofiltration membranes. Prior to the swelling experiments the support layer was removed from each membrane by separating the layers after immersion in liquid nitrogen. The remaining two layers were placed into a range of solvents with the swelling extent determined by the relative change in mass realised – results shown as Table 2.4. The authors found that with the exception of heptane (where compatible) water had the greatest swelling effect of the solvents tested, however the significance of this was not discussed apart from noting the same result was also found by Shukla and Cheryan (2002). In 2002 Ebert hypothesised the difference between dense and porous membranes. When a dense polymeric membrane swells the existing chains must move apart from each other

causing an increase in free volume throughout the structure, which would in turn lower the rejection characteristics. When a porous membrane swells the existing pores are constricted by the expanding material which would raise the rejection characteristics. To check whether the membranes used by Geens *et al* (2004) were technically porous or dense the authors used this hypothesis during the analysis of rejection experiments carried out using maltose which was reported in the same paper. It was determined that all three membranes operated in a porous fashion. It was concluded that the effects of swelling are more important on membranes with small pores due to the dual effects of diffusive and viscous transport which are affected by the changes.

Table 2.4 – Degree of swelling (in ml/g) of the membrane top layers in different solvents. (Geens *et al*, 2004)

2.3. Intermediate Conclusions

Membrane technology has come a long way since its birth in 18th century but it is the developments of the 1960's which changed this industry into what would now be regarded as the current processing technique. The development in question was composite membranes which allowed the active layer to become sufficiently thin, replacing its mechanical dependency with a support structure capable of performing such a role. With this advance, the throughput of membrane units was vastly increased whilst reliability and selectivity increased as well. From this discovery the whole field of reverse osmosis emerged as a viable technology and the importance of membrane separations increased.

This technology has developed over time to separate out a wider range of solutes from ever harsher environments, which have in turn necessitated that the membranes be adapted to cope with the conditions; this refinement gave birth to SRNF membranes. SRNF membranes are capable of functioning whilst filtering solutions composed of solvents such as heptane or xylene which other standard membranes can not. However their physical structure is changed by the presence of such solvents thereby altering their separation characteristics.

More recent work has focused on quantifying this swelling effect and trying to identify the apparent transport regime, however universal opinion has not currently been achieved as to which is correct. Two competing theories have arisen to explain solute transport differing by their fundamental assumptions. Solution diffusion states that the solutes dissolve into the active layer and diffuse down a concentration gradient, where as pore flow states that separation is achieved by a size exclusion technique utilising the transport regions in the structure of the active layer. Both theories have merit and both have been shown to work for different experimental conditions.

The main section of this thesis deals with the production and subsequent characterisation of composite SRNF membranes. From a review of the literature it is clear that the performance of commercially produced SRNF membranes varies greatly based on operational parameters such as solvent or solute type, operating pressure and even manufacturer, as it has been shown for identical conditions two membranes produced by different manufacturers can produce significantly different filtration characteristics. The aims of this work have been chosen to accommodate this acknowledged variance, by definably characterising the filtration characteristics of the membrane produced. Production of composite membranes is a pre-requisite for this work and, as such, needs no justification. Characterisation of PDMS is an important step as it has been shown that differently produced PDMS can behave in different ways. Achieving this aim will, besides proving that the polymer created is PDMS, identify which of the literature reported PDMS membranes most closely resembles the membranes created during this work. Typically the production method of SRNF membranes is not disclosed for confidentially reasons, however no such issue exists around the membranes created in this work, therefore by comparing the data collected to the literature examples previously described, indications of their production method can be inferred. As previously stated, universal opinion has not been achieved with regards to the transport mechanism within SRNF membranes – Identification of transport mechanism has been included as an aim for this reason. The only way universal opinion will be achieved will be by significant amounts of research into different membrane types and applications. Identifying the appropriate transport mechanism for the produced membranes will add weight to one side of the debate leading to a greater overall understanding. The final aim of this work, determination of effective pore size, exists because commercial membranes are sold based on their effective pore size, so determination of this value is an important step in truly charactering these membranes. As the field of membrane separations is vast that no single work could feasibly unite all aspects into a single unifying theory, however these

aims, which have developed from identifying gaps in the current state of research, will increase the current limit of knowledge in this field.

2.4. Nomenclature

${}_{g}\Delta_{\infty}H$	Enthalpy change (J)
${}_{l}\Delta_{g}H$	Molar vaporisation enthalpy (J mol^{-1})
A	Membrane area (m^2)
c	Molarity (mol l^{-1})
J	Solvent flux (l m^{-2} h^{-1})
L	Permeate volume (l)
P_s	Saturation vapour pressure (Pa)
R	Universal gas constant (J K^{-1} mol^{-1})
T	Temperature (K)
U	Molar cohesive density (MPa)
V	Molar volume (m^3 mol)
δ	Solubility parameter ($MPa^{0.5}$)
Π	Osmotic pressure (bar)

2.5. References

Ahmad A.L., Ooi B.S., Mohammad A.W., Choudhury J.P., 2004. Composite nanofiltration polyamide membrane: A study on the diamine ratio and its performance evaluation. *Industrial and Engineering Chemistry Research*, **43**, 8074-8082.

Albrecht W., Kneifel K., Weigel Th., Hilke R., Just R., Schossig M., Ebert K., Lendlein A., 2005. Preperation of highly asymmetric hollow fibre membranes from poly(ether imide) by a modified dry-wet phase inversion technique using a triple spinneret. *J. Membrane Science*, **262**, 69-80.

Baker R.W., 2004, *Membrane Technology and Applications*, 2nd Edn. John Wiley & Sons, Chichester.

Bhanushali D., Kloos S., Kurth C., Bhattacharyya D., 2001. Performance of solvent resistant membranes for non aqueous systems: Solvent permeation results and modelling, *J. Membrane Science*, **189**, 1-21.

Clarson, S.J. & Semlyen, J.A., 1993, *Siloxane Polymers*, PTR Prentice Hall, New Jersey.

Cocchini U., Nicolella C., Livingston A.G., 2002a. Braided silicone rubber membranes for organic extraction from aqueous solutions: I. Mass transfer studies. *J. Membrane Science*, **199**, 85-99.

Cocchini U., Nicolella C., Livingston A.G., 2002b. Braided silicone rubber membranes for organic extraction from aqueous solutions: II. Application to contained liquid membranes. *J. Membrane Science*, **199**, 101-115.

Darvishmanesh S., Degreve J., van der Bruggen B., 2009, Comparison of pressure driven transport of ethanol/n-hexane mixtures through dense and microporous membranes, *Chemical Engineering Science*, **64**, 3914-3927.

Dijkstra M.F.J., Bach S., Ebert K., 2006. A transport model for organophilic nanofiltration. *J. Membrane Science*, **286**, 60-68.

Doig S.D., Boam A.T., Livingston A.G., Stuckey D.C., 1998. Mass transfer of hydrophobic solutes in solvent swollen silicone rubber membranes, *J. Membrane Science*, **154**, 127-140.

Ebert K., Fritsch D., Koll J., Tjahjawiguna C., 2004. Influence of inorganic fillers on the compaction behaviour of porous polymer based membranes, *J. Membrane Science*, **233**, 71-78.

Ebert K., Koll J., Dijkstra M.F.J., Eggers M., 2006. Fundamental studies on the performance of a hydrophobic solvent stable membrane in non-aqueous solutions, *J. Membrane Science*, **285**, 75-80.

Elias H.G., 1997, *An Introduction to Polymer Science*, VCH Verlagsgesellschaft GmbH, Weinheim.

Ellis H, 1984, *Revised Book of Data*, Longman Group, Essex

Geens, J., Van der Bruggen, B., Vandecasteele, C., 2004, Characterisation of the solvent stability of polymeric nanofiltration membranes by measurement of contact angles and swelling, *Chemical Engineering Science*, **59**, 1161-1164.

Geens J., 2006, Mechanisms and modelling of nanofiltration in organic media, PhD thesis, Katholieke Universiteit Leuven.

Gekas, V., 1988, Terminology for pressure-driven membrane operations, *Desalination*, **68**, 77-92.

Gevers L.E.M., Meyen G., De Smet K., Van De Velde P., Du Prez F., Vankelecom I.F.J., Jacobs P.A., 2006. Physico-chemical interpretation of the SRNF transport mechanism for solutes through dense silicone membranes, *J. Membrane Science*, **274**, 173-182.

Guizard, C., Ayral, A., Julbe, A., 2002, Potentiality of organic solvents filtration with ceramic membranes. A comparison with polymer membranes, *Desalination*, **147**, 275-280.

Hill, D.J.T., Preston, C.M.L., Salisbury, D.J., Whittaker, A.K., 2001, Molecular weight changes and scission and crosslinking in poly(dimethyl siloxane) on gamma radiolysis, *Radiation Physics and Chemistry*, **62**, 11–17.

Ho W.S.W. & Sirkar K.K., 1992, *Membrane Handbook*. Van Nostrand Reinhold, New York.

Holdich R.G., 2002, *Fundamentals of Particle Technology*, Midland Technology and Publishing, Shepshed.

Kallioinen, M., Pekkarinen, M., Manttari, M., Nuortila-Jokinen, J., Nystrom, M., 2007, Comparison of the performance of two different regenerated cellulose ultrafiltration membranes at high filtration pressure, *J. Membrane Science*, **294**, 93-102.

Kolf W.J., Berk H.T., 1944. The artificial kidney: A dialiser with great area, *Acta Medica Scandinavica*, **117**, 121-134.

Kusakabe K., Yoneshige S., Morooka S., 1998, Separation of benzene/cyclohexane mixtures using polyurethane-silica hybrid membranes, *J. Membrane Science*, **149**, 29-37.

Lin J.C.-T., Livingston A.G., 2006. Nanofiltration membrane cascade for continuous solvent exchange. *Chemical Engineering Science*, **62**, 2728-2736.

Loeb S., Sourirajan S., 1963. Demineralisation by means of an osmotic membrane, *Advances in Chemistry*, **28**, 117-132.

Machado, D.R., Hasson, D., Semiat, R., 1999, Effect of solvent properties on permeate flow through nanofiltration membranes. Part I: investigation of parameters affecting solvent flux, *J. Membrane Science*, **163**, 93-102.

Mulder M., 2000, *Basic Principles of Membrane Technology*, 2nd Edn. Kluwer Academic Publishers, London

Persson, K.M., Gekas, V., Tragardh, G., 1995, Study of membrane compaction and its influence on ultrafiltration water permeability, *J. Membrane Science*, **100**, 155-162.

Peterson, R.A., Greenberg, A.R., Bond, L.J., Krantz, W.B., 1998, Use of ultrasonic TDR for real-time noninvasive measurement of compressive strain during membrane compaction, *Desalination*, **116**, 115-122.

Polk D.W., 2001, Synthesis and characterisation of alternating poly(arylene ether phosphine oxide)-b-siloxane and segmented nylon 6,6-b-siloxane copolymers. PhD thesis, Virginia Polytechnic Institute and State University.

Reinsch, V.E., Greenberg, A.R., Kelley, S.S., Peterson, R., Bond, L.J., 2000, A new technique for the simultaneous, real-time measurement of membrane compaction and performance during exposure to high-pressure gas, **171**, 217-228.

Robinson J.P., 2004, The selective removal of components from gasoline using membrane technology, PhD thesis, Loughborough University.

Robinson J.P., Tarleton E.S., Millington C.R., Nijmeijer A., 2004. Solvent flux through dense polymeric nanofiltration membranes, *J. Membrane Science*, **230**, 29-37.

Robinson, J.P., Tarleton, E.S., Ebert, K., Millington, C.R., Nijmeijer, A., 2005, Influence of Cross-linking and process parameters on the separation performance of poly(dimethylsiloxane) nanofiltration membranes, *Industrial and Engineering Chemistry Research*, **44**, 3238-3248.

Santos J.L.C., Hidalgo A.M., Oliveira R., Velizarov S., Crespo J.G., 2007, Analysis of solvent flux through nanofiltration membranes by mechanistic, chemometric and hybrid modelling, *J. Membrane Science*, **300**, 191-204.

Schafer A.I., Fane A.G. & Waite T.D., 2005, *Nanofiltration Principles and Applications*, Elsevier Advanced Technology, Oxford.

Szilasi, S.Z., Kokavecz, J., Huszank, R., Rajta, I., 2011, Compaction of poly(dimethylsiloxane) (PDMS) due to proton beam irradiation, *Applied Surface Science*, **257**, 4612-4615.

See Toh Y.H., Loh X.X., Li K., Bismarck A., Livingston A.G., 2007. In search of a standard method for the characterisation of organic solvent nanofiltration membranes, *J. Membrane Science*, **291**, 120-125.

Sherwood T.K., Brian P.L.T., Fisher R.E., 1967. Desalination by reverse osmosis, *Industrial and Engineering Chemistry Fundamentals*, **6**, 2-12.

Shukla, R., Chervan, M., 2002, Performance of ultrafiltration membranes in ethanol–water solutions: effect of membrane conditioning, *J. Membrane Science*, **198**, 75-85.

Song S., Khang D.Y., Kim M.J., Park J.E., Lee H.H., 2007. Asymmetric porous thin film preparation by controlled solvent absorption using PDMS, *J. Membrane Science*, **305**, 5-12.

Szymczyk A., Labbez C., Fievet P., Vidonne A., Foissy A., Pagetti J., 2003. Contribution of convection, diffusion and migration to electrolytr transport through nanofiltration membranes. *Advances in Colloid and Interface Science*, **103**, 77-94.

Tarleton E.S., Robinson J.P., Millington C.R., Nijmeijer A., 2004. Non-aqueous nanofiltration: Solute rejection in low-polarity binary systems, *J. Membrane Science*, **252**, 123-131.

Tarleton E.S., Robinson J.P., Smith S.J., Na J.J.W., 2005. New experimental measurments of solvent induced swelling in nanofiltration membranes, *J. Membrane Science*, **261**, 129-135.

Tarleton E.S., Robinson J.P., Millington C.R., Nijmeijer A., Taylor M.L., 2006a. The influence of polarity and rejection behaviour in solvent resistant nanofiltration - Experimental Observations, *J. Membrane Science*, **278**, 318-327.

Tarleton E.S., Robinson J.P., Salman M., 2006b, Solvent-induced swelling of membranes – measurements and influence in nanofiltration, *J. Membrane Science*, **280**, 442-451.

Tarleton E.S., Robinson J.P., Low J.S., 2009, Nanofiltration: A technology for selective solute removal form fuels and solvents, *Chemical Engineering Research and Design*, **87**, 271-279.

Teixeira M.R., Rosa M.J., Nystrom M., 2005. The role of membrane charge on nanofiltration performance, *J. Membrane Science*, **265**, 160-166.

Ulbricht M., 2006. Advanced functional polymer membranes, *Polymer*, **47**, 2217-2262.

Vankelecom I.F.J., De Smet K., Gevers L.E.M., Livingston A., Nair D., Aerts S., Kuypers S., Jacobs P.A., 2004, Physico-chemical interpretation of the SRNF transportmechanism for solvents throughdense silicone membranes, *J. Membrane Science*, **231**, 99-108.

Verhoef A., Figoli A., Leen B., Bettens B., Drioli E., van der Bruggen B., 2008. Performance of a nanofiltration mambrane for removal of ethanol from aqueous solutions by pervaporation, *Separation and Purification Technology*, **60**, 54-63.

Verliefde A.R.D., Cornelissen E.R., Heijman S.G.J., Verberk J.Q.J.C., Amy G.L., van der Bruggen B., van Dijk J.C., 2008, The role of electrostatic interactions on the

rejection of organic solutes in aqueous solutions with nanofiltration, *J. Membrane Science*, **322**, 52–66.

Wang X.L., Tsuru T., Nakao S.I., Kimura S., 1997. The electrostatic and steric-hindrance model for the transport of charged solutes through nanofiltration membranes, *J. Membrane Science*, **135**, 19-32.

White L.S., 2006. Development of large-scale applications in organic solvent nanofiltration and pervaporation for chemical and refining processes, *J. Membrane Science*, **286**, 26-35.

Yang X.J., Livingston A.G., Freitas dos Santos L., 2001. Experimental observations of nanofiltration with organic solvents, *J. Membrane Science*, **190**, 45-55.

Yaroshchuk A.E., 1995. Solution-diffusion-imperfection model revised, *J. Membrane Science*, **101**, 83-87.

Yoo J.S., Kim S.J., Choi J.S. 1999. Swelling equlibria of mixed solvent/poly(dimethylsiloxane) systems, *J. Chemical & Engineering Data*, **44**, 16-22.

3. Characterisation of Membranes

This chapter focuses on PDMS which has been manufactured in house by a catalyst based crosslinking procedure. Catalysis is only one way to produce functional polymers; other techniques include heat (thermal) or irradiation. Thermal crosslinking is a suitable method for producing membranes where the active layer is measured in microns, however when the active layer is measured in millimetres (as for the polymer slabs tested in this work) this is not an option. Thermally irradiating larger membranes results in a non-uniform crosslinking as the exposed surface forms bonds and effectively shields the centre of the polymer leading to little stabilisation of the internal structure. Chemically induced crosslinking circumvents this problem by dispersing a homogeneous catalyst within the fluid monomer melt to ensure the formation of a uniform crosslinking density assuming a sufficient dispersal can be achieved. Another typical production method is phase inversion where a solvent rich polymer melt is spread evenly on a non porous material (normally glass) which is then immersed into a bath of water. The solvent diffuses out from one side only, resulting in a difference of polymer structure throughout the depth of the polymer. Due to the fact that as the solvent exits the interface, it hardens which slows further leaching of solvent and results in a dense layer forming on top of a relatively open layer, all produced from the same material. This method has been reported by several authors (Ebert *et al,* 2004, Silva *et al,* 2005, Ulbricht, 2006) as a viable means of production, however, this method produces thin films and was not used in this project for the same reasons as radiation crosslinked polymers, i.e. the method can not be used to produce the thick slabs required in the initial stages of testing.

The membrane used throughout this work was a composite material consisting of three layers. The first layer was a nonwoven cellulose support, which takes no part in the separation and was only present to provide mechanical strength for the other layers. Bonded to the cellulose was a backing layer of polyacrylonitrile (PAN) which also takes no part in the separation but provides both mechanical strength and a level surface for the final layer to adhere to. A selective layer of polydimethylsiloxane (PDMS) was bonded to the backing layer; this material is a dense polymer which provides the separation properties of the membrane. Both the PAN layer and the PDMS layer were in a liquid state when applied to the support layer meaning that they filled any available gaps in its surface. If the PAN layer was not present, the thickness of the PDMS layer would not be as constant, providing uneven separation properties, and as the PAN

does not take part in the separation the overall thickness of this layer was not critical. Polymerisation of the active layer was a necessary step in the manufacture process and is usually initiated by the application of heat or irradiation; however the membranes used in this work were produced using a catalyst crosslinking method instead.

3.1. Polymer Tests

3.1.1. Manufacture of Polymer Slabs

Cylindrical polymer slab (26 mm diameter and around 2 mm high) have been produced to confirm the effects of free polymer swelling without the inherent restrictions bonding to a support layer produces. It is envisioned that that by knowing the maximum extent of pure polymer swelling and comparing this data to membrane swelling (detailed in Section 3.5) additional insight into the process can be gained. The PDMS used in this study was obtained from Techsil Ltd as a two part kit; a silicon containing pre-polymer and a dibutyl catalyst. This kit has previously been used by Gevers *et al* (2006a) as a source of PDMS for nanofiltration membranes. The catalyst was incorporated in amounts ranging from 0.1 to 0.5 wt%, which allowed for some control over the physical properties of the PDMS produced.

The polymer slabs were produced in batches of twelve at a time in order to reduce the variance in any individual piece and provide some allowance for failed tests. By preparing sufficient monomer to cast twelve slabs at once the amount of catalyst increased to a more reproducible value around 0.1 g; the catalyst suspension was quite viscous and introducing amounts less than 0.1 g accurately tended to be difficult.

Producing the polymer slabs in batches of twelve ensured a sufficient quantity so that each of the eight solvents used could be tested against the exact same composition of polymer. This is important as although the compositions have been referred to as 0.1%, 0.2% etc in practise the actual composition was subject to variance so values such as 0.104%, 0.099% or 0.206% could occur. If each polymer was made individually the bulk variance in the tests would have introduced a small, but ultimately unnecessary, error into the experimental procedure. After blending of the monomer and the catalyst, the liquid was evenly distributed into twelve 30 mm square casting trays

and then left for at least 48 hours at ambient conditions to allow polymerisation to occur.

3.1.2. Polymer Swelling

After casting, each PDMS slab was shaped into a cylinder 26 mm in diameter and *ca.* 2.25 mm in height. These dimensions were dictated by the internal space of the available test cell. The exact height of the cylinder was then measured by dial gauge and the plan view was photographed so that computer image analysis could subsequently be used to calculate the initial size of the sample. The sample was secured in the test cell and 30 ml of solvent introduced before the cell was sealed to prevent loss of solvent through evaporation over the course of the experiment. A digital dial gauge was connected to the polymer expansion by recording the movement of a plunger which rested upon the test sample. Once expansion had occurred (22+ hours) the final dial gauge reading was recorded, the cell opened and a second photograph taken. The mass of the polymer cylinder before and after was also recorded. From the data recorded the relative change of three parameters was able to be calculated; mass, height and plan area.

A standard method for polymer swelling is relative change by mass, due to the fact that for thin films the change in height is difficult to measure and plan area doesn't change due to the restrictions of the support layer, however these parameters are important in the swelling of unbacked PDMS slabs. The initial test run was conducted using 0.3% DBT catalyst PDMS slabs and eight different pure solvents (as detailed in Table 3.1) chosen for the range of solubility parameters they represent. An extension to this test was also completed where the samples were left for over 70 hours to check the extent of expansion which had been reached after 22 hours. The third test set used 0.3% DBT catalyst PDMS slabs of varying initial heights to confirm the effect of height on relative change values. The fourth test used 0.1% DBT, 0.3% DBT and 0.5% DBT catalyst polymer slabs with three different solvents to confirm the effect of catalyst concentration on the relative parameters. Summary of the tests performed are shown as Table 3.1.

Test Designation	Solvents Tested (Solubility Parameter, $MPa^{0.5}$)		Catalyst Amount (wt%)	Test Duration (Hours)	Sets (Tests)
Test A	i-octane (14.3) i-hexane (14.7) n-hexane (14.9) n-heptane (15.3)	xylene (18.2) n-propanol (24.9) ethanol (26.5) methanol (29.2)	0.3	22~24	2 (16)
Test B	i-octane (14.3) i-hexane (14.7) n-hexane (14.9) n-heptane (15.3)	xylene (18.2) n-propanol (24.9) ethanol (26.5) methanol (29.2)	0.3	70~72	2 (16)
Test C	n-heptane (15.3)		0.3	22~24	1 (9)
Test D	n-heptane (15.3) xylene (18.2) ethanol (26.5)		0.1 0.3 0.5	22~24	2 (6)

Table 3.1 – Polymer swelling test matrix.

The rig used throughout these tests is shown as Figure 3.1. It consisted of a test cell which housed the polymer sample and an actuated plunger which allowed for transient measurements to be recorded throughout the duration of a test. This cell ensured that no solvent was lost due to evaporation and allowed the polymer slab to expand without outside disturbance.

A polymer slab was placed into the test cell of the rig and the housing closed, the test solvent(s) were then introduced through the injection ports on the top of the cell before the cell was sealed. A magnetically coupled stirrer was in operation throughout the duration of the test to ensure immersion of the slab.

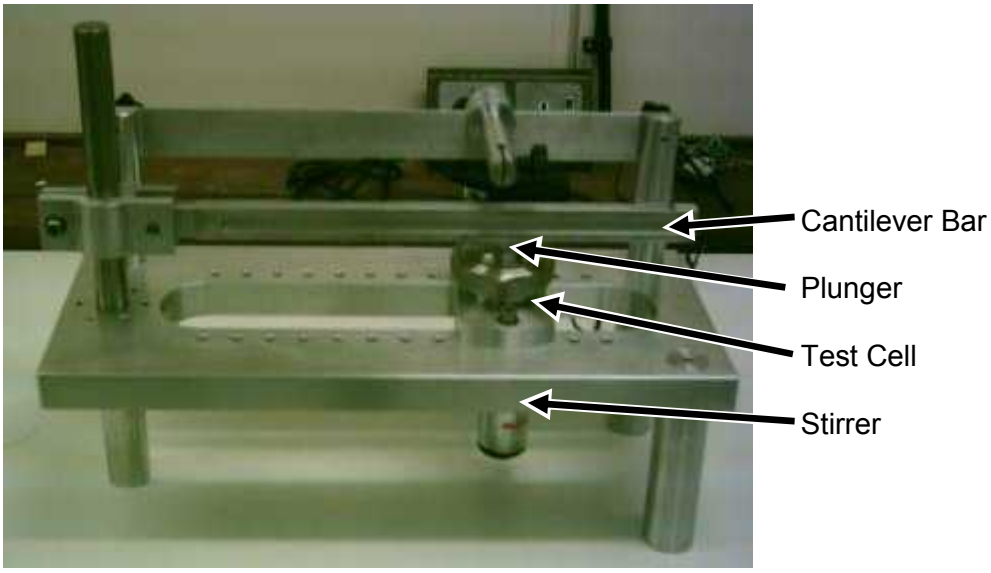

Figure 3.1 – Photograph of polymer swelling experimental rig.

As the sample swelled it pushed the plunger up, which in turn moved the needle of the digital dial gauge mounted on top, allowing for transient swelling readings to be taken at any time interval which was deemed relevant. At the end of a test, the cell was dismantled and the sample removed. The weight of the polymer sample was measured before and immediately after the test. The sample was placed upon a calibration grid and photographed to assess the change in plan area.

The sealed test cell on this rig was the main advantage of this apparatus ensuring that the evaporation of solvents was minimised. However, it is acknowledged that this rig is not without its problems, one of the main ones being that any polymer sample placed into this rig will swell in all directions. The rig will only measure expansion perpendicular to the angle of the plunger, i.e. no readings are taken of the increase of cross sectional area, which was the reason for photographing the samples immediately before and after each test. The initial photograph did not cause a problem as the polymer was stable. The final photograph was more time critical as the swollen membrane was leaching solvent from the instant it was removed from the cell, so a proportional error was introduced here, with the higher swelling solvents, like heptane, leaching quicker than the poorer swelling solvents, like ethanol. The effect of this evaporation rate is discussed in Section 3.1.4.

A second potential issue was that an amount of friction formed at the moving points of the set up, which would affect the reading on the digital dial gauge. The plunger had to move with the expansion of the polymer slab, however the cell had to be vapour tight

so a fixed seal was mounted into the lid of the cell and for the plunger to move it had to overcome the friction generated at this point. This second point was also countered by photographic analysis, as once the polymer was restrained in one direction (vertically) it would simply expand in the path of least resistance (laterally), and an increase in surface area would be observed.

At the end of the polymer test duration; 22 to 24 hours for tests one, three and four, and 70 to 72 hours for test two, the separate pieces of data were collected in a specific order, first the lateral swelling extent was recorded from the digital dial gauge as this value could be obtained without disturbing the test cell. Then the polymer slab was taken from the test cell and any excess solvent removed before the weight was recorded. The difficulty of this step was dependent on the solvent used, for solvents with a solubility parameter greater than 20 $MPa^{0.5}$, such as ethanol, the final weight was almost a static value, and so it was easy to record. The same was not true for solvents with solubility parameters in the region of 15 $MPa^{0.5}$, significant variance in weight with time was noted, resulting in the constant decrease in mass with time. To ensure a consistent baseline this section of the test was completed in less than 20 seconds from removal from the solvent to recording of the final mass. With this complete the polymer slab was sandwiched between two optically clear glass plates for the second photograph to be taken. The restrained polymer was then placed upon a calibration grid of known size and photographed. Preparation in this way had several benefits; it reduced the evaporation rate of the entrained solvent by minimising the surface area open to the air, it kept the polymer flat preventing the curling caused by evaporation from one polymer face, additionally it protected the calibration grid from being damaged by contact with volatile solvents. Figure 3.2 shows a polymer sample on top of the calibration grid, this photograph was from the end of a test run and was taken with the two glass plates in place; however as they are optically clear they are not visible from the photograph. The measurement taken from the calibration chart is the relative size of the squares printed.

Figure 3.2 – Representative photograph of polymer sample on calibration grid.

3.1.2.1. Analysis of Data

Scion Image was used to analyse the initial and final photographs. The program counts the number of pixels inside the boundary of the polymer and compares that to the length of a line on the calibration chart, to produce an accurate value for the size of the polymer. Comparing this value before and after allows for the relative increase to be determined. The use of the calibration chart ensures that the true change can be obtained by relative scaling of a known item common to both images. The equation for this comparison is shown as Equation (3.1).

$$AD = \left(\left(\frac{Final\ \ Area}{Length\ \ of\ \ Calibration\ \ line} \right) \Big/ \left(\frac{Initial\ \ Area}{Length\ \ of\ \ Calibration\ \ Line} \right) \right) \times 100 \quad (3.1)$$

In addition to area degree (AD) there were two other parameters calculated for each test, namely swelling degree (MD) and height degree (HD). Swelling degree was carried out as per the method devised by Ho & Sirkar (1992) and subsequently used by Stafie *et al* (2004) and Geens *et al* (2004). This method is shown as Equation (3.2), where the change in mass was considered between the initial and final states. Similarly height change, Equation (3.3), is based on the initial and final thicknesses of the polymer slab.

$$MD \cdot (\%) = \left(\frac{(M_{wet} - M_{dry})}{M_{dry}} \right) \times 100 \quad \text{Where M denotes mass} \quad (3.2)$$

$$HD \cdot (\%) = \left(\frac{(H_{wet} - H_{dry})}{H_{dry}} \right) \times 100 \quad \text{Where H denotes height} \tag{3.3}$$

Both of these analytical functions have been contrasted against varying amounts of catalyst and varying solution compositions. These two formulas might initially seem to yield the same result, however, MD takes into account all changes to the size and shape, and HD only accounts for changes in height, not an increase in surface area. HD was included for comparison as a membrane made from the given polymer would be restrained and generally the increase in height is a more pertinent factor. MD is a widely reported standard method for reporting swelling of polymer slabs due to its simplicity. Direct measurements of the change in height were able to be achieved when the polymers initial height was around 2 mm, however measuring the same relative increase in the order of microns was quite difficult so swelling by mass has gained in popularity as a method that was accurate and can be related to the change in height and as such will be the main parameter compared to other authors' results.

3.1.2.2. Results – Effects of Solvent Type

Figure 3.3 shows the results from test A (0.3% DBT), and Figure 3.4 shows the results from test B (0.3% DBT). The axes are common to both charts where a value of 100% on the y-axis indicates no change, and a value of 200% indicates a doubling of the parameter. Any values less than 100% indicate a decrease, and as the number of polymer chains did not alter throughout the run this indicates that certain solvents encourage the chains already present into a closer arrangement, reducing the overall size.

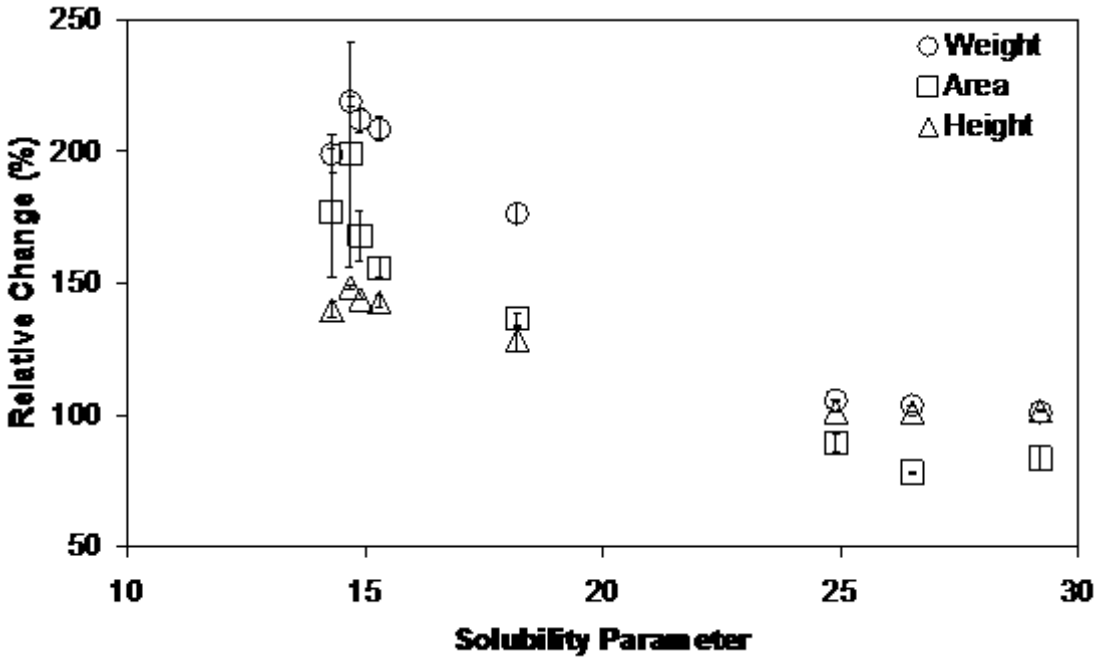

Figure 3.3 – Effect of solvent type – Single day test.

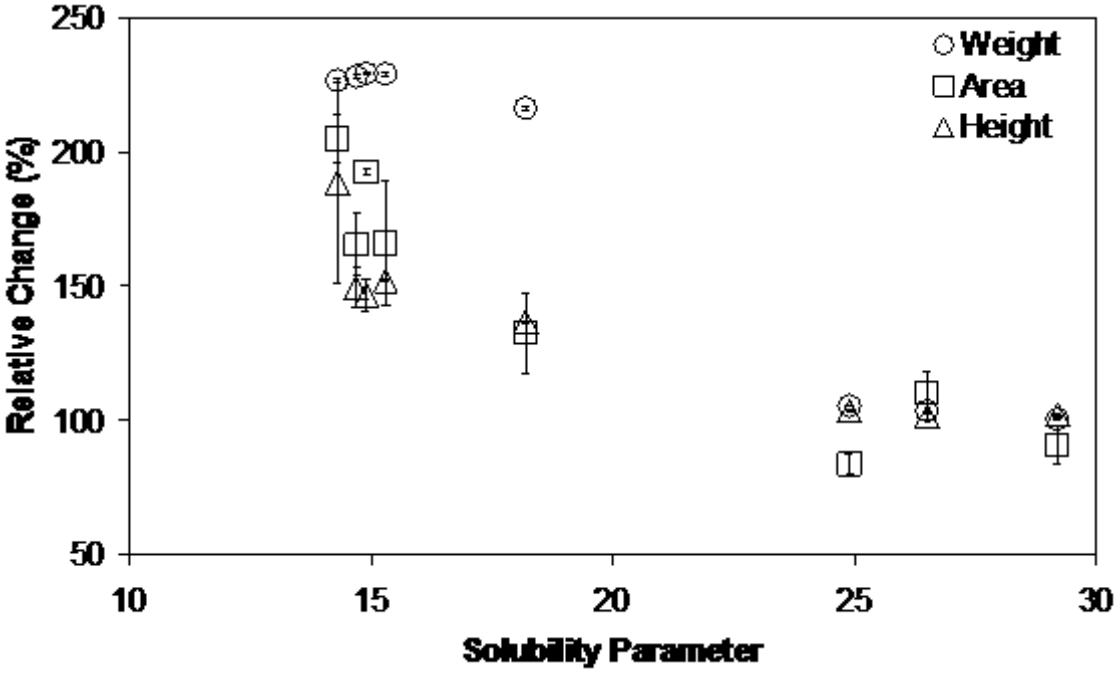

Figure 3.4 – Effect of solvent type – Three day test.

A curved relationship similar to that found by other authors (See Figure 2.10) between solubility parameter and relative parameter change was evident in both charts. The

solubility parameter for PDMS is 15.5 $MPa^{0.5}$ so solvents close to this value are likely to swell the polymer the most, and values far from this will have little to no effect on swelling, i.e. non polar solvents swell the membrane and polar solvents do not, which was comparable with the findings of Gevers *et al* (2006a) who found that separation of polar solvents by PDMS was 'limited'. A similar effect has also been noted by Dewimille *et al* (2005), Doig *et al* (1998), Low (2009) and Yoo *et al* (1999). This trend was able to be seen best in the weight data for test A, where an initial peak in seen around 15.5 $MPa^{0.5}$ which trails off to settle just above 100% at the higher end of the solvent solubility parameters, see Figure 3.3.

On each chart the relative change in height was the least affected parameter, then relative change in area and relative change in weight was the most affected parameter for any single run. As no other research stating the relative change in area could be found it is unclear whether or not this trend is correct, however it does make sense. SRNF polymers swell because they retain some of the chemical species passing through them and as a result the polymer chains move further apart as the inter-polymer spaces are filled. Fundamentally this effect occurs right through the bulk of the material and is therefore independent of direction. Height was the least affected parameter and it is a linear dimension, area was the next affected parameter and it is a squared dimension, and weight was the most affected parameter which is a third order dimension (technically, volume is of order three and is proportional to mass by the bulk density). So it appeared that the magnitude of the relative change was able to be predicted based on the order of parameter concerned.

The purpose of conducting polymer swelling test B was, apart from confirming the results of test A, to check the extent of maximum swelling which was reached after 22~24 hours. This was achieved by comparing any differences between the results from polymer test A and test B. The first thing of note is that both charts are quite similar in appearance with both being displayed on identical axis scales. One point of note was regarding the weight results for the four lowest solubility parameter solvents (i-octane, i-hexane, n-hexane, n-heptane). After 24 hours a relative change in the region of 200~220% is observed with some scatter present, but at 72 hours the range is more settled at about 230% with very close agreement between repeated runs. This change was also paralleled in the xylene results where HD increases from 175% to 215%. Overall the results after 24 hours were only about 10~15% lower than the results for 72 hours of immersion, meaning that 24 hours was an adequate amount of time to allow polymer slabs of this type to expand.

Overall the extent of polymer block swelling was comparable with literature data for PDMS membrane swelling. The blocks swell to around 175% of their size in heptane and only increase by around ten percent in ethanol, which was the same extent reported by Tarleton *et al* (2005) and shown as Figure 2.10. The relative extent of swelling is specific to the polymer type and so this mirroring of trend implies that functional PDMS has been created using the manufacturing process detailed in Section 3.1.1.

3.1.2.3. Results – Effect of Initial Polymer Thickness

Polymer test C was devised to check whether or not thick polymer slabs could be used to accurately predict the behaviour of the active layer of a composite membrane some 100 times thinner than the polymer slabs. To achieve this, a selection of polymer slabs all with different heights were prepared and tested in the same manner as those described in test A. In this case only n-heptane solvent was tested as this was the one proven to swell PDMS the most and therefore elicit the greatest response. The consequence was that the only process variable was the initial height of the polymer therefore if swelling was independent of initial height these should present a series of horizontal lines. The results of this test are shown as Figure 3.5, and it can be seen that apart from the 50 μm run, relative change by weight, area and height are largely independent of initial height; with weight in the region of 200%, area in the region of 170% and height in the region of 140%. These values were in line with the experimental results of test A, but to prove this relationship conclusively, further tests need to be conducted at the lower end of initial heights. The reason that the results for the 50 μm test vary from the expected were probably due to error in the data recording of this run; for this test the polymer slab was very thin and did not have a backing attached so that when it was removed from the solvent it immediately curled up and proved very difficult to get accurate values for either the weight or the area. Reduced force generated by the thinner polymer layer not overcoming the base level of friction imposed by the experimental apparatus is thought to be the reason for the lower HD.

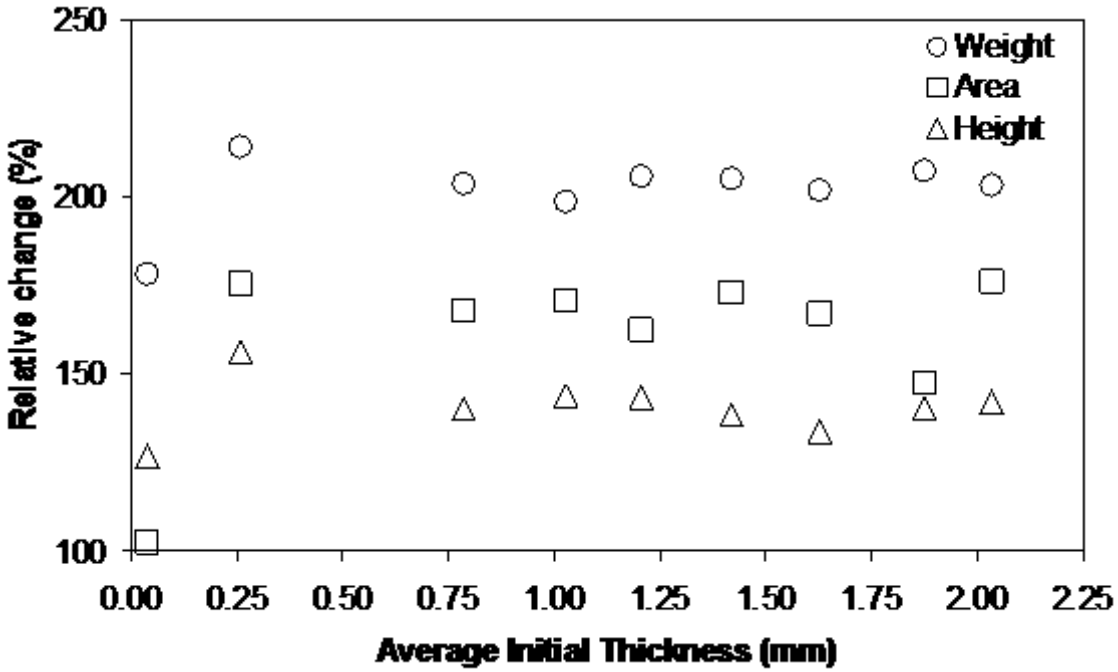

Figure 3.5 – Initial thickness of PDMS – variance results.

3.1.2.4. Results – Effect of Catalyst Concentration

All the testing reported so far was conducted using polymers with as close to 0.3% DBT as was possible, so the purpose of polymer test D was a check into the dependence of catalyst amount on swelling. This test used three different compositions of polymer and three solvents from the range already tested. The results are shown as Figure 3.6. The average expansion in height has been plotted as a representative parameter, as the charts look similar regardless of which degree was plotted. From the data it appears that catalyst amount has little effect on swelling. If a trend was to be assigned to the data it could be argued that a slight negative relationship exists with the higher catalyst amount polymers swelling fractionally less than the lower catalyst amount polymers, however this trend is nowhere near as evident as the effect of solvent type. For xylene the expansion recorded decreased with increasing catalyst amount however such a result for heptane and ethanol did not present, as in both cases the 0.3% DBT grade swelled the least. This outcome was probably noted due to the total range of expansion recorded being small and the tendency of experimental data to fluctuate. Overall the effect of polymer grade on swelling extent seems negligible. The extent of swelling based on solvent type is constant and in line with the results shown in Figures 3.3 and 3.4. Heptane swells the polymer slab by around 1 mm which on an original height of 2 mm was a 50% increase consistent with the previous

extent noted. Xylene and ethanol also swell the polymer to similar extents to those previously noted.

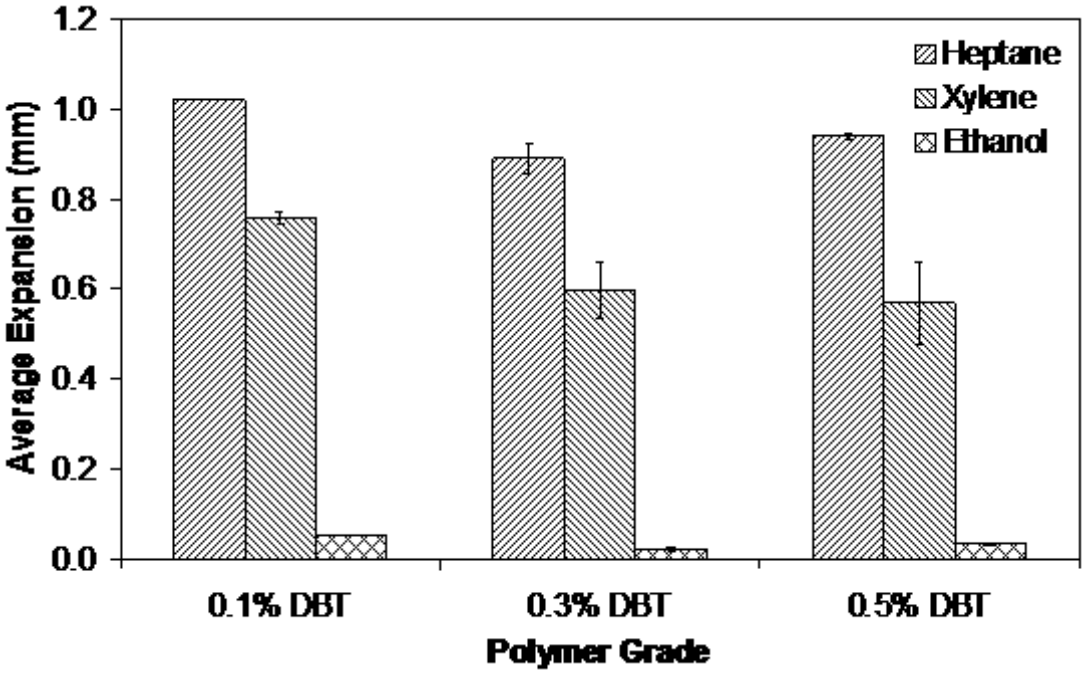

Figure 3.6 – Effect of solvent and membrane grade on average polymer slab expansion.

3.1.3. Determination of Young's modulus

As part of the characterisation of the PDMS produced one of the desired mechanical properties to be measured was Young's modulus. Young's modulus is a measure of the stiffness of a material, and can potentially be used to infer the degree of crosslinking present. The higher the degree of crosslinking, the more bonds the polymer matrix has, therefore the more resistant to deformation the matrix becomes, and so Young's modulus is higher. As a well researched material, the literature value of Young's modulus for PDMS is in the range 0.2 ~ 9.4 MPa (Chaudhury, 2005).

3.1.3.1. Polymer Strength Test Discussion

Square cross section 'beams' of PDMS of 50 mm x 4 mm x 4 mm were produced in compositions of 0.1% DBT, 0.2% DBT, 0.3% DBT, 0.4% DBT and 0.5% DBT. The beams were then sequentially balanced on two knife edges positioned 45 mm apart and loaded with a series of known weights. Photographs of the subsequent bending

were taken and later analysed to determine the extent of deflection, Figure 3.7 shows a schematic of the arrangement.

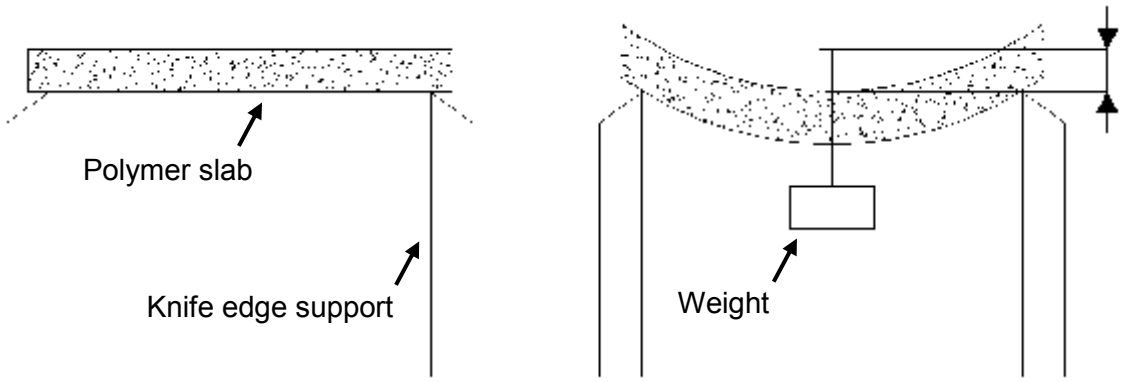

Figure 3.7 – Schematic of experimental set up for loaded beams. Left: The unloaded polymer bar was balanced upon two knife edge supports; Right: When weighted the total deflection was measured.

Several bars were produced for each catalyst amount and the results shown as Figure 3.8 are from one typical set. The loading of the beam was achieved by an under-hanging basket with a single contact line on the beam. The basket weighed 0.85 g and was loaded in three stages; 3 g, 5 g and 10 g, to produce four loading values for each test. The absolute value of Young's modulus should be independent of the loading amount provided the deformation stays within the elastic region, however, when the values were calculated it was common to have a variance of around 30% between the lightest and heaviest loading for the polymer sample. It should be noted that this variance however was due to a single value, as of the four results, three were in very close agreement with one, either the 0.85 g or the 10 g, offset from the group, i.e. with the result removed the remaining points formed an almost perfect (R^2>0.9) straight line.

3.1.3.2. Theory

Equations (3.4) and (3.5) (Roark, 1965) have been used to calculate the Young's modulus for the varying catalyst amounts. These equations are the standard formulas for working out Young's modulus of a bar freely supported at both ends, with a single centre loading. As the bars had a square cross section, b = h = 4 mm (0.004 m), so I_x had the constant value of 2.133×10^{-11} m^4 throughout all the tests.

$$I_x = \frac{bh^3}{12} \tag{3.4}$$

$$E = \frac{1}{48}\left[\frac{Wl^3}{yI_x}\right] \tag{3.5}$$

where b is width of polymer bar, h is height of polymer bar, E is modulus of elasticity, W is applied load (force), l is bar length, y is deflection and I_x is moment of inertia.

3.1.3.3. Results – Young's modulus

At the end of the testing phase 16 different polymer bars had been characterised; four at 0.1% DBT and three for each of the remaining compositions, which resulted in a total of 324 (4*3^4) different combinations each of which was to be checked against the expected trend. As the amount of catalyst directly affects the amount of crosslinking the expected trend was linear, with an increase in catalyst amount producing an increase in Young's modulus. The product moment correlation coefficient (PMCC) of each combination was checked to find the most appropriate approximation of linearity, and so the value of Young's modulus was determined for each polymer. The typical results obtained are shown as Figure 3.8, where it can be observed that by varying the catalyst amount, Young's modulus values ranging from 0.75 to 2 MPa can be achieved. This range falls inside that found by other authors (Chaudhury *et al,* 2005, Tonelli, 2001 and Armani *et al,* 1999), indicating that this was an appropriate value for this material. It should be noted that compared to polymers in general the Young's modulus of PDMS is low, where values in the range of GPa are common.

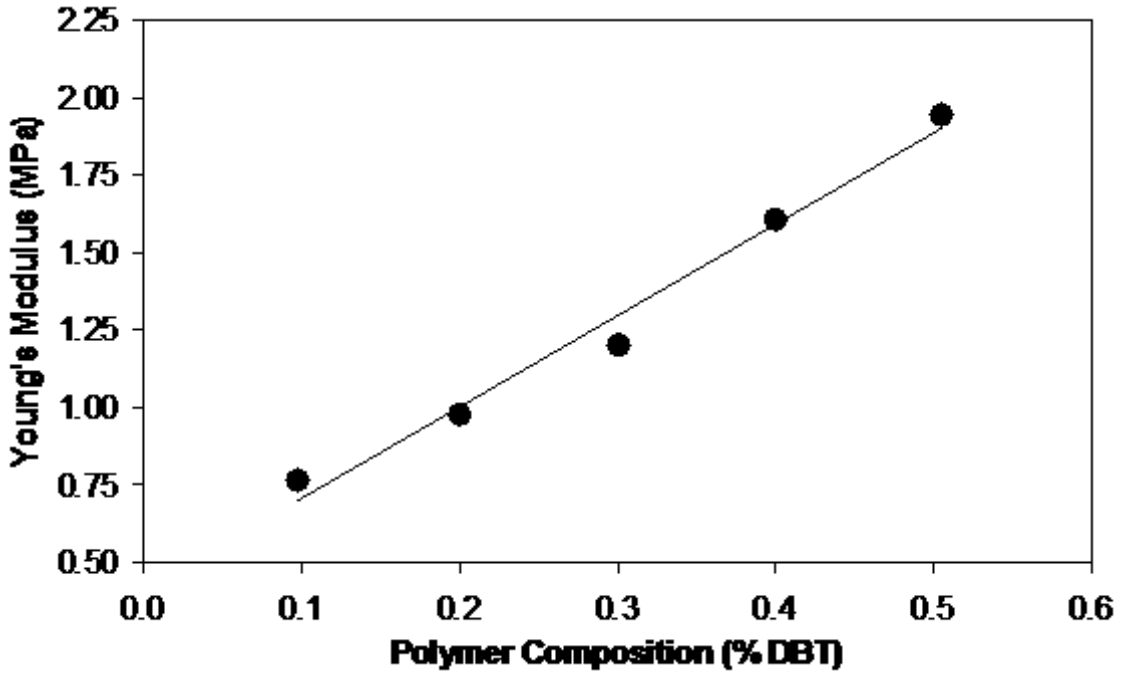

Figure 3.8 – Young's modulus variance for PDMS.

The result that Young's modulus was linearly dependent on catalyst concentration is logical, because, the more catalyst there is, the more crosslinking takes place, which in turn stiffens the polymer and leads to a higher Young's modulus. There was an anomaly, however, when this result was compared to the findings of test four, which found only slight dependence between swelling degree and crosslinking density. It was believed that the degree of swelling and the internal rigidity (and therefore Young's modulus) of a polymer should be linked. A 0.1% DBT polymer is less stiff than a 0.5% DBT polymer and it was postulated that this meant a 0.1% DBT polymer would swell relatively more than a 0.5% DBT polymer under similar conditions. However the extent of swelling recorded was only marginally affected by the levels of DBT present, and considering Young's modulus doubles over the range tested, such a small effect seems disproportionate.

3.1.4. Solvent Evaporation Rate

Once a swollen polymer slab is removed from a solvent, the solvent starts to evaporate out of the matrix, reducing the bulk weight and the slab eventually returns to its original size. To record the change in mass of swollen polymer slabs the slabs had to be removed form the solvent and weighed, which could potentially introduce a source of error due to evaporation. This test was devised to quantify the error introduced by the

weighing procedure. The tests involved placing a swollen polymer slab on a balance and record the changing weight with time. The polymer slabs used in these tests contained 0.3% DBT and were produced using the standard method already described. Before testing they were immersed in pure heptane for a week to ensure maximum swelling had been achieved, and removed immediately prior to recording. Several runs were completed and Figure 3.9 shows a representative experimental set.

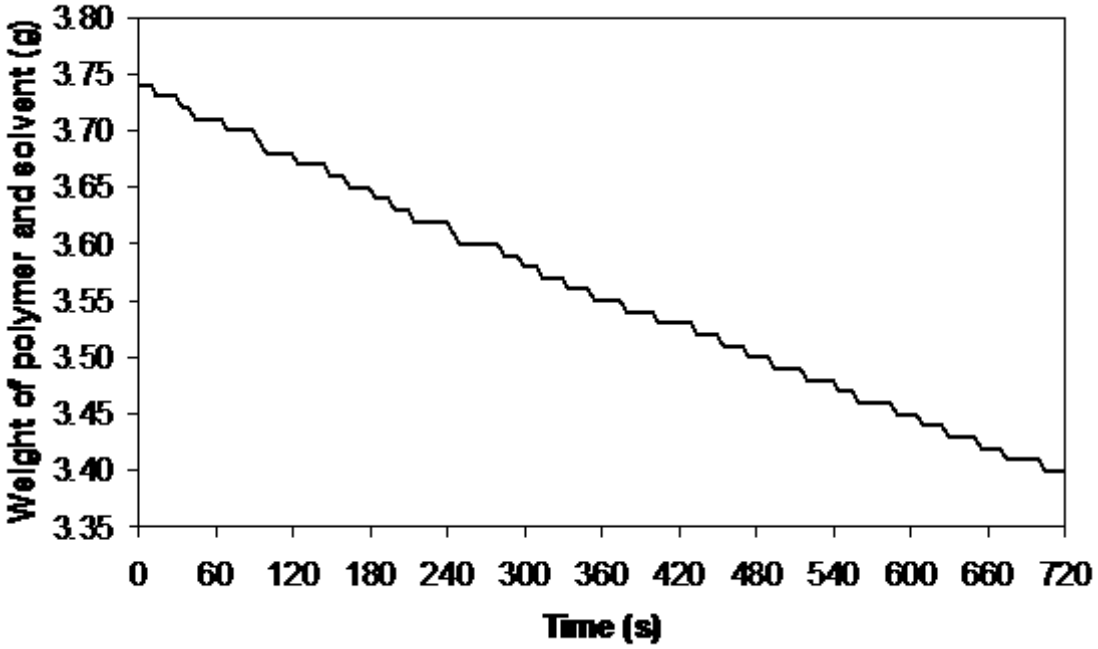

Figure 3.9 – Evaporation rate of heptane from polymer slab.

Over the time period recorded the profile was linear which implies that diffusion of entrained solvent from the polymer matrix to the surface is the limiting factor. From the above results it was not possible to deduce the mechanism for the entire leaching process as towards the end, when the total number of solvent molecules was low the trend may not be linear. Depletion to this extent takes several hours and was deemed unimportant to this stage of research. The test was halted after 12 minutes as at this time almost a ten percent decrease in weight had been recorded, which would introduce a sufficient error on its own to negate the test run if this occurred on an experimental run. This result validates the experimental procedure used for polymer tests A ~ D. The removal of the polymer, surface drying and weighing took around 20 seconds to achieve and as can be seen from the chart a drop of only 0.02 g was recorded in this time interval, meaning that the swelling values were accurate as this loss of mass equated to less than 0.25% of the total mass.

3.2. Manufacture of Composite Nanofiltration Membranes

3.2.1. Review of Potential Production Methods

As stated in the introduction the membranes used throughout this work will be produced in house so that more details of the manufacturing procedure are known. The determination of the exact method did prove to be less than straightforward. From research carried out for the literature survey there were a number of options available for synthesis method namely phase separation, interfacial polymerisation or solution coated (adapted from Baker, 2004). The methods are outlined here to aid the overall structure. The following is an outline of each process and the reasons why it was or was not used for the final synthesis method.

3.2.1.1. Phase Separation – Leob-Souiriajan Method

This classic method was the first one to bridge the gap between natural and synthetic membranes making high rejection thin anisotropic membranes (as outlined in Section 2.1.1). It involves creating a water-miscible solvent / polymer mixture which is cast onto a glass plate or similar. The plate is then immersed into a water bath and as the solvent leaches out the polymer solidifies into a porous substructure with a dense top layer, meaning the support and active layers are both formed of the same material. This method was ultimately not chosen as the membranes created for this work utilise discrete support and active layers made from different materials.

3.2.1.2. Phase Separation – Solvent Evaporation Method

This method also forms membranes from a single substance and was similarly not used. Briefly the polymer is mixed with two differently volatile solvents and cast on a glass plate (or similar). Instead of being immersed in water the mixture is allowed to evaporate in air and as the solvents evaporate at different rates the membrane is formed. This method typically takes longer and produces membranes with larger pores than the Leob-Souiriajan method. Song *et al* (2007) have devised a variation of this process where by a plate, which will readily absorb the solvent, is placed upon the top of the mixture to speed up manufacturing time.

3.2.1.3. Phase Separation – Precipitation by cooling

This method involves using a polymer and solvent which only form a soluble mixture at elevated temperatures. Upon cooling spontaneous formation of the membrane occurs with the solvent trapped in the membrane pores. This solvent remains and has to be flushed out prior to the initial use of the membrane. Successfully applying this method would have required detailed knowledge of the chemistry of PDMS which was not readily available. Additionally this method produces isotropic membranes which would have not been able to be compared with the existing membranes.

3.2.1.4. Interfacial Polymerisation

This process uses a separate microporous support layer and is the main process through which reverse osmosis membranes are made. First a reactive pre-polymer blend is deposited into the structure of a microporous support, and then the entire support is immersed into a water immiscible solvent solution which contains a corresponding reactant (Mulder, 2000). The polymerisation reaction occurs at the interface and forms a very thin but dense crosslinking layer. This method is used to produce R.O. membranes and was not used as PDMS cannot be made dense enough to form an R.O. selective layer. Additionally PDMS is not hydrophilic which is another pre-requisite for R.O. separation.

3.2.1.5. Solution Coated– Water Casting

The polymer is mixed with a volatile water insoluble solvent and then floated upon the surface of a filled water bath between two Teflon rods (or similar rigid material that will not be dissolved by the solvent or bonded with the polymer). As the two rods are moved apart the polymer mixture is evenly spread thin across the surface of the water. A microporous support is then carefully laid upon the polymer, lifted and left to dry. If the contact between polymer and support was good the resultant membrane has an active layer thickness of around 0.5~2.0 μm and is very uniform. This method was not used due to the low success rate encountered. The point at which the support layer is bonded to the polymer layer is critical and until expertise is obtained many failures would likely have been recorded. For time concerns this method was dismissed as easier options exist.

3.2.1.6. Solution Coated– Direct Casting

This method is the one which was ultimately used and is explained fully in Section 3.2.3. The polymer is mixed with a volatile solvent and used to coat a restrained microporous support. As the solvent evaporates the polymer is deposited upon the surface of the support and forms the active layer. This method requires careful selection of the support layer, as the structure must allow the polymer to form as an even layer. Uneven layer thickness will result in varying flux and rejection characteristics across the final membrane.

3.2.2. Support Layer Selection

In addition to the method for synthesis, a choice of support layer was available – between Sepro PAN200 and Pall Versapor. Both of these supports were composed of cellulose fibres with polyacrylonitrile (PAN) used to bridge the gaps between the individual cellulose fibres, however the configuration was different. The PDMS/PAN composite membrane is a standard membrane that has been previously applied by several authors' (Dijkstra *et al*, 2006, Ebert *et al,* 2006, Low 2009, Tarleton *et al*, 2005). Figures 3.10 and 3.11 show SEM images of each of the supports available in the 'as received' condition. As can be seen from the images the Sepro PAN200 support has its PAN as a discrete layer on top of the cellulose where as the Pall Versapor has its PAN dispersed throughout the whole of the cellulose fibres. It is noted that the jagged edge seen on the Sepro image was due to problems with preparing a sample for SEM analysis and is not thought to be part of the original structure.

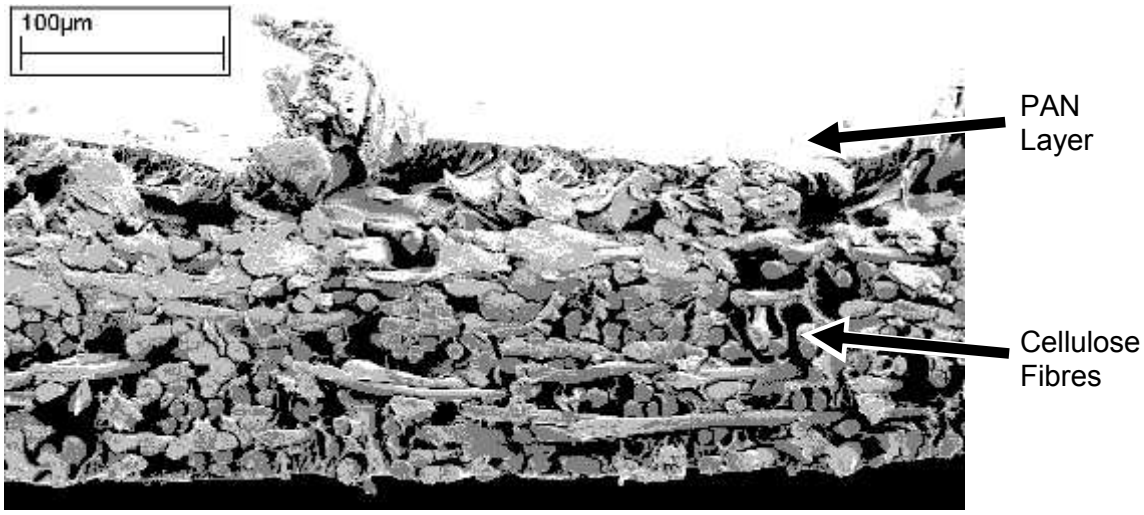

Figure 3.10 – SEM image of Sepro PAN200 support layer alone.

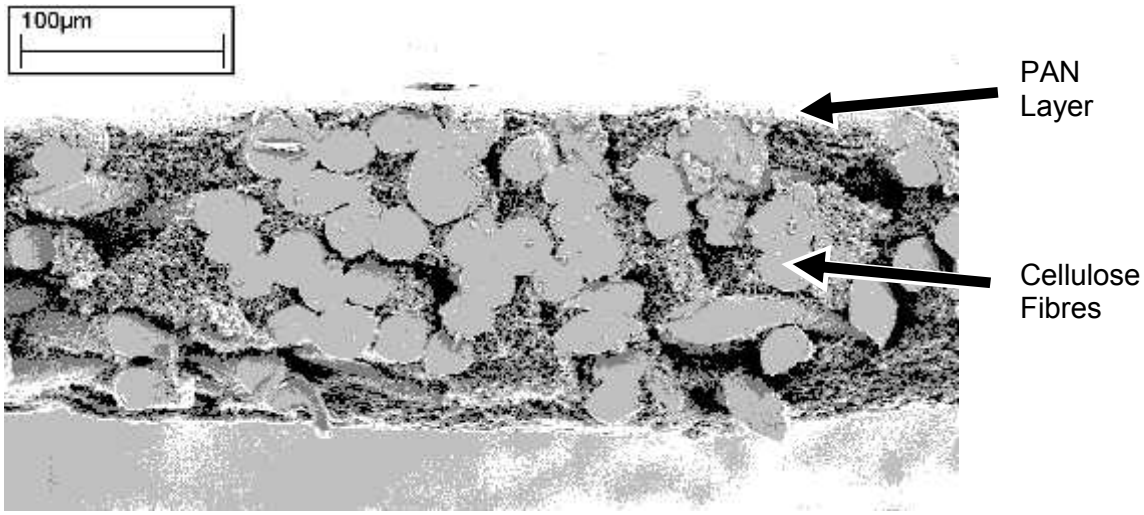

Figure 3.11 – SEM image of Pall Versapor support layer alone.

During testing to find the correct method both supports were used, however it was found that the Sepro backed membranes failed inside the test cell 100% of the time, the PDMS top layer simply swelled under the influence of the test solvent and the bonding between the active and support layers was insufficient to counteract this effect. The active layer separated itself from the support leading to little or no separation occurring. By comparison the Pall based membranes failed about 5% of the time during the refinement of the synthesis method, and progressive refinement led to no failures at all. This difference was thought to be due to the structures that can be seen in the SEM images. The PAN layer in the Sepro membrane is simply too smooth and does not provide enough bonding sites for the PDMS to adhere to, whereas the Pall backing allowed PDMS to in effect 'permeate' through the structure obtaining a sufficient hold to withstand the ultimate swelling. 'Bonding' in this sense refers to the relative surface roughness and as the Pall membrane had a rougher surface the PDMS could 'bond' better as there was increased surface contact. This theory is validated by two further SEM images, Figure 3.12 and Figure 3.13, which show the corresponding layers with the addition of PDMS. The Sepro membrane has the PDMS on top which has clearly started to lift away due to the preparation method to take the photograph. For the Pall backing it is hard to pick out the PAN clearly as the PDMS has covered the entire depth of the support.

In an effort to salvage the Sepro support a section of it was taken and treated to remove some of the PAN layer or at least increase its surface roughness. To do this some parts were lifted using adhesive and other sections were thinned down by acid

etching, neither of these approaches worked as the thinned down layer provided uneven separation and still ultimately failed, whereas the acid etched sections dissolved completely including the underlining cellulose strands. These results confirmed that the Sepro backing was unsuitable and thus all subsequent work utilised the Pall Versapor as the support layer.

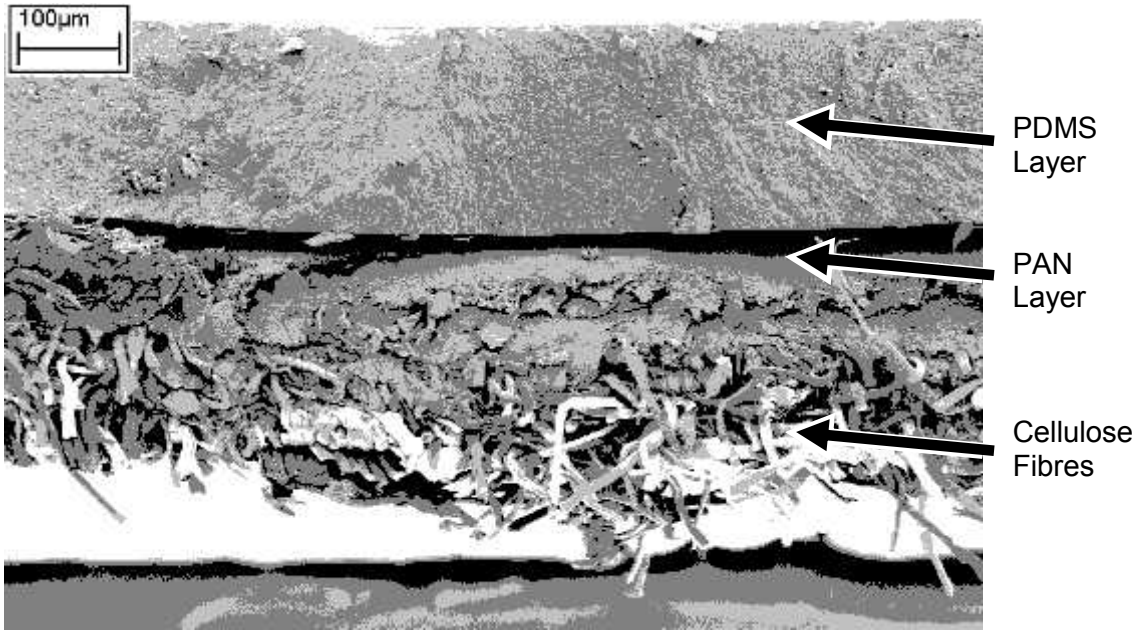

Figure 3.12 – SEM image of Sepro PAN200 support layer with a PDMS top layer.

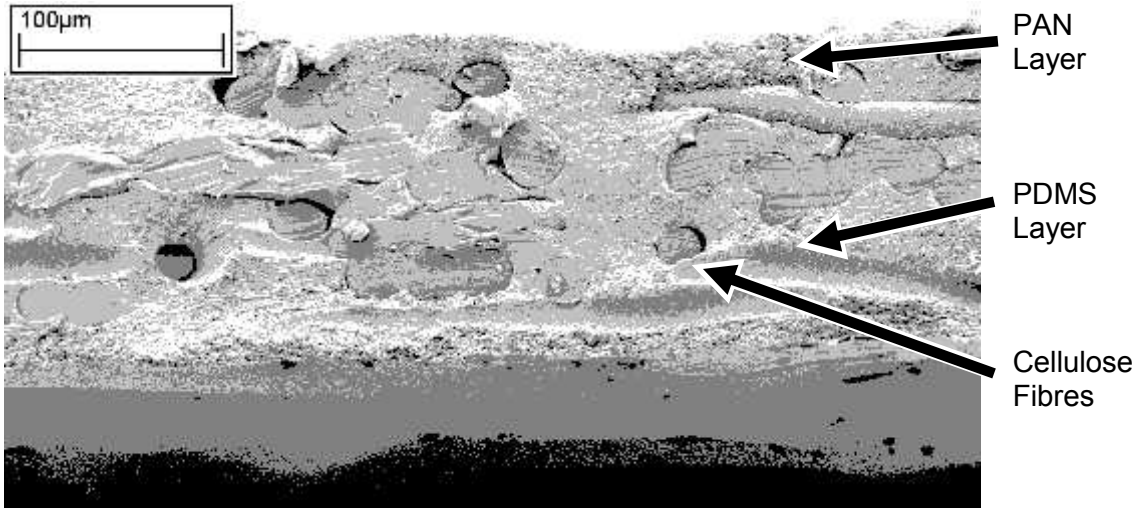

Figure 3.13 – SEM image of Pall Versapor support layer with the addition of PDMS.

3.2.3. Chosen Method and Reasoning

The final method chosen for membrane synthesis was the solution coated composite and the procedure was as follows. The surface of a metal casting tray was first cleaned

with pure ethanol to ensure the casting area was clear of dust or other particles. A 150 mm diameter circular Pall Versapor support layer was placed centrally in the tray and the edges restrained. 1 g of pre polymer was weighed into a separate metal container and the appropriate amount of catalyst was added. The two components were mixed for five minutes before 20 ml of n-hexane was added and mixing resumed. When the polymer had completely dissolved the mixture was poured over the support layer and placed in a fume cupboard to flash off the solvent. When complete the tray was covered and moved out of the path of direct sunlight for 24 hours, at normal room temperature. Removal from direct sunlight was an effort to prevent uneven heating, not because of any radiation based effects. Finally the restraints were removed from the support layer to free the membrane.

This method worked as the solvent ensured an even coating layer and when evaporated a uniform polymer thickness remained. One thing to note was that the support layer had to be restrained otherwise it floated upon the mixture resulting in the polymer coating both sides and ultimately making the composite non-uniform. Membranes created by this method take a support layer in the region of 170~180 μm and turn it into a composite membrane of dimensions 210~220 μm.

3.3. Materials

3.3.1. Solvents

Three solvents were used extensively in this work; heptane, xylene and octane. These solvents are typical of those found in industrial processes including fuel processing and pharmaceutical. The solvents were chosen for the range of solubility parameters represented. Solvents with different solubility parameters swell the active layer of the composite membranes to different degrees affecting both the solvent flux and solute rejection. All solvents used were obtained from Sigma-Aldrich and were CHROMASOLV grade. The solvents were used in their ‘as received’ state with no additional processing completed. Key information regarding the physical properties of the solvents is given in Table 3.2, where the solubility parameter of PDMS was taken to be 15.5 $MPa^{0.5}$.

Solvent	Surface Tension (mN/m)	Viscosity (cP)	Solubility Parameter, δ ($MPa^{0.5}$)	$\Delta\delta_{(Solvent\text{-}PDMS)}$
Xylene	30.10	0.65	18.2	2.7
Octane	21.62	0.46	14.3	1.2
Heptane	20.14	0.39	15.3	0.2

Table 3.2 – Solvent physical properties.

3.3.2. Solutes

Three solutes have been used extensively in this work; 9,10-diphenylanthracene (910), iron (III) naphthenate (I3N) and iron (III) acetylacetonate (I3A). These solutes were selected based on solute size, solubility in the solvents used and distinctive UV/VIS profiles. I3A and I3N are organometallics and 910 is a poly-nuclear aromatic. The solutes were used at levels around 30 ppm but due to the small quantities involved levels from 27~33 ppm were possible. Slight deviations in feed concentration have already been shown to have no effect on separation properties (Robinson, 2004). Table 3.3 shows relevant physical information on the solutes used in this study. The characterisation of the solutes was obtained using Chemdraw Pro V12. The cylinder dimensions were calculated by the program which fitted the smallest volume cylinder around the solute molecule in 3D space. The aspect ratio was calculated as the ratio of diameter to length.

Solute	Molecular Weight (g/mol)	Solute Cylinder Length (nm)	Solute Cylinder Diameter (nm)	Aspect Ratio
Iron (III) Acetylacetonate	353	0.9883	0.9822	0.994
Iron (III) Naphthenate	373	1.6054	1.1614	0.723
9,10-Diphenylanthracene	330	1.4523	0.9428	0.649

Table 3.3 – Solute physical properties.

3.4. Membrane Characterisation

3.4.1. Feasibility Tests

The next stage of membrane manufacture was feasibility trials to check the filtration characteristics of the produced membranes and to eliminate any defective membranes from the later testing stages. At this point neither the crossflow rig nor its operation has been discussed but it is important for the structure of this thesis that the feasibility tests occur here, whilst all other crossflow tests are covered in Chapter four. A general description of the apparatus used is given in Section 4.1.2, the test method is detailed in Section 4.1.2.2 and the sample analysis is given in Section 4.1.2.3. For the initial feasibility tests the solution chosen was 9,10-diphenylanthracene in n-heptane. This combination was chosen because 9,10-diphenylanthracene has a strong trace when analysed in a UV/VIS spectrophotometer and so its presence will be simple to detect. n-heptane was chosen as the solvent because it had been shown to elicit the greatest swelling extent (Section 3.1.2.2), therefore putting the membranes under the greatest stress. Each membrane produced by the method outlined above had been tested in the crossflow rig for flux and rejection using the method outlined in Section 4.1.2.2. As a baseline two samples of GKSS membranes were obtained and tested in the same fashion to the membranes produced – selected results can be seen as Figure 3.14 for flux data and a comparable set of rejection data can be seen as Figure 3.15. The results plotted in Figure 3.14 and Figure 3.15 were all from membranes close to 0.3%

DBT. The 0.1% DBT and 0.5% DBT membranes have not been plotted in an attempt to make the charts more readable, but do show similar trends.

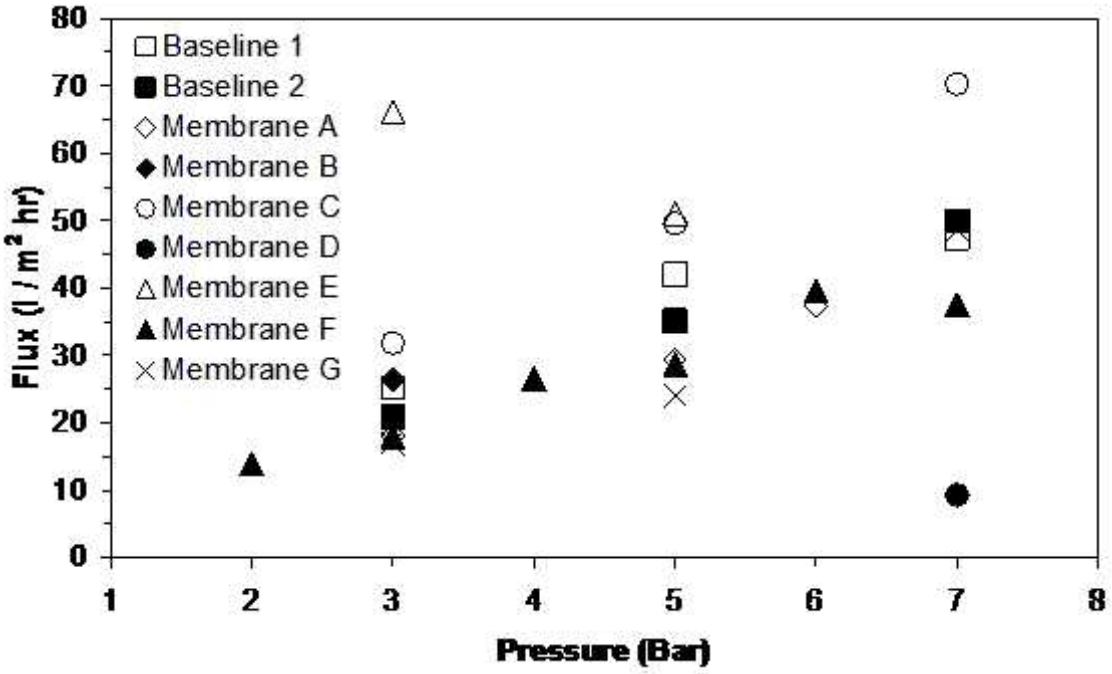

Figure 3.14 – Selective feasibility data – Flux version.

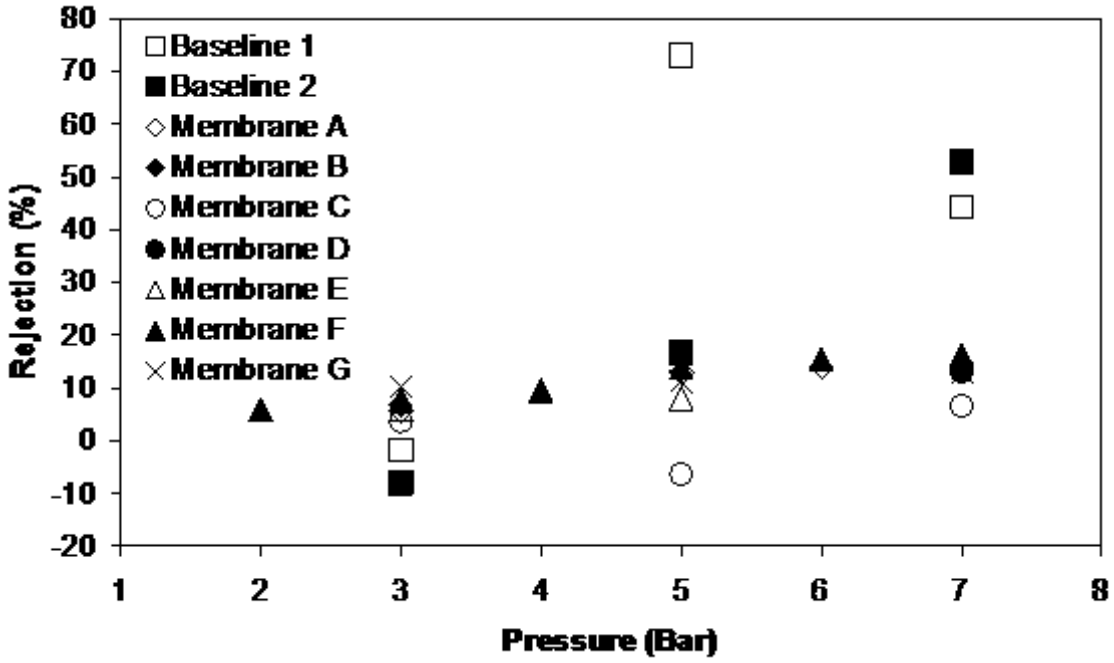

Figure 3.15 – Selective feasibility data – Rejection version.

As can be seen from Figure 3.14 most of the membranes produce flux values of the expected trend with a few notable outliers. Generally the 0.3% DBT membranes have flux values within the range of 15 ~ 50 l / m^2 hr when applied with pressures in the range 2 ~ 8 bar. This positive trend shows that the majority of the membranes produced were acting correctly, i.e. as predicted, however some of the manufactured membranes do not in terms of either flux, rejection or both. Notable examples include the 7 bar flux result for membrane D and the 3 bar flux result for membrane E. In each of these cases the actual result falls outside the expected by a considerable margin, and were examples of 'failed' membranes, something had occurred during the curing process to make these membranes operate differently (see also Section 3.5.3). The GKSS membranes tested are identified as baseline 1 & baseline 2, and produce some of the most varying results of all the membranes tested, although the exact reason for this is unknown.

The rejection data (Figure 3.15) was slightly more complicated to analyse. Again, it shows the same positive trend as the flux data, however, the scatter present was higher for specific runs. The rejection at the higher pressures with GKSS membranes was higher than any of the membranes produced, however as this chart only shows the 0.3% DBT membranes this was not a problem, it simply implies that a higher amount of catalyst was required to get results comparable to the GKSS membranes. Overall this chart showed promise and allowed for the pass / fail assessment of produced membranes to be made. The difference in results between a successful and a failed membrane was so wide that no specific metric beyond common sense was required. The important thing to note in these charts is the relative trends rather than the absolute values; this is because the GKSS membranes are irradiation crosslinked where as the membranes produced here are catalyst derived.

3.4.2. Selection of Membranes for Further Study

To maintain consistency each membrane was made using the same type of support layer (i.e. Pall Versapor) and all support layers came from the same batch. Despite this some membranes produced did not operate in the expected manner, and such membranes were discarded. The point of this initial testing on the produced membranes was two fold. First, it allowed a check to be carried out on the membranes as they were made, so that checks could be carried out to see if the production method was correct. Second it ensured that any defective membranes did not get used in the main testing section, i.e. membranes MTN6 and MTN7 failed based on flux. This

method ensured that all the membranes used for crossflow filtration experiments (Chapter four) operate both as expected and in a similar fashion to each other.

The reproducibility of results obtained from the crossflow experiments was determined by conducting a series of repeat experiments using the same conditions. All the tests used 9,10-diphenylanthracene and heptane at pressures of 3, 5 and 7 bar. Each combination was tested five times with the results shown as Figures 3.16 for flux and Figure 3.17 for rejection, where the error bars represent one standard deviation either side of the mean result. Overall the charts demonstrate a high level of repeatability with flux being accurate to plus or minus 5 l/m^2hr and rejection accurate to plus or minus 4 percent. Time constraints dictated that not every test could be repeated five times so the repeatability demonstrated in Figures 3.16 and 3.17 was important for validating the conclusions drawn from only one test run.

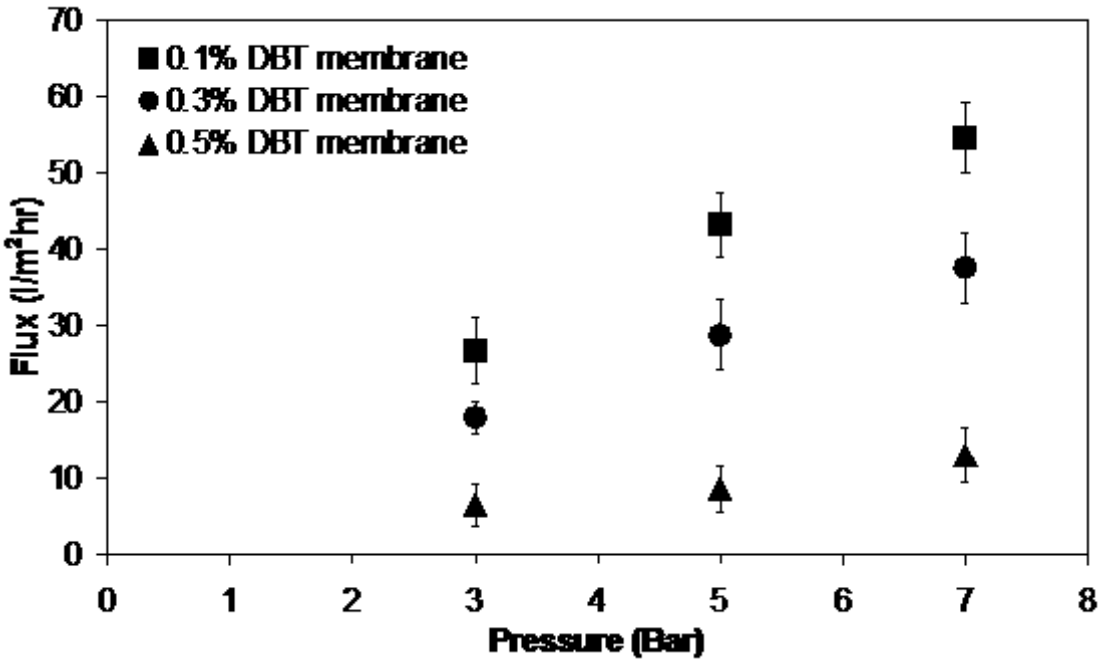

Figure 3.16 – Membrane repeatability data – Flux version.

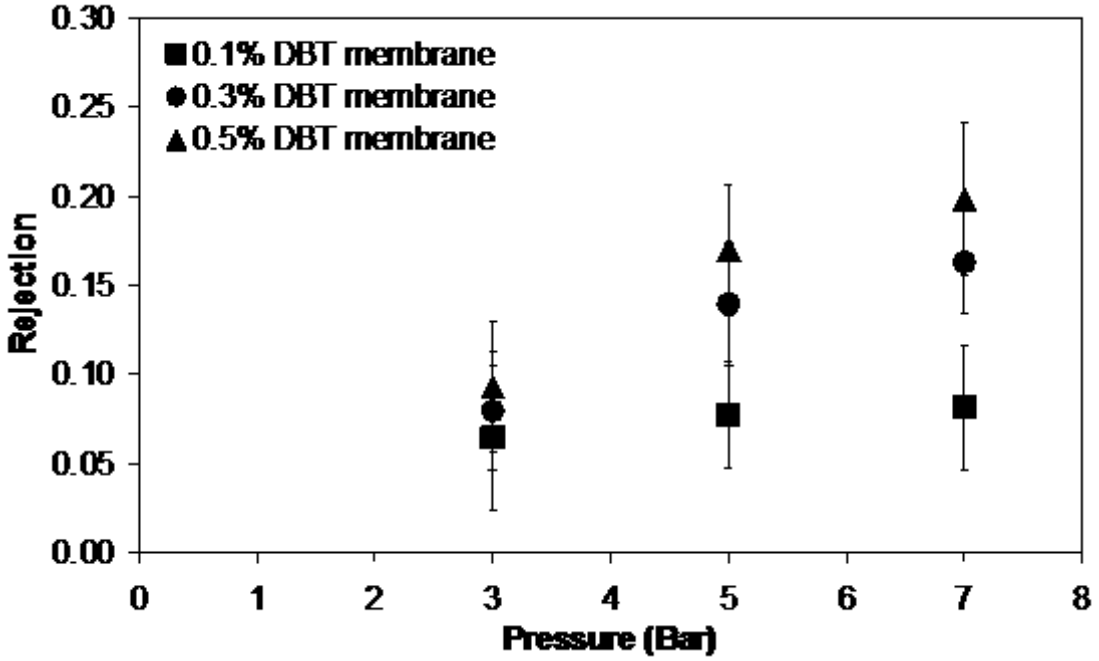

Figure 3.17 – Membrane repeatability data – Rejection version.

3.4.3. SEM Analysis

An SEM image was taken of each membrane grade produced (0.1% DBT, 0.3%DBT and 0.5% DBT) to see if any discrepancies could be noted between the different membranes. The membrane samples used in the following SEM images have not been altered from their initial produced state; the samples were prepared using a razor blade and coated with a layer of gold particles to help with generating the required charge needed to produce this type of image. Figures 3.18, 3.19 and 3.20 show the cross sectional view of the 0.1% DBT membrane, the 0.3% DBT membrane and the 0.5% DBT membrane respectively.

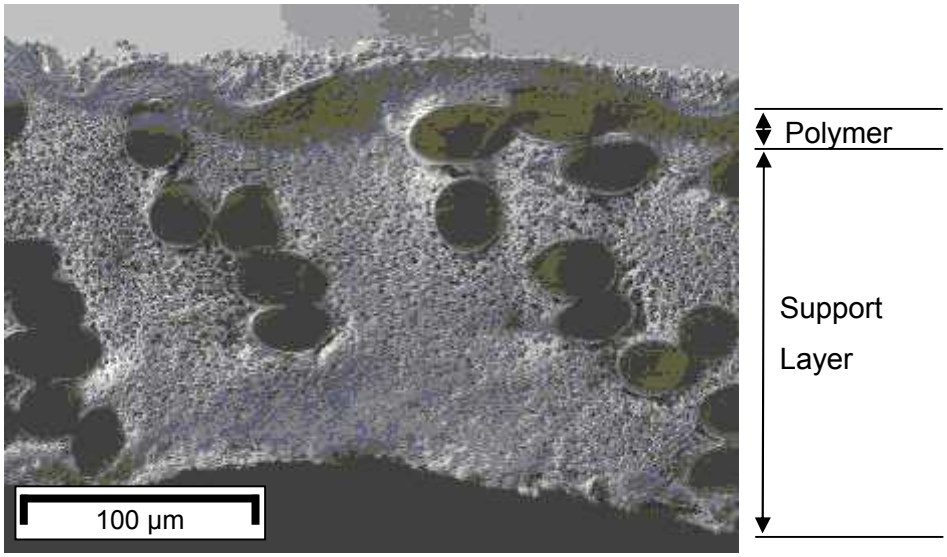

Figure 3.18 – SEM image of a representative 0.1% DBT membrane.

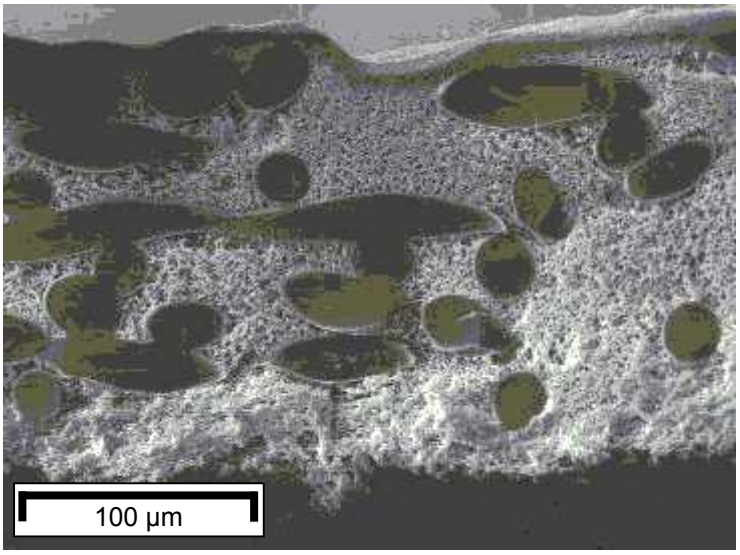

Figure 3.19 – SEM image of a representative 0.3% DBT membrane.

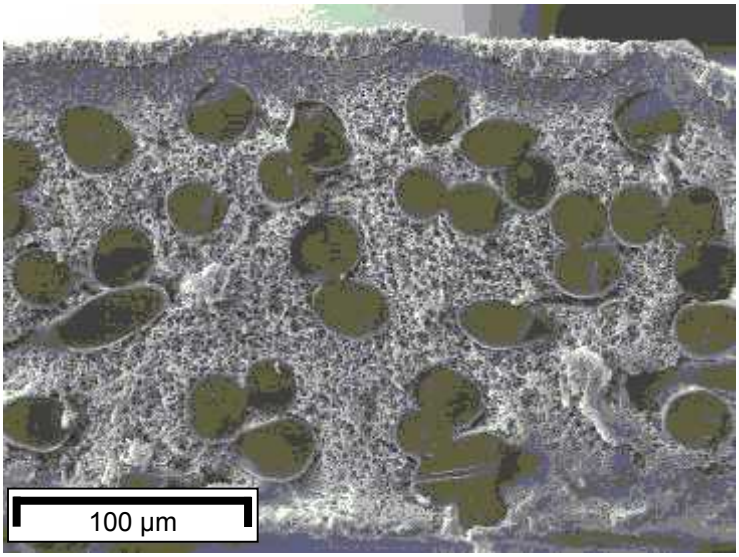

Figure 3.20 – SEM image of a representative 0.5% DBT membrane.

There are several key points to note in these images, both as a group and individually. The total depth of the membranes seems to be quite variable. This was especially apparent in Figure 3.19 where a dip can be seen in the centre of the image, which corresponds to the arrangement of the cellulose fibres beneath. Variation within membrane thickness was to be expected when using a non woven support but as the depth of the selective layer is largely constant throughout all the images the effect of the overall membrane thickness changing is thought to be negligible. The increase in area generated by this variance it thought to be the reason for the increased success noted in using the Pall support layer over the Sepro support layer.

From these images the random arrangement of the support layer was able to be assessed, and the variation in the cellulose fibres can be noted; the general arrangement seems to indicate a crosshatch layout with parallel lines of fibres passing perpendicular to each other, this can be seen very well in Figure 3.19 where several lateral fibres have been sliced through. There was one more point of note taking these images as a group and that was regarding the configuration of the PDMS. The initial feasibility image (Figure 3.13) taken during the membrane refinement stage seemed to show an essentially uniform section of PDMS filling in all the space around the support structure, however these images show a more fibrous arrangement with transport regions between the polymer sections. Obviously this change must have occurred during the refinement process. The PDMS now exists as both a solid band (present at the top edge of each of the membranes) as well as throughout the entirety of the membrane. It was believed that most of the separation occurs at the top “active” layer rather than throughout the depth of the membrane. This theory was supported by

taking additional SEM images at a higher magnification to check the internal membrane structure. Additional SEM images were of each membrane grade however they were largely similar so only the 0.3% DBT membrane is shown as Figure 3.21 as it is typical of the set. Figure 3.21 shows an enlargement of the main support layer structure at the centre of the membrane. Overall these images are positive, they show that the polymer had completely covered the support layer meaning that transport through the PDMS layer must be responsible for the separation.

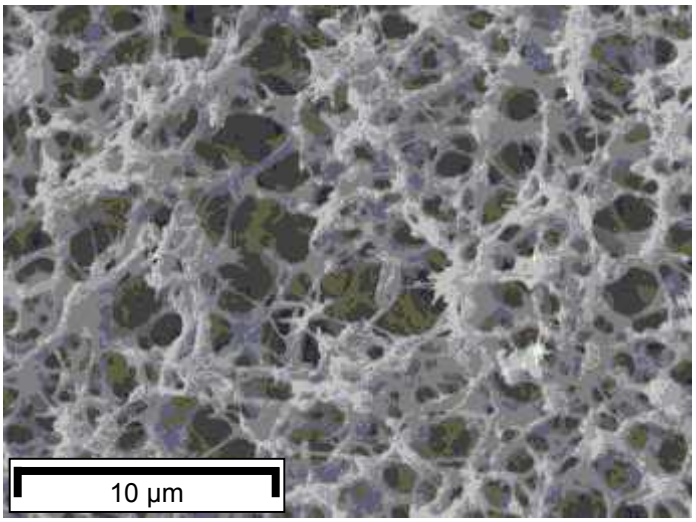

Figure 3.21 – Enlargement of SEM image (0.3% DBT membrane).

3.5. Membrane Swelling

3.5.1. Introduction

Determining the extent of swelling in the membranes produced was an important step in fully classifying their behaviour, as when swelled the filtration properties would be different to the filtration properties in their non-swelled state. The work presented here on membrane swelling consisted of three distinct experiments – an initial feasibility test followed by two more detailed investigations; one on swelling with variable pressure and the other on swelling with fixed pressure. The feasibility test involved measuring the thickness of membrane samples before and after immersion in various solvents to determine the extent of swelling. The swelling with variable pressure test involved initially swelling a sample in solvent and measuring its thickness under sequentially heavier loads and then sequentially lighter loads. This test was used to determine if hysteresis was present in the samples as well as deducing any solvent/membrane

trends, where hysteresis was defined as the difference between compression results for the same pressure (increasing and decreasing). The swelling with fixed pressure test involved measuring the thickness of a compressed sample before and after immersion in solvent to determine the limits of swelling under pressure.

3.5.2. Description of Apparatus

As the membranes produced are significantly thinner than the polymer slabs previously discussed, a different experimental rig was required for swelling measurements. The produced membranes have an initial thickness of around 190 μm whereas the polymer slabs were around 2 mm, so the membrane swelling apparatus had to be capable of working at the micron scale. The equipment used for measurement of membrane swelling consisted of an inductive probe which was actuated by a loading bar. This set up had been previously used by other authors Low (2009) and Robinson (2004), a schematic can be seen in Figure 3.22.

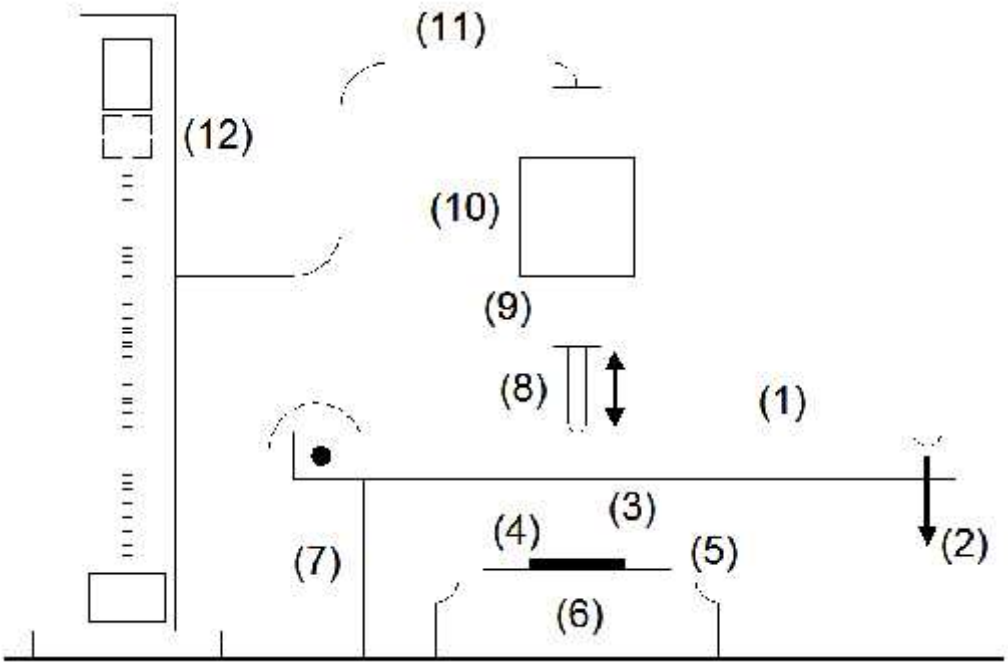

Figure 3.22 – Schematic diagram of membrane swelling rig. (1) cantilever bar; (2) weight; (3) spacer; (4) membrane sample; (5) solvent retaining dish; (6) comparator stand; (7) cantilever bar support frame; (8) measurement tip; (9) inductive probe; (10) probe support (partially omitted for clarity); (11) data cable; (12) electronic gauge column.

The main function of the rig was to accurately measure expansion or contraction in a polymer or membrane sample which can be placed under varying loads through the loading arm and under immersion in various solvents by the retainer. The operation principle is described here with some specifics highlighted in Sections 3.5.4 and 3.5.5. The membrane sample to be tested was placed in the centre of the dish with the spacer located on top. The loading arm was lowered and slotted upon the spacer. The loading arm had 15 holes in the bottom side into which the spacer directly fits. These holes have been termed 'Positions' such that the hole closest to the pivot is termed 'Position 1' and the one furthest from the pivot is termed 'Position 15'. Throughout this work 'Position 2' has been used for all the experimental tests. The probe was then introduced directly above the centre of the spacer. To ensure this was done precisely the top of the loading arm was notched corresponding to the holes underneath. The probe had a resolution of 0.1 µm, a travel length of 5000 µm and was connected to a digital gauge column, for ease of recording. By suspending different loads from the free end of the arm different amounts of pressure were able to be applied to the sample to restrict swelling or induce compression. The pressure applied has been calculated by taking a moment around the pivot point W as shown in Figure 3.23 and equation (3.6).

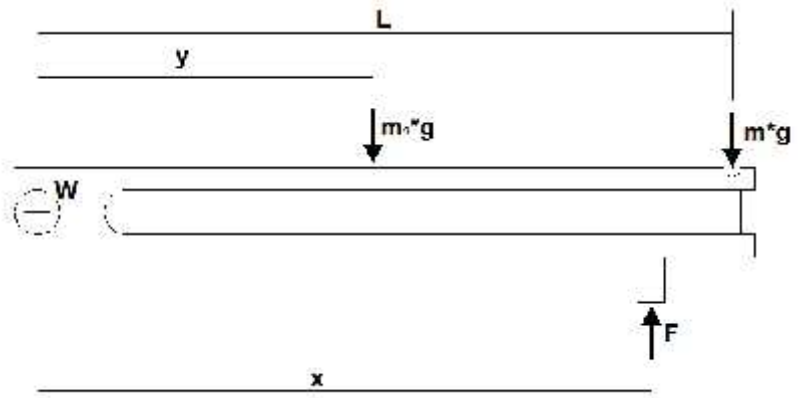

Figure 3.23 – Schematic of bar loading forces.

The moment around W must be zero as the bar was stationary so,

$$P = \frac{F}{A} = \frac{\left(\frac{mLg + m_1 yg}{x}\right)}{A} \tag{3.6}$$

where A is the area of the spacer in contact with the membrane (7.854×10^{-5} m^2) and g is acceleration due to gravity (9.81 m/s^2). This calculation also takes into account the

mass of the loading arm itself. The arm used in this work was an aluminium I-bar (the cross-section resembles the shape of a capital letter I when viewed from the end) which differs from the arm used in Low (2009) which was steel. Even using the lighter bar an amount of pressure will be generated by the bar itself which has been calculated as 1.10 bar. This value was a constant throughout all the tests completed as the spacer position was kept constant throughout all the tests. For any desired pressure the smallest load that was able to be applied was found when the spacer was as close as possible to the pivot (forming a third class lever) and multiplying the effect of the load. In practice the design of the support frame made it impossible to use the closest hole to the pivot so the second locator was used exclusively in this work to keep the required load to a minimum. The weights added were all identical and calculated using the Equation (3.6) to result in a cumulative pressure of 2.94, 5.89, 8.83, 11.77 and 14.71 bar respectively applied to the membrane sample.

This experimental set up was used to run two similar but crucially different experiments; swelling with variable and fixed pressure. In the variable pressure method, loads are sequentially added to and removed to measure hysteresis in the membrane sample. In the fixed pressure method a dry membrane sample was compressed and the expansion due to immersion in solvent was measured.

3.5.3. Membrane Swelling Feasibility Study

The thickness of samples of each of the three membranes was measured and then completely immersed into one of three different solvents (heptane, xylene or octane). The membranes were allowed to reach equilibrium swelling before being removed and their thickness measured again. In this way the expansion of each membrane under no applied pressure in each solvent was recorded (the cantilever bar was not in use in this test). Each sample once measured was left for at least a day before being used again to ensure the sample had returned to its original state. Each solvent / membrane combination was tested at least six times. The aim of this test was to determine if the membranes swelled a measurable amount and to give an indication of which solvents or grades elicited the greatest effect. The average results are shown as Figure 3.24 with the error bars extending one standard deviation above and below the mean. In addition to testing each membrane grade a sample of the support layer was tested in as received condition using the same procedure, however the support did not swell in any of the solvents used and so the data has not been included in Figure 3.24.

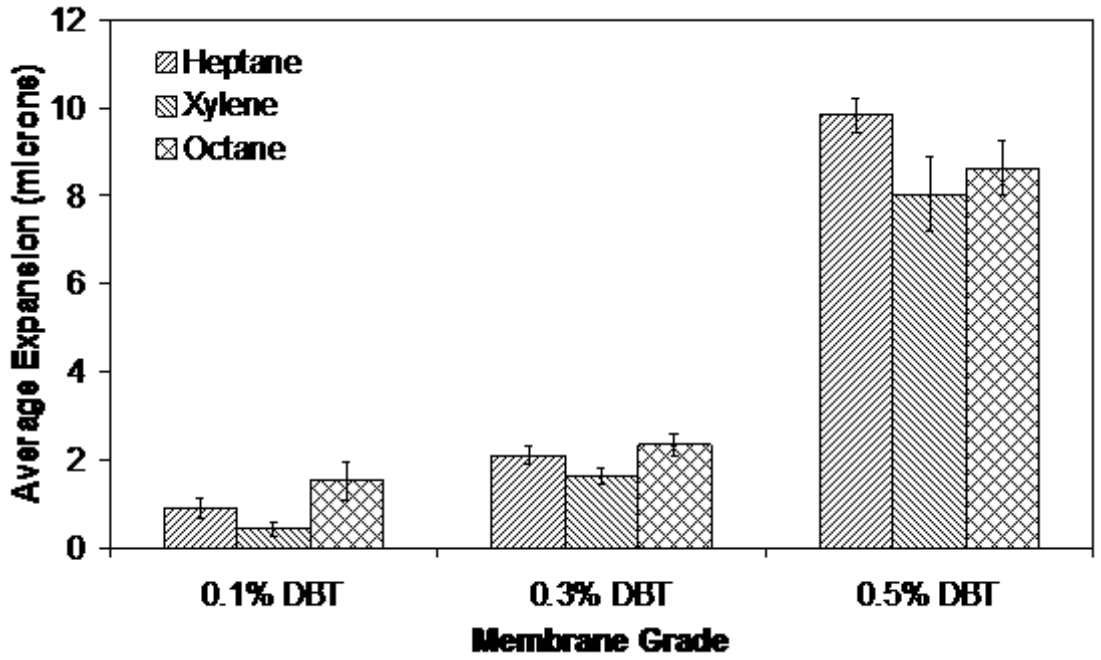

Figure 3.24 – Effect of solvent and membrane grade on average membrane expansion.

The membranes expand to a measurable degree, the extent of expansion by different solvents mirrors the work on polymer swelling with the heptane and octane solvents (solubility parameters of 15.3 $MPa^{0.5}$ and 14.3 $MPa^{0.5}$ respectively) having a greater effect than xylene (solubility parameter of 18.2 $MPa^{0.5}$ (Section 3.1)). This result was in line with the work of Gevers *et al* (2006b) who found non-polar solvents swell PDMS membranes to a greater extent than polar solvents. Of the two solvents, heptane and octane, it was assumed that heptane would have the greater effect as it was closer to PDMS solubility of 15.5 $MPa^{0.5}$ however this was only the case for the 0.5% DBT membrane. The reason for this was thought to be that the expansion of the other two grades was significantly less pronounced than the expansion of the 0.5% DBT membrane and therefore due to the closeness of the solvents the true order can only been clearly observed at the larger expansions.

The effect of expansion with regards to membrane grade was also of note. Originally it was believed that the different membranes were formed with different degrees of crosslinking by adding different amounts of homogeneous catalyst into the pre-polymer liquid during manufacture. It was assumed that the more catalyst that was added the greater the extent of crosslinking that would be formed in the final membrane. This is due to the fact that as the amount of catalyst added is increased the total number of reaction sites this provides is also increased. This result was supported by the finding of Section 3.1.3 where it has been shown that Young's modulus increases linearly with

catalyst amount and has been supported by Section 3.4.3 as the SEM photos taken of the membranes show a higher amount of branching in the larger catalyst amount membranes. However the results of these expansion tests seem to contradict this assumption as the 0.5% DBT membrane swells around five times as much as the others and the 0.1% DBT membrane expands the least. It seems logical that crosslinking should retard expansion as the more bonds between a single polymer chain and its neighbours, the less free it is to move and slide past its neighbours during expansion.

It is also important to consider the actual mechanism by which the expansion occurs. The structure of PDMS had previously been described as a liquid-like matrix by Merkel *et al* (1999) which the results of this work seem to agree with. PDMS matrices expand in the presence of certain solvents, such as heptane. The heptane molecules diffuse through the internal spaces or chambers formed between polymer chains and exert a repulsion force enlarging the chamber at the same time, this allowed more heptane molecules to enter and enlarge the chamber to an equilibrium limit, whilst at the same time the original heptane molecules have diffused further into the matrix and the whole process repeats. Ultimately the expansion stops when the expansive force on the polymer chains from the heptane molecules is equal to the contractive force of attraction between the atoms in the polymer chains. In an ordered matrix each polymer chain could freely expand to its limit, not constrained by being coiled around other chains. A polymer matrix with few crosslinks would be too tangled to expand freely. In this way a more densely crosslinked polymer could expand more than a lightly crosslinked one.

The fact that the expansion trend was opposite to the expected was interesting, one possible explanation was to do with order. Each chemical bond has a certain flexibility in relation to the atoms around it and any pair of non-bonded atoms exerts a certain repulsion upon the other proportional to the distance between them. The specific size of these parameters was not important in this discussion. It was known that the silicon-oxygen backbone which forms the core of PDMS is relatively flexible compared to carbon based molecules (Section 2.2.4.2) and in simulations an identically sized chain can twist itself into a seemly infinite number of configurations, any (or all) of which could be found in the polymer during membrane manufacture. If there was no crosslinking all the chains would be tangled around each other in a disarrayed fashion, however as soon as the first crosslink was formed two chains were joined and the repulsion from the linking atoms makes the other non active chains move away from

the join. In this case two C-H bonds were replaced by a single C-C bond, which is fewer total atoms but as a carbon atom is eight times bigger than hydrogen atom a bond of this type will exert significantly greater repulsion than before the joining. As the other chains are reordered the original two have a greater chance of forming a second bond between as the number of adjacent chains has decreased. Two crosslinks between the same chains will also repulse and the chain will tend to straighten out rather than form a tight coil. As the formation of crosslinks is a somewhat random process on a macro scale this straightening effect will be more noticeable the more catalyst is present leading to a more ordered chain arrangement, which in turn will lead to more swelling as each chain will be able to swell freely without being tangled around other chains, as they would be in a truly random matrix.

This explanation also holds for explaining the yield stress phenomenon already discussed (Section 3.1.3). An ordered matrix would be rigid as each bond would be taking an equal portion of the stress loaded upon it meaning that the total resistance to deformation was high, whereas a non-ordered matrix would have localised stress points arising at certain bonds and other bonds taking little stress at all leading to an overall weakening of the superstructure. To check the orientation of the polymer chains in the formed membranes would require specialist equipment which was not available, however this explanation seems to be the most logical reasoning for the observed phenomenon.

From this initial feasibility testing it was decided to continue with the swelling experiments using all three membrane grades and the three solvents, heptane, xylene and octane. To confirm that the support layer does not swell and to check its baseline compression under pressure the swelling with variable pressure test also included a fourth sample which was a untreated support layer from the same batch that was used to form the support layer of the produced membrane grades.

3.5.4. Swelling with Variable Pressure

A piece of membrane was located in the retainer and under the swelling probe with the cantilever bar set to Position 2 as described in Section 3.5.2. The retainer was then filled with the sample solvent sufficient to completely immerse the membrane sample, and after 3 minutes the value on the electronic gauge column (total membrane expansion) was recorded and the first weight added. After a further 3 minutes the total expansion was recorded again and the second weight was added to the first. This

process was repeated until a total of five weights were suspended from the bar. After 3 minutes the total expansion was recorded and a single weight removed. In a similar fashion all the weights were removed sequentially with the final reading being the unloaded arm.

Testing in this way provided a way to measure the effect of sequential pressure loading on a membrane sample which uncovered any time-based swelling effects, this is different to the fixed pressure tests presented in Section 3.5.5 which only measure the effect of a single load. This method also provides a measurement of the hysteresis inherent in the membranes by measuring the differences between increasing and decreasing applied pressure. The common time step of 3 minutes was determined during an initial trial which found that the membranes typically finished expanding (or contracting) within the first minute therefore after 3 minutes the reading on the tower had become static. Generally hysteresis is not an important factor when considering membrane operations however the nature of this test allowed for it to be measured.

Four membrane samples (0.1% DBT, 0.3% DBT, 0.5% DBT and Pall Versapor backing) were tested using this method, and each membrane was tested against three solvents; heptane, xylene, and octane. The four samples are composed of the three that were produced during the course of this work and the untreated Pall Versapor backing layer, which was chosen to give a baseline for compression. The twelve solvent/membrane combinations were each tested four times.

3.5.4.1. Results and Discussion

Each of the twelve different combinations tested demonstrated an amount of hysteresis between identical loads on the ascending and descending sections. The overall compression of the membrane was greater during decreasing loading pressure than for a similar load during the initial compression and the compression did not return to zero at the end of the test meaning that some deformation of the membrane had occurred. Table 3.4 shows this discrepancy by displaying the extent of hysteresis as a percentage of the maximum compression recorded, for example the 0.1% DBT membrane in heptane compressed a maximum of 42.875 μm and the remaining compression after the pressure was removed was 8.049 μm giving a discrepancy of 18.77% - the equation used is shown as Equation (3.7). The percentage values have been reported, rather than the absolute to normalise the data set. The extent of the hysteresis between maximum and final compression varied between different

combinations, but ranged between 13.7% (for 0.5% DBT membrane in xylene) to 35.5% (for Pall Versapor in heptane).

The fact that the membranes show the phenomenon must mean that the membranes do retain a memory of their previous states, at least temporarily. This means that in real life, if these membranes were over-pressurised the filtration properties will not instantaneously return to the previous desired dynamics.

$$Hysteresis\ (\%) = \frac{Final\ Compression\ Extent}{Maximum\ Compression\ Extent} \times 100 \tag{3.7}$$

For example, using data from 0.1% DBT membrane and heptane

$$18.77\% = \frac{8.049}{42.875} \times 100 \tag{3.8}$$

Solvent	Membrane Grade			S.D.
	0.1% DBT	0.3% DBT	0.5% DBT	
Heptane	18.77	23.04	17.95	2.73
Xylene	31.36	22.31	13.68	8.84
Octane	24.41	25.36	20.77	2.42
S.D.	6.30	1.60	3.57	

Table 3.4 – Extent of hysteresis (%) recorded in compressed membranes.

Across the different membrane grades it can be seen that both heptane and octane have relatively small standard deviations compared to the deviation attributed to xylene. This deviation was caused by the large variance noted between the different membrane grades with the 0.1% DBT membrane having more than twice the difference observed in the 0.5% DBT membrane. This phenomenon was able to be explained by noting the swelling parameters involved. Any swelling within the membrane would cause it to be more resilient to this kind of pseudo-permanent deformation as a swelled polymer will return to its original shape quickly, and the value in the table will be small. Heptane and octane both swell PDMS better than xylene (Section 3.1) and so it was logical for the highest recorded amount of hysteresis to be found in the xylene experiments, i.e. a slightly swelled membrane will be deformed to a greater extent than a highly swelled membrane. The slope of the trend in the xylene experiments also

supports the earlier findings from the feasibility study (see Figure 3.24). The smallest xylene difference was in the 0.5% DBT membrane which correspondingly swelled the most when tested, adding more weight to the logic of tying these observations into the solubility parameter. Of the membrane grades, the totals of the 0.1% DBT membrane and 0.3% DBT membrane are almost identical with the 0.5% DBT membrane being significantly different. This result was similar to the one shown in Figure 3.24 where the swelling of the 0.1% DBT and 0.3% DBT membranes is similar and the 0.5% DBT significantly different.

In all but one case the 0.1% DBT membrane compressed the least and the 0.5% DBT membrane compressed the most, irrespective of the solvent applied. The one case where this did not happen was the octane tests where the 0.3% DBT membrane compressed marginally less than the 0.1% DBT membrane; the minimum membrane thickness recorded was 128.6 μm for the 0.1% DBT membrane and 130.1 μm for the 0.3% DBT membrane. As all these membranes had the same backing the differences in compression characteristics must arise from the polymer layers. The fact that the choice of solvent had no effect on the general trend of swelling was a good result with regards to the membrane manufacture as it means that the behaviour of the polymer layer was constant.

Another concept to consider from the swelling with variable pressure tests was the magnitude of the compression which was able to be attributed to the backing itself. So far, only the membrane as a whole were discussed but by measuring the compression of a fresh blank backing sheet using the same method that was used to test the membranes, the compression due to the backing was able to be allowed for, meaning that the compression of the polymer layer alone can be calculated or inferred. This was done by taking the compression of the backing layer away from the total compression of the membrane. The advantage of this procedure was that it allows for a value to be determined for the polymer layer compression which would be very difficult to obtain directly. Both the small size and difficulty of stripping the polymer layer intact from the membrane make direct measurement almost impossible and mean that inference from the total was the only practical method. The disadvantage of this procedure was that it implicitly assumes that the compression of the backing was identical with and without the polymer layer which may not be the case. Figure 3.25 explains this logic, in which the relative sizes of the individual layers had been exaggerated for clarity.

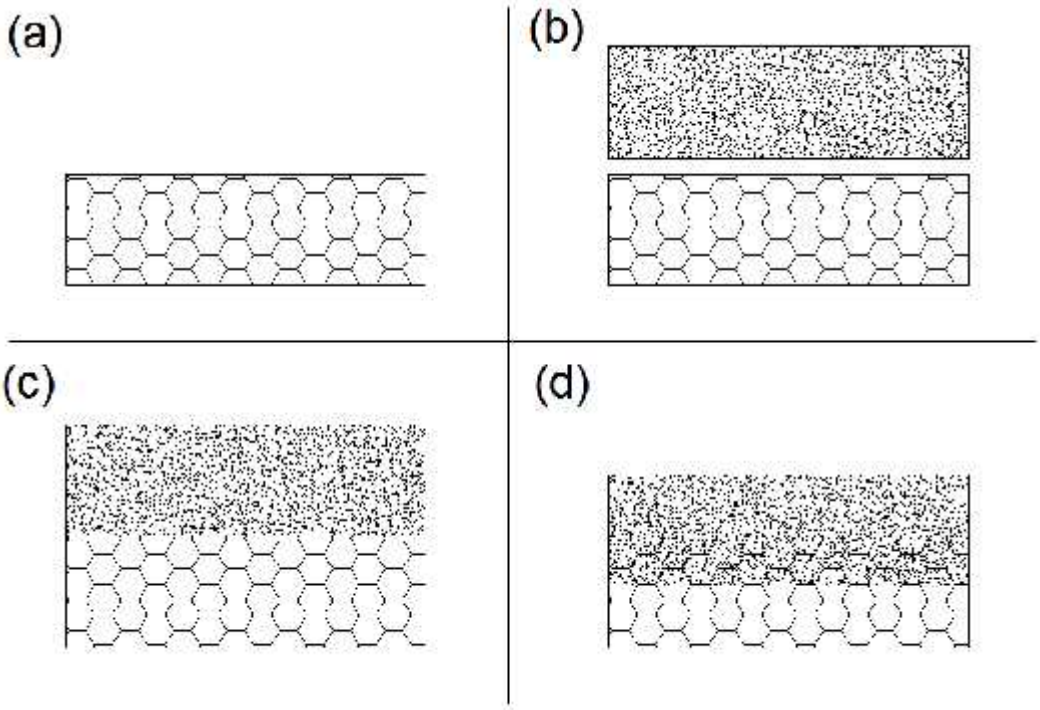

Figure 3.25 – Idealised membrane configurations. a: Backing layer, b: Backing layer and polymer layer – not bonded, c: Backing layer and polymer layer – bonded, d: backing layer and polymer layer combined.

A single uniform slab of any material will compress in a repeatable fashion when exposed to outside influence (see Figure 3.25a). This is also true when considering stacks of material (identical or different) which are simply residing upon each other with no permanent bond between the layers (Figure 3.25b). The complications arise when the two materials are bonded together to form a single structure (Figures 3.25c and 3.25d) as in most composite membranes. In this case when the structure is compressed, stresses are transferred between the two materials via the bond. If the two materials vary in rigidity the stronger material will reduce the compression of the composite compared to the individual materials. Figure 3.26 shows this effect where Figures 3.26a and 3.26b show the idealised compression of a single material and Figures 3.26c and 3.26d show the compression of a composite. In Figure 3.26d the total compression has been reduced by the strengthening effects of the support material.

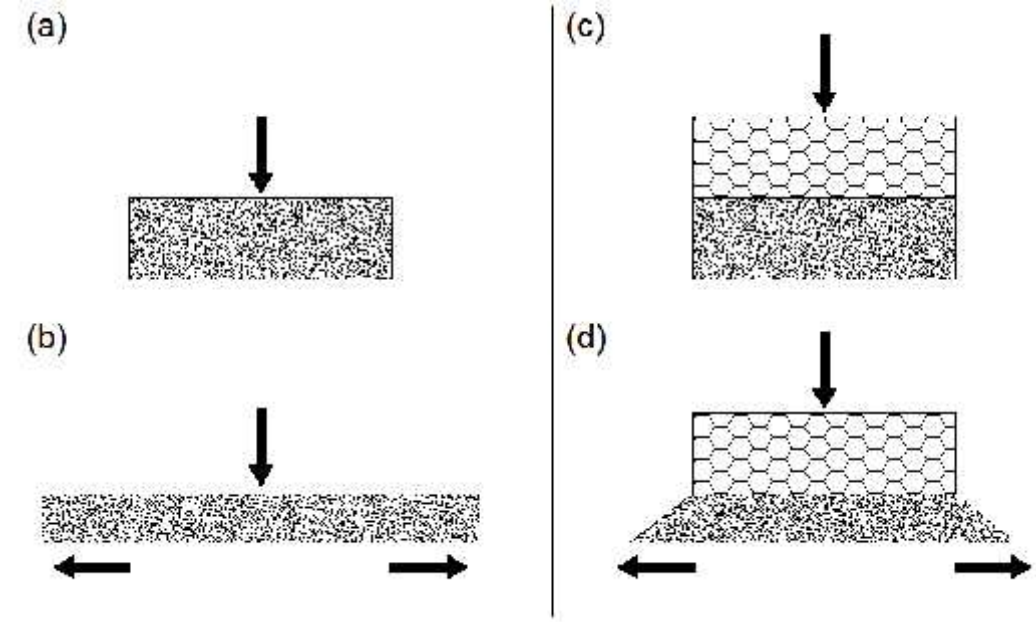

Figure 3.26 – Idealised polymer compression behaviour.

The data was used to calculate the value of compression of the polymer by taking the backing compression extent away from the membrane compression extent. Figure 3.27 shows the polymer compression results for the heptane solvent where a negative value indicates that the backing alone compressed more than the total membrane.

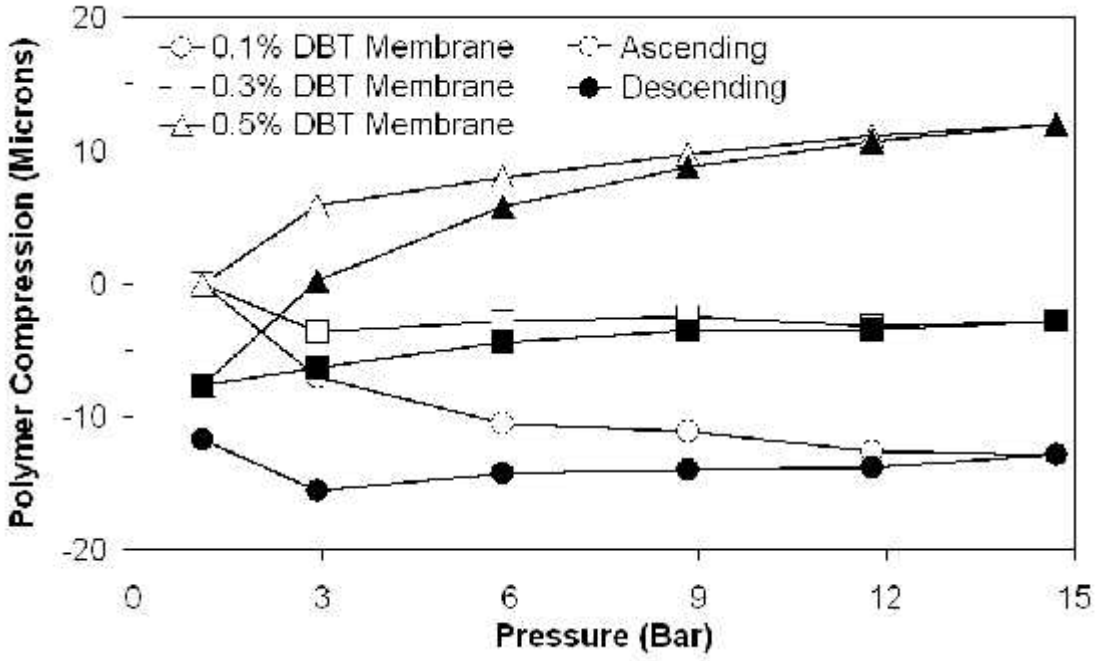

Figure 3.27 – Polymer compression results for the heptane tests.

Although a similar chart to Figure 3.27 could be produced for xylene and octane, heptane results will be used here for ease of discussion. The first thing of note in Figure 3.27 was that two of the membranes (the 0.1% DBT membrane and the 0.3% DBT membrane) exist entirely in the negative region of the chart. This means that for these cases the inclusion of the polymer actually retarded the compression of the backing with the 0.1% DBT membrane providing greater protection than the 0.3% DBT membrane. This would add weight to the theory about having extra polymer inside the backing structure, as the 0.1% DBT membrane is less rigid and so it would be able to penetrate deeper than the relatively more rigid 0.3% DBT membrane blend and having more polymer in the support resists compression. Following the same logic the 0.5% DBT membrane exists mostly in the positive region of the chart meaning that this grade compressed more than the backing alone. Which would make sense as the 0.5% DBT membrane was the most rigid and would therefore penetrate the support layer the least, and without the polymer filling the support layers substructure, it was more easily deformed leading to a positive total compression. The 0.5% DBT membrane was the one closest to having distinct bonded layers (Figure 3.25c) and the 0.1% DBT membrane was the closest to having merged layers (Figure 3.25d). This analysis shows that the measurement of polymer compression by inference was not sufficient to determine the extent of polymer swelling in this type of membrane, as the fact that some negative values were determined proves that the baseline was not constant.

3.5.4.2. Intermediate Conclusions

Overall, several different trends and theories have been deduced from the results of the swelling with variable pressure tests. Hysteresis within the sample tested has been confirmed, the extent of which varies by both membrane grade and solvent applied. The 0.5% DBT membrane has been shown to compress the most irrespective of other factors and heptane has been shown to make the membranes the most resistant to compression – this conclusion was logical as heptane had already been shown to swell PDMS the most. Finally the idea of inferring pure polymer compression has been tried but it was found that interactions with the support layer cloud the results obtained from such analysis.

3.5.5. Swelling with Fixed Pressure

Swelling with fixed pressure was the second of the detailed investigations and it was based on a method that had been previously used by other authors (Low, 2009) to assess membrane swelling. A dry membrane sample was located under the spacer with the loading arm and probe located to position 2. A load was added and the membrane sample was allowed to compress to equilibrium. When compression was complete the solvent was added and the membrane was allowed to expand to equilibrium again. The volume of solvent added was sufficient to completely immerse the membrane sample at all times. The difference between the two equilibrium values was recorded as the expansion due to solvent immersion. The same loads were used for the fixed pressure tests as for the variable pressure tests, i.e. 2.94, 5.89, 8.83, 11.77 and 14.71 bar respectively. This method was similar to the one used for the feasibility test, however, through the use of the cantilever bar a small amount of pressure generated by the rig itself means that direct comparison to the feasibility study results was not possible.

3.5.5.1. Results and Discussion

A typical set of raw data for the swelling with fixed pressure tests obtained using xylene solvent are shown as Figure 3.28. The expansion results from this series of experiments mirror that found for the feasibility test and a similar logic can be used to explain their significance. For every solvent tested the 0.1% DBT membrane expanded the least with the 0.3% DBT membrane swelling only marginally more and the 0.5% DBT membrane swelling at least twice as much as the 0.3% DBT membrane. This was similar to the results of the feasibility test however the factor difference between the 0.3% DBT and 0.5% DBT membranes was smaller – two to three times rather than four to five times.

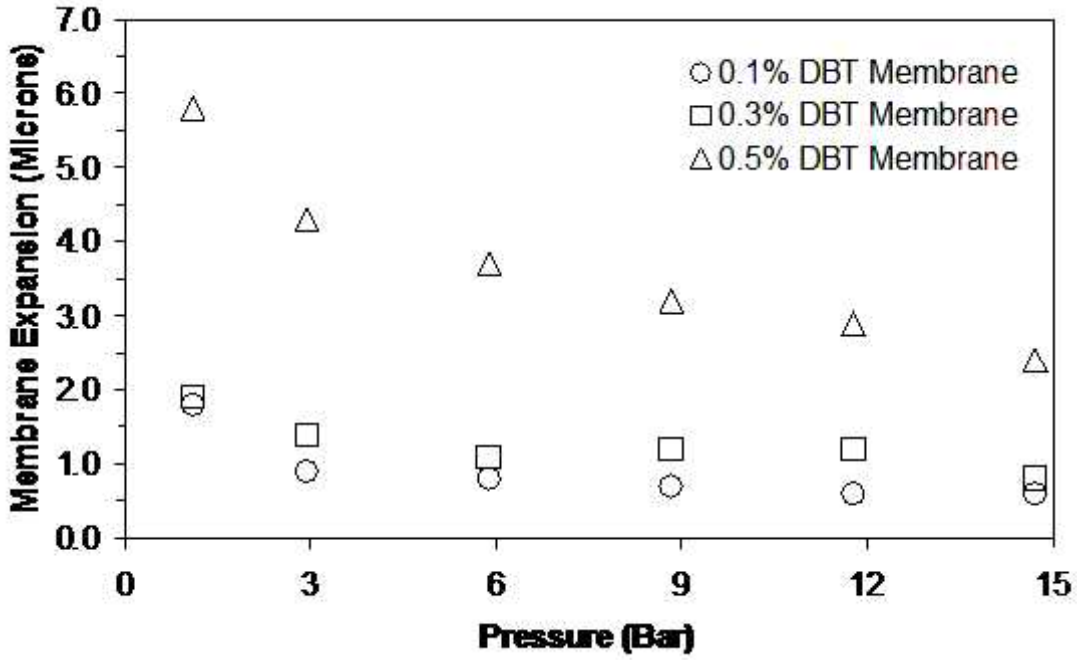

Figure 3.28 – Fixed pressure results for xylene solvent.

Considering solvent type; for all the membranes tested xylene produced the smallest expansion – except for the result for the 0.1% DBT membrane, unloaded where it expanded only 0.2 µm more than heptane. Heptane and octane were found to expand the membrane samples to a comparable extent. One of the advantages of the fixed pressure test over the variable pressure test was that it provided data on the effect of increasing pressure on the expansion of the membranes. It had already been discussed that the swelling of the polymer layer of composite membranes was a problem and most of the work conducted seems to involve developing models to predict this expansion and associated change in filtration properties, but another way round this problem is to simply apply direct pressure to stop the polymer expanding in the first place. It can be seen from Figure 3.28 that the result of applying 14.71 bar to the membrane sample causes the extent of expansion to be halved compared with the minimum force tested. The true extent of retardation of swelling cannot be measured by this method alone, as the rig always applies a small amount of force but by comparing the results to the results in Figure 3.24, it can be determined that the expansion for the 0.5% DBT membrane at maximum force was 45%, 30% and 41% of the average maximum expansion recorded for heptane, xylene and octane respectively. The ability to constantly compress membranes during crossflow filtration was outside the scope of this thesis but could be considered as an avenue for future work (discussed in Chapter 7). The swelling with fixed pressure test had produced

results which were comparable to earlier work (Low, 2009) reinforcing the findings and extending it for a range of loading forces.

3.5.6. Comparison of Membrane Swelling Methods and Results

There were several functional differences between the two methods, the first of which being duration. The swelling with variable pressure tests, due to the way in which the loading and unloading was consecutive, produced the entire data set within half an hour so any local effects such as temperature or humidity were minimised. Compare this to the results for the swelling with fixed pressure tests which could only be taken once a day as after each time a membrane sample was used, it had to be left for at least a day to return to its original state before it could be used again – this led to a greater variance in the local environment. The fixed pressure experiments could have all been conducted on the same day if several membrane samples had been used however this would have introduced a new source of error into the results, specifically error arising from the variation in membrane samples. As the effect of local environment was deemed to be less pronounced than different membranes it was decided to run the experiment over several days. The local temperature and humidity were recorded during the curing process with a negligible change in humidity and at maximum a 0.6 °C temperature fluctuation.

Another point to be considered was the variance between different sections of the same membrane sample. As the variable pressure tests were conducted consecutively, the region of the membrane directly under the probe was constant. However with the fixed pressure tests the membrane was moved between results (conducted on consecutive days) so the potential for slight variation existed.

Comparisons can also be drawn between the data obtained not just the methodology. In the swelling with variable pressure tests the 0.5% DBT membrane compressed the most and in the swelling with fixed pressure tests it expanded the most. This was a logical conclusion as the polymer that was the least resistant to expansion will also be the one least resistant to compressive forces. The fact that the polymer in question was supposedly the stiffest grade was intriguing and the discussion on ordered polymers is offered as the underlying reason behind this.

Considering solvents, in the majority of the tests heptane and octane produced almost identical results with xylene producing a marked distinction from the others. This was true in all cases except for the 0.1% DBT membrane for variable pressure. This has been attributed to solubility parameters and entropy. The largest compression / largest

expansion mechanic was in evidence again and has already been explained in the previous paragraph.

Overall the two different approaches have similar trends within the same sample set (Figures 3.27 and 3.28) and have each provided different viewpoints on the same phenomenon. The variable pressure tests have provided method for measuring hysteresis within a membrane sample. The results from the fixed pressure tests have confirmed the findings of the feasibility study and provided a direct quantification of the extent of swelling within the membrane samples.

3.6. Comparison of Polymer and Membrane Swelling

To compare these two different sets of experiments some refinement was initially required. As it had already been shown that the membrane based tests covered in Section 3.5 all demonstrate different aspects of the same trend, this comparison does not need to be covered here again, therefore throughout this section the feasibility test data will be used where applicable for consistency.

The effect of catalyst amount on polymer swelling is shown as Figure 3.6 and Figure 3.24 for membrane swelling. These charts show the extent of height change upon immersion for identical solvents – Both tests used heptane and xylene, with the polymer experiments focusing on ethanol whilst the membrane experiments utilised octane.

The experimental data shows that there was no correlation between catalyst amount and swelled height for the polymer based tests but there was a strong correlation found within the membrane based data – with the 0.1% DBT membrane swelling the least, the 0.3% DBT membrane swelling around a third more and the 0.5% DBT membrane swelling around five times as much as the others. The reason for this discrepancy must be due to the differences inherent between the manufacture process of the polymer slabs and composite membranes. The polymer slabs tested upon immersion were able to relatively freely expand in any of three dimensions. Compare this to the produced membranes, the polymer of which was restrained along the planar face of the support media and expansion was only free perpendicular to this plane. The polymer slabs expanded up to twice their original size, the membranes which underwent fixed pressure tests expanded two to three times their original size and the membranes used

in the feasibility tests expanded four to five times their original size. By restraining, or at least restricting, the polymer layer, the total expansion increased in the last free direction. This means that by eliminating all the expansion possibilities except for depth, the thickness increase has become noticeable. This result implies that the well documented membrane swelling that occurs in the presence of solvents is actually a side effect of the inclusion of the support layer and the associated restriction this produces.

Expansion by solvent type produces a comparable trend. In both cases expansion due to heptane was larger than expansion due to xylene, but the extent of the expansion (relative to initial height) was different. For the polymer slabs the expansion was averaged as 43% and 30% for heptane and xylene respectively. However the relative expansions of the membrane were 2.3% for heptane and 1.8% for xylene. In both cases the result for heptane was around 35% higher than the xylene result which means that the polymer behaviour in the two states must be the same with an external effect altering the magnitude. The fact that the membrane swelling was absolutely smaller can be explained by the attachment to the support, which retards the overall expansion which can be realised.

It has been shown that the swelling behaviour of the polymer material was comparable in both produced forms to the behaviour of PDMS detailed in published journal articles, and the measured Young's modulus was also comparable to other polymers. This comparison had to be completed to ensure that any future conclusions drawn between the membranes produced in house and industry standard membranes were valid.

3.7. Intermediate Conclusions

Initially the purpose of this chapter was to detail the effects of polymer swelling including the manufacture of both dense PDMS slabs and composite nanofiltration membranes, however during its completion significant parallels have been drawn between different sections such that this work unifies different aspect of the same swelling phenomenon rather than simply being a record of different experiments.

One of the aspects of this work has been the conformation of the swelling dependence on solubility parameter. In every composition of polymer, in both slab and selective

layer forms, the maximum extent of swelling was found to be elicited by the addition of solvents which have a solubility parameter close to that of PDMS (i.e. 15.5 $MPa^{0.5}$). Swelling extent was found to decrease when using solvents above or below this parameter. The upper limit to this phenomenon was found to exist around 26.5 $MPa^{0.5}$ (the solubility parameter for ethanol) as this was the point where swelling was reduced to almost nil. The result of this was that the swelling phenomenon must be an inherent property of the polymer matrix and independent of the produced polymer block size.

The effect of catalyst concentration was also covered in this chapter with seemingly contradictory evidence being evident. The higher catalyst concentration samples have been shown to be stiffer (possessing of a higher Young's modulus) but at the same time have been shown to compress the most under loading. The higher catalyst concentration samples were recorded as swelling the most when part of a composite membrane but when part of a PDMS slab no discernable catalyst concentration / swelling relationship was noted. These differences have been put down to the dynamics of swelling at different polymer layer sizes. At small sizes the total number of polymer chains was less, meaning that the material was able to be deformed easier, but at larger sizes more non-planar bonds were able to be formed (as the surface area to volume ratio was more favourable) solidifying the entire structure. Therefore it was believed that changing the catalyst concentration had an effect on the filtration properties of the selective layer, however at least in part this effect was being masked by the macro level effect of polymer thickness.

3.8. Nomenclature

A	Plan area of spacer (m^2)
b	Width of polymer bar (m)
E	Modulus of elasticity (Pa)
F	Compressive force (N)
g	Gravity ($m\ s^{-2}$)
h	Height of polymer bar (m)
I_x	Second moment of inertia (m^4)
l	Bar length (m)
L	Length of cantilever bar (m)
m	Mass of applied weight (kg)

m_1	Mass of cantilever bar (kg)
P	Applied pressure (Pa)
W	Suspended weight (kg) or Pivot point (-)
X	Distance from pivot to spacer (m)
y	Beam deflection (m) or Centre of gravity of cantilever bar (-)

3.9. References

Albrecht W., Kneifel K., Weigel Th., Hilke R., Just R., Schossig M., Ebert K., Lendlein A., 2005. Preparation of highly asymmetric hollow fibre membranes from poly(ether imide) by a modified dry-wet phase inversion technique using a triple spinneret. *J. Membrane Science*, **262**, 69-80.

Armani D., Lui C., Aluru N., 1999. Re-configurable fluid circuits by PDMS elastomer micromachining, *Twelfth IEEE International Conference on Micro Electro Mechanical Systems*, pp. 222-227, Orlando.

Baker, R.W., 2004, *Membrane Technology and Applications*, 2nd Edn. John Wiley & Sons, Chichester.

Chaudhury M.K., Finlay J.A., Chung J.Y., Callow M.E., Callow J.A., 2005. The influence of elastic modulus and thickness on the release of the soft-fouling green alga Ulva linza (syn. Enteromorpha linza) from poly(dimethylsiloxane) (PDMS) model networks, *Biofouling*, **21**, 41-48.

Dewimille L., Bresson B., Bokobz L., 2005, Synthesis, structure and morphology of poly(dimethylsiloxane) networks filled with in situ generated silica particles, *Polymer*, **46**, 4135–4143.

Dijkstra M.F.J., Bach S., Ebert K., 2006. A transport model for organophilic nanofiltration. *J. Membrane Science*, **286**, 60-68.

Doig S.D., Boam A.T., Livingston A.G., Stuckey D.C., 1998. Mass transfer of hydrophobic solutes in solvent swollen silicone rubber membranes, *J. Membrane Science*, **154**, 127-140.

Ebert K., Fritsch D., Koll J., Tjahjawiguna C., 2004. Influence of inorganic fillers on the compaction behaviour of porous polymer based membranes, *J. Membrane Science*, **233**, 71-78.

Ebert K., Koll J., Dijkstra M.F.J., Eggers M., 2006. Fundamental studies on the performance of a hydrophobic solvent stable membrane in non-aqueous solutions, *J. Membrane Science*, **285**, 75-80.

Geens J., van der Bruggen B., Vandecasteele C., 2004. Characterisation of the solvent stability of polymeric nanofiltration membranes by measurement of contact angles and swelling, *Chemical Engineering Science*, **59**, 1161-1164.

Gevers L.E.M., Meyen G., De Smet K., van de Velde P., Du Prez F., Vankelecon I.F.J., Jacobs P.A., 2006a. Physico-chemical interpretation of the SRNF transport mechanism for solutes through dense silicone membranes, *J. Membrane Science*, **274**, 173-182.

Gevers L.E.M., Vankelecom I.F.J., Jacobs P.A., 2006b. Solvent-resistant nanofiltration with filled polydimethylsiloxane (PDMS) membranes, *J. Membrane Science*, **278**, 199-204.

Ho W.S.W. & Sirkar K.K., 1992, *Membrane Handbook*, Van Nostrand Reinhold, New York.

Low, J.S., 2009, A Study of Organic Solvent Nanofiltration, PhD thesis, Loughborough University.

Merkel T.C., Bondar V.I., Nagai K., Freeman B.D., Pinnau I., 1999, Gas Sorption, Diffusion and Permeation in Pol(dimethylsiloxane), *J. Polymer Science*, **38**, 414-434.

Mulder, M., 2000, *Basic Principles of Membrane Technology*, 2nd Edn. Kluwer Academic Publishers, London.

Roark R.J., 1965, *Formulas for Stress and Strain*, 4th Edn McGraw-Hill, New York.

Robinson J.P., 2004. The selective removal of components from gasoline using membrane technology, PhD thesis, Loughborough University

Silva P., Han S., Livingston A.G., 2005. Solvent transport in organic solvent nanofiltration membranes, *J. Membrane Science*, **262**, 49-59.

Song S., Khang D.Y., Kim M.J., Park J.E., Lee H.H., 2007. Asymmetric porous thin film preparation by controlled solvent absorption using PDMS, *J. Membrane Science*, **305**, 5-12.

Stafie N., 2004. Poly(dimethylsiloxane)-based composite nanofiltration membranes for non-aqueous applications, PhD thesis, University of Twente.

Tarleton E.S., Robinson J.P., Smith S.J., Na J.J.W., 2005. New experimental measurments of solvent induced swelling in nanofiltration membranes, *J. Membrane Science*, **261**, 129-135.

Tonelli A.E., 2001, *Polymers from the Inside Out*, John Wiley & Sons, New York.

Ulbricht M., 2006. Advanced functional polymer membranes, *Polymer*, **47**, 2217-2262.

Yoo J.S., Kim S.J., Choi J.S. 1999. Swelling equlibria of mixed solvent/poly(dimethylsiloxane) systems, *J. Chemical & Engineering Data*, **44**, 16-22.

4. Filtration Experiments

To complete two of the aims of this project (identification of transport mechanism and determination of effective pore size) filtration data was needed. The data was obtained by completing a series of crossflow filtration tests at several different pressures. The PDMS/PAN composite membranes were tested to determine their flux and rejection characteristics. This was achieved by subjecting the membranes to a series of crossflow tests at different pressures, using different solvents and solutes. To check the effect of membrane swelling a range of solvents were tested from heptane (previously shown to swell the membrane the most), to xylene (shown to have little effect on membrane swelling) and including octane (falls between the other two solvents in terms of membrane swelling). The effect of catalyst concentration on separation dynamics was studied. This chapter covers all the remaining filtration characterisation testing conducted with Chapter five detailing the transport mechanism work.

4.1. Crossflow Rig Tests

4.1.1. Design of Test Cell

The main testing rig detailed in this chapter is a crossflow rig which has been used in the past by other authors (Tarleton *et al,* 2009, Robinson, 2004, Low, 2009). The test cell which the previous researchers had used had a 100 mm diameter circular test area, which was too large for testing the membranes produced throughout the course of this study. From the feasibility tests conducted on membrane manufacture it was unlikely that a membrane of that size would be able to be produced without inherent defects. Therefore there were two rational ways to resolve this problem. Either the current test cell had to be modified or a new test cell had to be designed to take its place. The former of these ideas was ruled out on inspection of the present cell, the location of the retentate removal pipe prevents any modification to the absolute size of the test area. Due to this, a new cell had to be designed and can be seen as Figure 4.1 which shows three potential cell designs each capable of taking a different size of membrane. The cell was produced from stainless steel and sized to take 50 mm circular diameter membranes. The segmented base of the cell was angled to allow the permeate to flow out of the cell and during operation the structure was covered by a

porous plate. The cell used in this work had an effective permeation rate of one quarter of the cell used by other authors (Tarleton *et al,* 2009, Robinson, 2004, Low, 2009) and a removable top plate to alter the internal reservoir's volume. The existing cell had a clearance of 3 mm between the membrane and the top plate, the new cell had a clearance of 12 mm between these two parts to keep the same total volume in the hold up space. As well as this, a 9 mm thick spacer had been produced which can be bolted into the top plate to reduce the clearance back to 3 mm, inline with the existing configuration. So the cell used in this work was able to be operated with the same hold up volume as the original cell or it was able to be operated with the same total clearance as the original cell. This provides an extra level of customisation and allows different phenomena to be investigated.

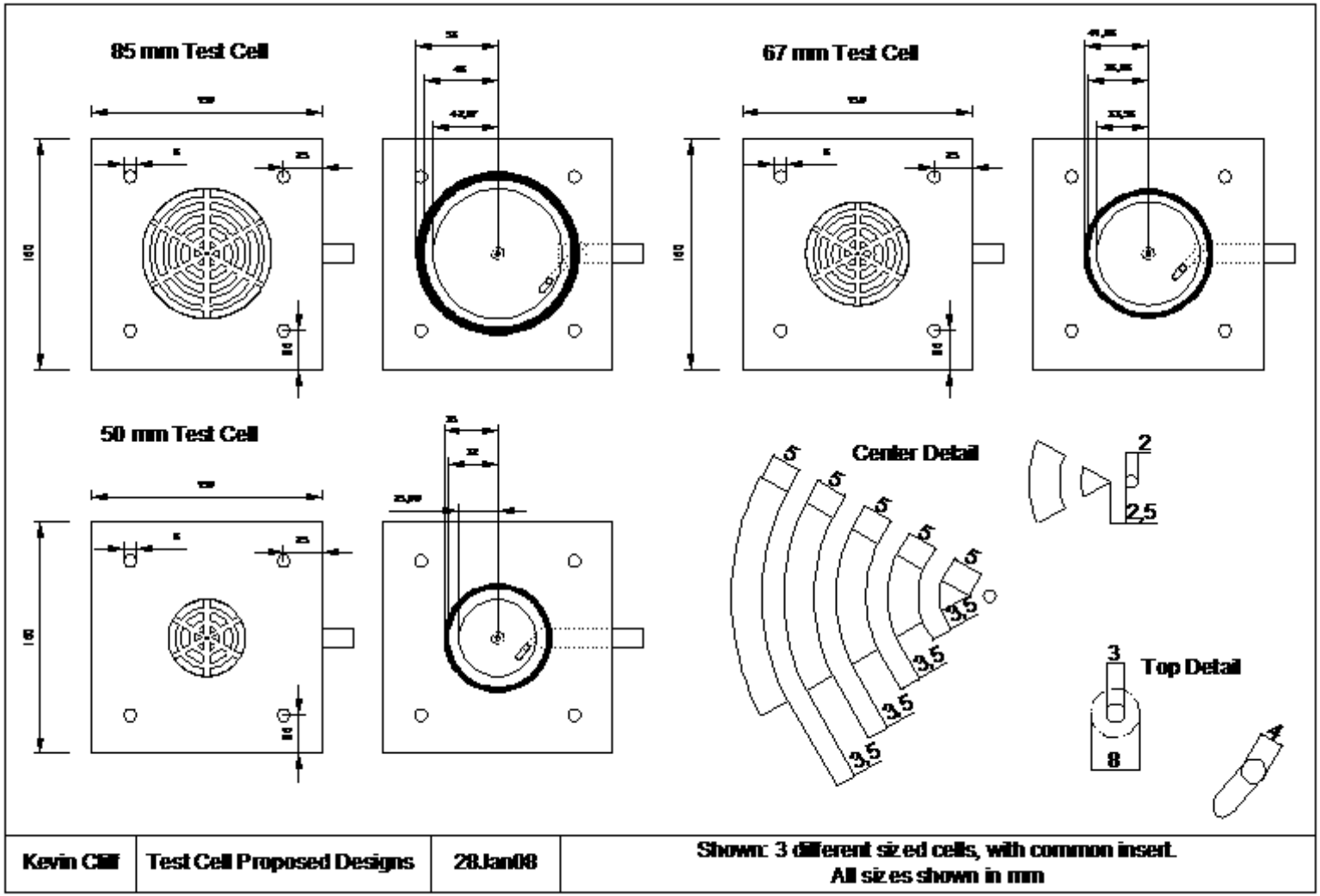

Figure 4.1 – Schematic diagram of test cell design potentials – 50 mm cell produced.

4.1.2. Crossflow Rig Description

A photograph of the crossflow rig is shown in Figure 4.2, whilst a schematic diagram is presented in Figure 4.3. The set up of the crossflow rig featured a closed loop system in which the retentate from the test cell was recycled back into the reservoir tank. The mechanical force was provided by an air driven magnetically coupled pump which had the dual benefits of being self contained (the motor's lubricating oil cannot enter the process stream) and providing cooling (the exhaust gas from the pump was passed through a cooler to maintain the temperature of the process stream. The permeate stream could be made to bypass the collection vessel and routed back into the reservoir tank if required. The test cell and all pipework were removable to aid with cleaning.

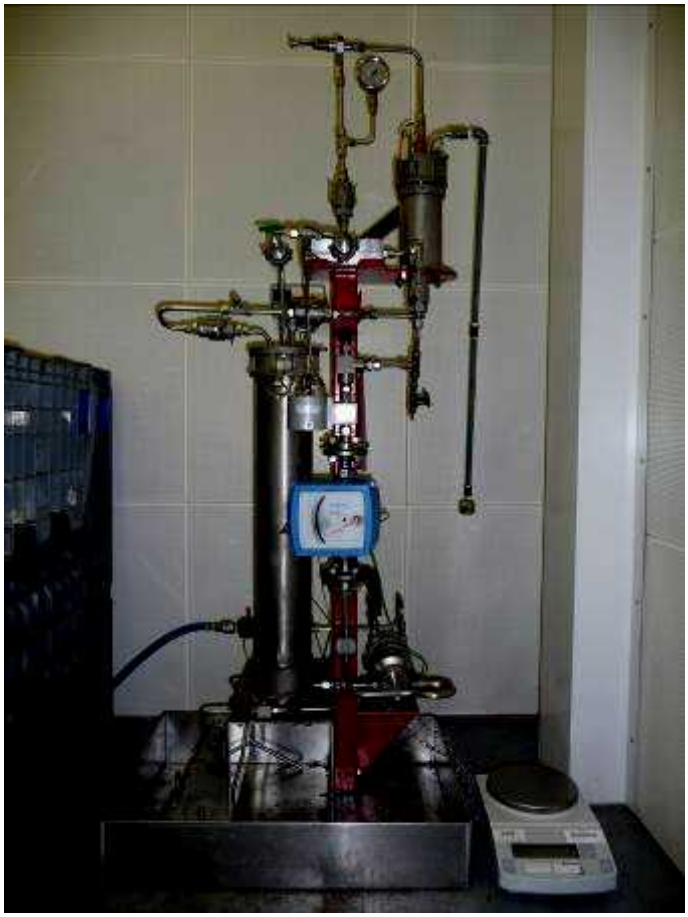

Figure 4.2 – Photograph of the crossflow rig.

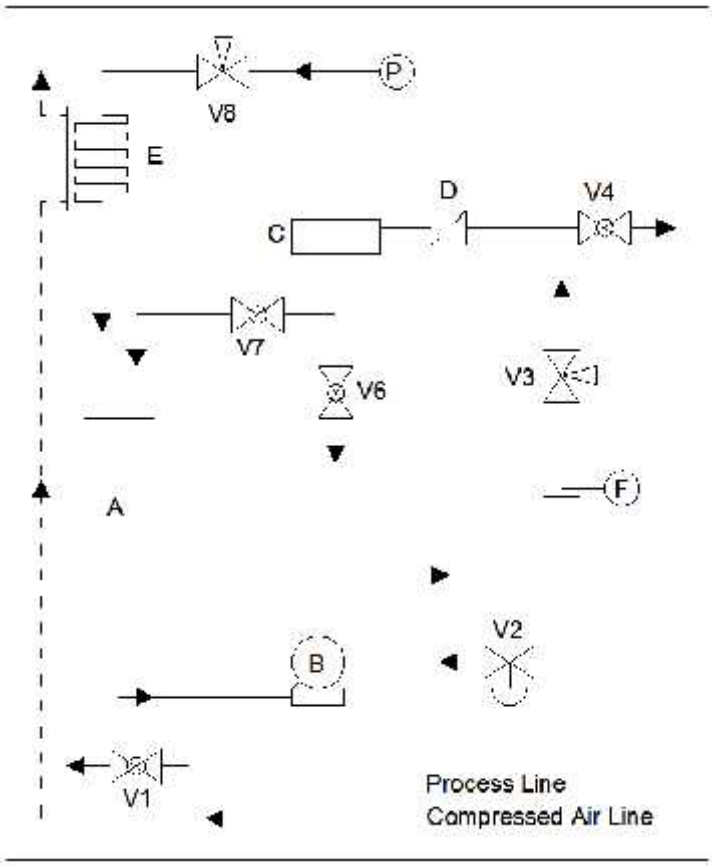

Key:

V1 – Reservoir Drain Valve
V2 – Compressed Air Regulator Valve
V3 – Flow Fine-Adjust Valve
V4 – Test Cell Drain Isolation Valve
V5 – Test Cell Drain Valve
V6 – Permeate Sampling Valve
V7 – Permeate Return Valve
V8 – Pressure Regulator Valve

A – Reservoir
B – Air Driven Pump
C – Test Cell
D – Filter
E – Cooler
F – Flow Meter
P – Pressure Gauge

Figure 4.3 – Schematic diagram of the crossflow rig.

4.1.2.1. Crossflow Rig Overview

When the compressed air line valve was opened the pump draws fluid from the reservoir and passes through a sampling point, flowmeter, second sampling port and a filter before entering the upper part of the test cell. From there the fluid was able to either leave through the top (retentate) or it was able to leave though the front of the

lower section of the test cell after passing through the membrane (permeate). A needle valve and pressure gauge mounted on the upper exit line from the test cell allow for the back pressure to be regulated altering the pressure difference over the membrane. The upper stream was then passed through a cooler with the exhaust gas from the pump acting as the cold stream. From there both streams fed back to the reservoir. On the permeate side of the rig just before the reservoir return there was a permeate sampling port to allow for an assessment of the flux and rejection of any particular membrane to be determined. A similar arrangement had previously been applied successfully by Peeva *et al* (2004).

4.1.2.2. Operation of a Single Test

Bracketed items in this section refer to the objects identified in Figure 4.3.
This section briefly covers the operation of the crossflow rig and details the sampling procedure.
Each test started with 1 litre of solvent containing an approximately 30ppm solute solution, and finished when 100 ml of permeate had been produced (10% stage cut). A sample of the starting solution was taken and labelled at 'bulk – initial'. The test cell was fitted with the relevant membrane and sealed. The solution was circulated for 5 minutes, to remove trapped air from the system, with all permeate formed being recycled back to the reservoir, after which a second sample labelled 'bulk – circulated' was taken. Any differences found between the first two bulk samples must have arisen due to the rig not being cleaned properly and the 'bulk – circulated' sample picking up impurities from inside the rig. These two samples were used as cleaning validation. Valve (V6) was opened and (V7) closed forcing the permeate into the collection vessel. The duration between the valve switching and 100 ml of permeate being collected was recorded and used with the exact mass of permeate collected to work out the flux rate. A sample of the collection vessel fluid was taken and labelled as 'permeate – averaged'. A sample of the permeate at the end of the experiment was also taken to assess if the membrane has filtered consistently; it was labelled 'permeate at end'. The solution remaining in the reservoir after a test had been completed was also taken and labelled as 'bulk – final'.

4.1.2.3. Analysis of Samples

Each of the five samples were run through a Perkin Elmer Lambda 12 UV/VIS spectrophotometer, scanning over the range of 200~500 nm recording absorbance

every 1 nm at a rate of 240 nm/min. An example of the resultant chart is shown in Figure 4.4, for n-heptane and 9,10-diphenylanthracene. On this chart samples one and two were identical, proving the rig was sufficiently cleaned and samples three and four were identical proving the membrane operated consistently. A baseline scan was performed using a pure sample of the same solvent which was in the test solution, in this case n-heptane, so the traces shown were solely because of the solute (9,10-diphenylanthracene). From the chart two distinct areas were able to be seen. Between 300 nm and 500 nm a three peaked smooth curve was present and from this section the results have been taken. However between 200 nm and 300 nm a distorted region exists, this was because the spectrophotometer encounters interference at the lower end, no results will be taken from this section. The entire range has been scanned as the characteristic shape of the trace was completely dependent on the solvent/solute combination and the possibility existed that another combination would work in the range 200 nm to 300 nm and so scanning the full range was deemed good practice. From this chart the absorbance value at a single wavelength had been noted for use later. For the n-heptane / 9,10-diphenylanthracene combination this wavelength was 392 nm, as it corresponds to the maximum of the rightmost peak. Selecting a peak absorbance ensured that constancy would be achieved for all similar tests.

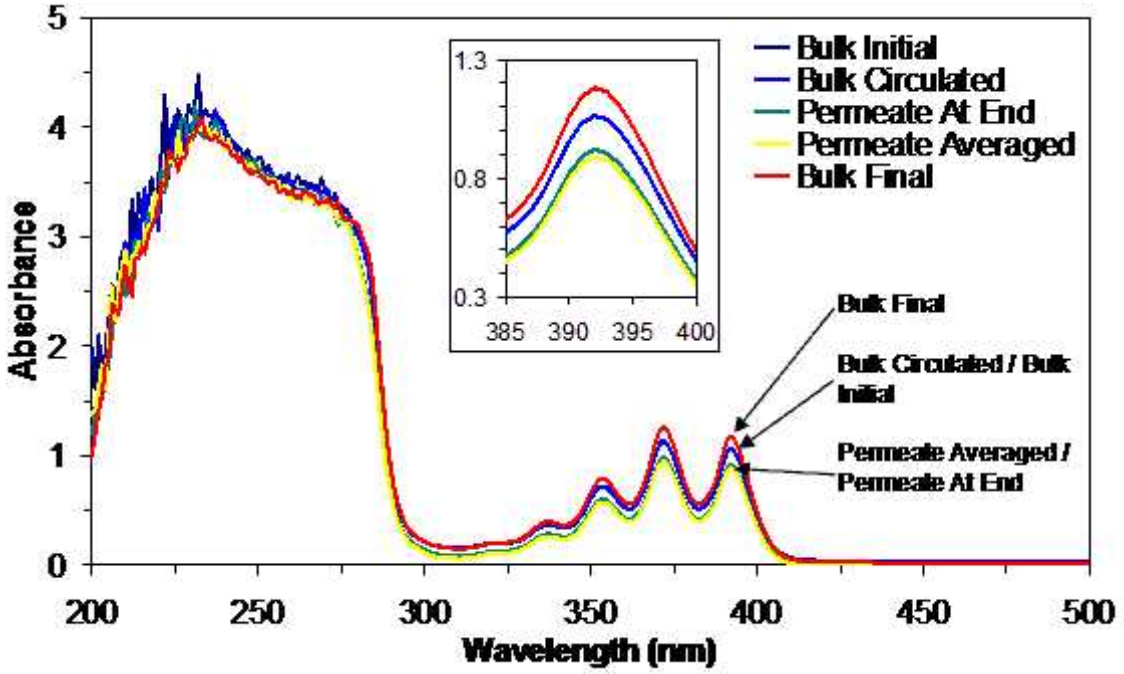

Figure 4.4 – Example UV/VIS traces for all five samples.

Figure 4.4 on its own does not give the rejection extent as the UV/VIS spectrophotometer records changes in absorbance of light not the actual composition

of the solution, so a calibration chart was required. The corresponding calibration chart to Figure 4.4 is shown as Figure 4.5. To produce this chart, known standards of range of concentrations were made up and analysed by spectrophotometry as detailed above. Taking the absolute absorbance of each of these traces at 392 nm allows for the conversion chart to be plotted, shown as Figure 4.6.

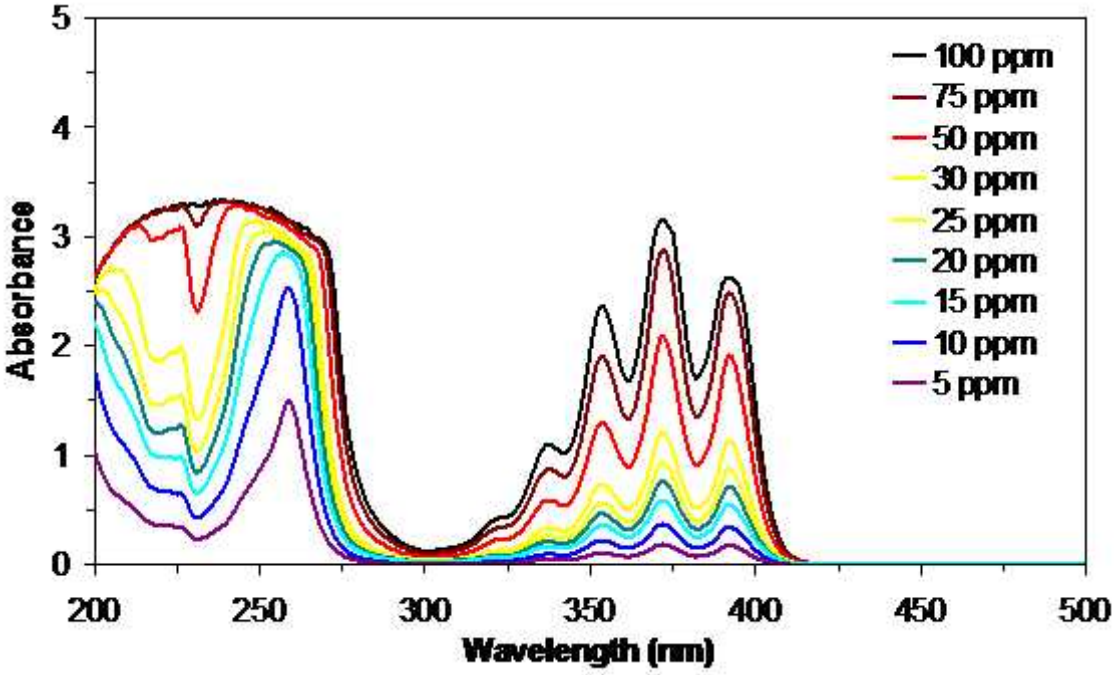

Figure 4.5 – Calibration chart for 9,10-diphenylanthracene in n-heptane.

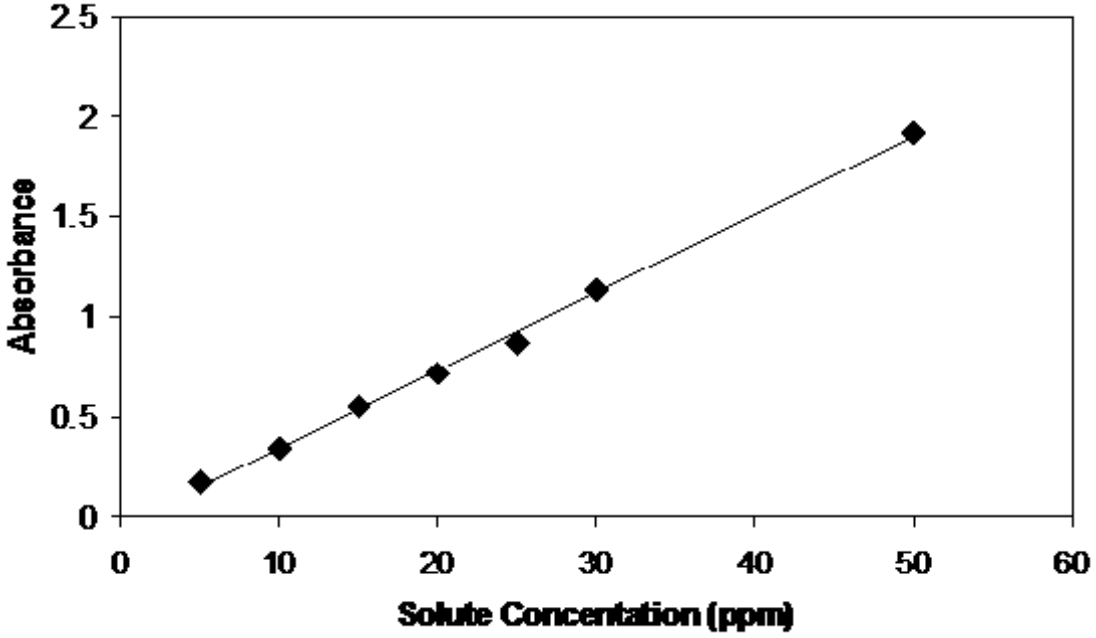

Figure 4.6 – Conversion chart for 9,10-diphenylanthracene in n-heptane.

As can be seen from the Figure 4.6, a linear relationship exists between concentration (ppm) and absorbance. This allows the absorbance values taken from Figure 4.4 to be changed to composition. With the concentration of the five samples known the rejection of the membrane was able to be calculated by comparing the concentrations of samples two (bulk – circulated) and four (permeate – averaged). In this case sample two was the retentate and sample four the permeate meaning that the rejection was given by Equation (4.1) (See Toh *et al*, 2007a, Baker, 2004 and Silva *et al*, 2005).

$$R\ (\%) = 1 - \left(\frac{C_{Permeate}}{C_{\mathrm{Re}\,tentate}} \right) \times 100 \tag{4.1}$$

These two samples were chosen as they best represent the change in composition throughout the course of the experiment. In practice it was found that samples three and four were identical for all tests so either could have been used.

4.2. Filtration Test Matrix

A total of 189 different crossflow experiments were completed (not including repeat runs). This number was reached by testing every combination of three solvents, three solutes, three membranes and seven pressures. As each run took between 2 and 5 hours to complete (dependent on membrane and pressure) each experimental combination was tested only once. The time required to complete duplicate experiments was prohibitive and so repeats were only conducted for failed runs. The three solvents used were heptane, xylene and octane, the reasons for choosing these was discussed in Section 3.3.1. 9,10-diphenylanthracene (910), iron (III) naphthenate (I3N) and iron (III) acetylacetonate (I3A) were the three solutes tested. Briefly these solutes were used due their distinctive UV/VIS profiles and range of solute size. Additionally a representative from each of the membrane grades, 0.1% DBT, 0.3% BDT and 0.5% DBT were used in the crossflow testing. Each combination was run at one of seven different fixed pressures ranging from 2 to 8 bar. This range of experimental parameters ensured that enough data was produced to meet the aims outlined in Section 1.2. 27 data sets (combinations of membrane/solute/solvent) each containing seven data points was sufficient for modelling purposes and to be sure that the trend produced was correct and not being affected by a single outlier. During the

feasibility stages only three pressures were completed for a run and it was deemed that a single outlier had too large an effect on the final trend, so a seven pressure system was adopted.

4.3. Membrane Performance Results

The remainder of this chapter is devoted to the discussion and analysis of the results from the completed crossflow experiments. The raw filtration data has been compiled into sets of paired graphs (one each for flux and rejection) showing the three membrane grades for a particular solvent/solute set. To aid with the discussion the membrane performance data has been split by solvent type, for convenience of discussion, before the overall effects of solute and solvent were considered. However, it was appropriate to discuss the general shapes of the flux and rejection profiles as these were common to all the tests performed.

4.3.1. Flux and Rejection Trend Shapes

A positive linear trend which passes through the origin was found to be a suitable fit for all flux vs. pressure data, with only the gradient varying between different solute/solvent/membrane combinations, a typical example is shown as Figure 4.7 for the tests using I3N solute and heptane solvent. This trend was logical as ultimately, this process was pressure driven, and with a higher pressure comes a higher driving force across the membrane therefore a higher flux was generated. The linear correlation found in the data sets was generally high with the average regression coefficient being greater than 0.9 (i.e. $R^2 > 0.9$).

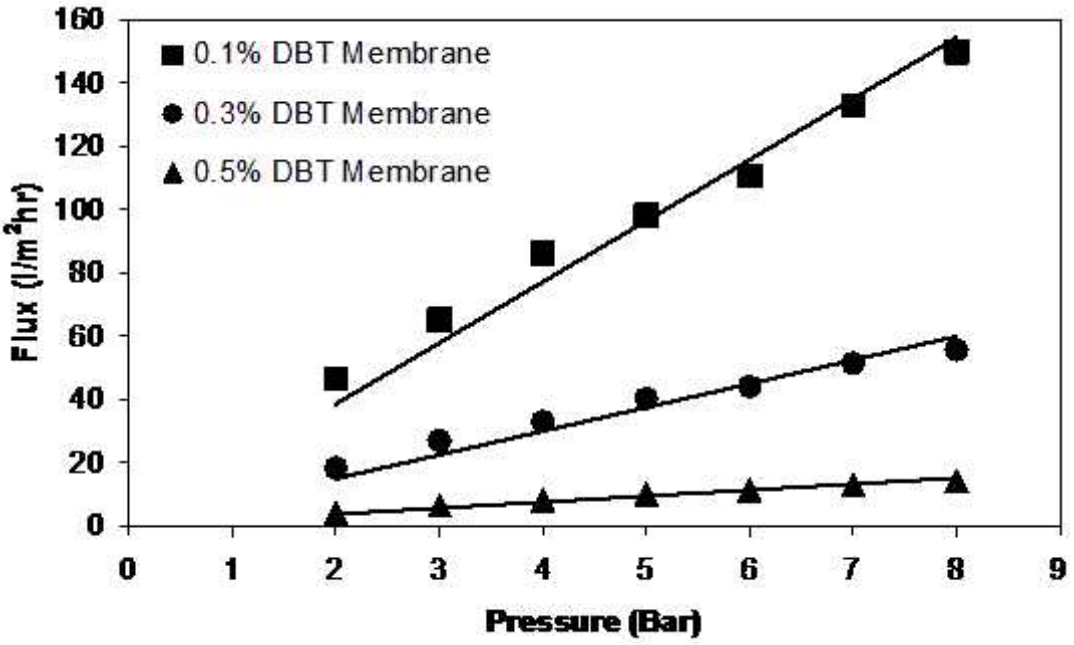

Figure 4.7 – Typical linear correlation within crossflow filtration flux data.

Darcy's law provides the reason behind the noted linearity. Darcy's law can be used to define the relationship between the applied pressure difference and solvent flux through a porous media. The formula for Darcy's law can be seen as Equation (4.2), with this form taken from Baker (2004).

$$J = \frac{k \cdot \Delta P}{\mu \cdot L} \tag{4.2}$$

where J is solvent flux, k is permeability coefficient, ΔP is trans-membrane pressure, μ is liquid viscosity and L is membrane thickness. As the viscosity and membrane depth were constant throughout all the experiments Equation (4.2) means that the solvent flux is proportional to the permeability coefficient multiplied by the pressure difference. As the value of permeability coefficient is fixed for any particular combination this means that the flux will be linearly dependent on pressure. This overall trend was in line with the data collected in the feasibility stages (Section 3.4.1) and in line with the work of Bhanshali *et al* (2001) who have noted that the solvent flux through polymeric membranes was dependent on parameters such as degree of crosslinking and solvent type which were constant throughout. Teixeria *et al* (2005) have also confirmed linearity between solvent flux and trans-membrane pressure for nanofiltration membranes.

Table 4.1 shows the gradients of the linear trendlines through the origin which were fitted to the data. As linearity has been shown to be applicable for flux predictions, differences in the gradients can be considered to highlight any underlying trends elicited by the parameter choice. For example when considering the effect of membrane grade the gradient increases over the order 0.1% DBT / 0.3% DBT / 0.5% DBT meaning that the membrane grade directly affects the resultant flux rate, and so on. The units of the gradient were l m^{-2} hr^{-1} bar^{-1}.

Solvent	Solute	Membrane Grade		
		0.1% DBT	0.3% DBT	0.5% DBT
Heptane	910	9.0	5.9	1.6
	I3N	19.2	7.4	1.9
	I3A	43.9	22.2	2.2
Xylene	910	9.9	7.9	1.2
	I3N	19.7	8.1	1.1
	I3A	45.2	21.8	1.3
Octane	910	13.5	4.9	1.5
	I3N	22.0	6.5	1.3
	I3A	29.4	11.2	1.4

Table 4.1 – Flux trendline gradients for all crossflow experiments.

There seems to be an increasing trend when considering different solutes over the order 910 < I3N < I3A which should not exist. The solutes were added at levels approximating 30 ppm and so should not have such a large effect on the flux rates (Robinson, 2004). Therefore using this data for cross comparison between solutes should not be considered. This finding was not applicable to the 0.5% DBT grade as the noted increase was not apparent in this set. Each membrane grade set can be considered on its own to be correct as it was just that the confidence level drops when considering across solute trends. The flux data obtained was still required for the model analysis detailed in Chapter five. Additionally the solute based flux effect was not present in the rejection data which means that data set is valid. The reason for this effect is unclear as it does not correlate with the testing order, but as the membrane did

not change during the space of a single experiment the validity in the individual data points was high.

The rejection data also appears to be linear at the lower end of the pressures tested but the gain in rejection for unit increases in pressure decreases towards the higher end making the overall trend obey a standard form logarithmic function, see Figure 4.8. Figure 4.8 shows the standard logarithmic form applied to the data produced from the crossflow filtration tests using 910 solute and heptane solvent.

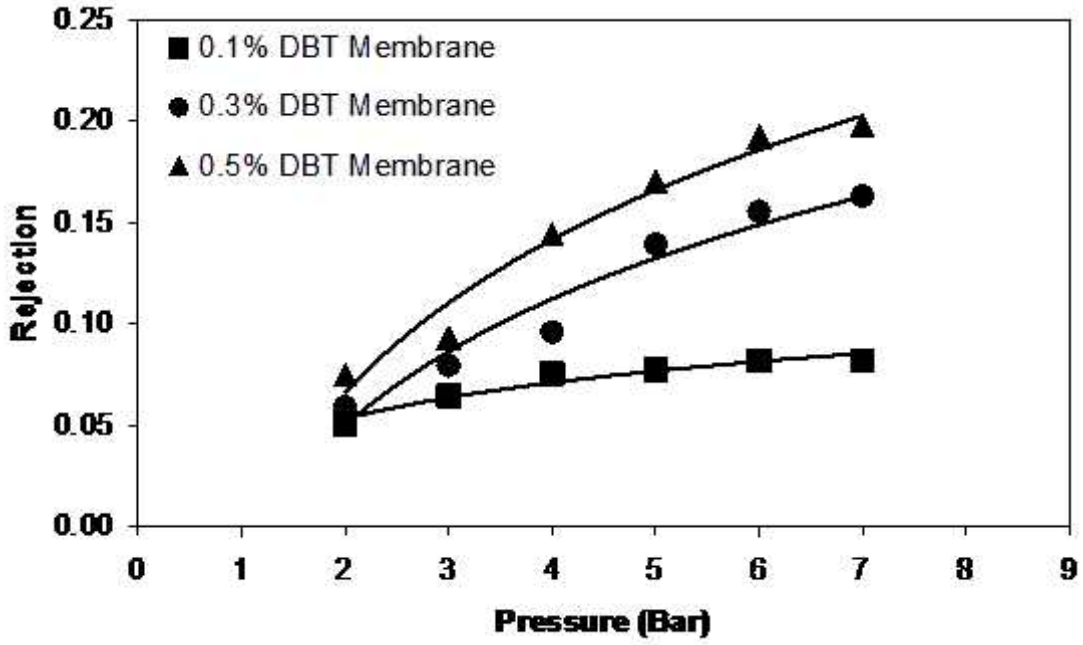

Figure 4.8 – Typical logarithmic correlation within crossflow filtration rejection data.

A logarithmic function (Equation 4.3) has been used to give an indication of trend. It is not intended to imply any physical meaning, although it does imply a significant membrane compaction effect is in evidence. Physical interpretations of data with models are stated in Chapter five. This trend means that, like flux, the efficiency of separation was aided by the increase in pressure, but only to a point. From a practical viewpoint this means that an optimum operating pressure must exist for each system which was a trade off between the beneficial separation dynamics and the detrimental increase in operating costs that operating at elevated pressures inevitably generates.

$$\text{Rejection} = A \bullet \ln(\text{Pressure}) \qquad (4.3)$$

where *A* is a trendline parameter chosen to minimise the total set error.

Table 4.2 shows the values of the fitting parameter *A* for the complete experimental set.

Solvent	Solute	Membrane Grade		
		0.1% DBT	0.3% DBT	0.5% DBT
Heptane	910	0.10	0.09	0.02
	I3N	0.08	0.03	0.19
	I3A	0.05	0.03	0.13
Xylene	910	0.01	0.02	0.10
	I3N	-0.02	0.04	0.14
	I3A	0.10	0.10	0.10
Octane	910	0.02	0.03	0.08
	I3N	-0.03	0.11	0.40
	I3A	0.01	0.01	0.16

Table 4.2 – Rejection trendline parameters (parameter A) for all crossflow experiments.

The first point of note within Table 4.2 was that two negative values exist, both for the 0.1% DBT membrane and both for the solute I3N. Both of these cases were on lines which were almost horizontal and the negative value exists as this was the best solution mathematically rather than practically. In reality the horizontal trend has occurred because either the experimental conditions have meant that the membrane was operating at the flat plateau to the right of the logarithmic trend line, or because the effect of pressure for this set of conditions was negligible, and the choice of a logarithmic trend was incorrect – these values were, however, still included for completeness. Of the two options the former seems more apt for this system but in any case the trend should be zero or slightly positive, rather than the slightly negative that has occurred.

The second point was that no consistent trend was able to be found in the values in the table, similar to that found in the table for flux (Table 4.1) for example the membrane grade order for the heptane was 0.5% DBT < 0.3% DBT < 0.1% DBT for 910 solute

and 0.3% DBT < 0.1% DBT < 0.5% DBT for both I3N and I3A solutes. A similar statement could be made for the other solvents and both solute and membrane grade. The fact that no underlying order was present was the reason why rejection characterisation was significantly more difficult than flux characterisation and it means that the following rejection analysis will have to be done on a case by case basis.

One way to characterise the rejection data was to look at the maximum separation that was achieved and average that across all completed tests using that substance. Table 4.3 contains this analysis along with the maximum and minimum individual results from that set. In Table 4.3 any obviously outlying points have been omitted to mitigate the effect these errors have. The values stated were percentages of total rejection, where 100% signifies complete rejection and 0% signifies no rejection. Sections 4.3.2 through 4.3.4 discuss the outlying points.

		Rejection (%)		
		Average	Minimum	Maximum
Substance ID	Heptane	20.35	8.18	36.17
	Xylene	38.73	11.71	69.13
	Octane	24.38	5.25	69.79
	910	15.65	5.25	37.89
	I3N	38.55	16.85	69.79
	I3A	29.26	8.03	69.13
	0.1	18.13	5.25	42.28
	0.3	23.86	9.17	49.32
	0.5	41.47	14.42	69.13

Table 4.3 – Analysis of maximum rejection results.

The correlation between the rejection data and the theoretical logarithmic fit that has been proposed was significantly lower than the correlation found between the flux data and the proposed linear fit, and as such the regression coefficient, product moment correlation coefficient (PMCC), was typically lower for the rejection data than the flux. On average, the PMCC for flux was 0.903 and for rejection, 0.504 – this calculation includes all outliers which were the main reason for this drop in confidence level. The visibly higher extent of scatter within the rejection data was inherent to the measuring

procedure and although this does not mean that the data produced was suspect in validity, it does mean that a simple PMCC calculation including all data points is.

The following sections detail the outliers and unexpended trends found in the raw data for each solvent. First the flux data was considered as a single set, and then the rejection data was considered as nine individual sets due to the increased scatter found. These sections primarily discuss results obtained which fall outside the previously determined repeatability limits for the produced membranes.

4.3.2. Heptane Based Tests

4.3.2.1. Flux Results

The flux results all conform to the linear trend explained in the last section with a regression coefficient of at least 0.8 and all but one of the tests conforms to a regression coefficient greater than 0.9. The test which has the lowest regression coefficient (i.e. the worst data set at proving linearity) was the heptane/910/0.1 set, which can be seen in Figure 4.9. The stepped nature of the data is thought to have arisen due to the feasibility testing already discussed in Section 3.4. As previously detailed the data points at 3, 5 and 7 bar are an average of the five tests completed in the feasibility stage, compared to the other points in this set which were from single tests. A similar pattern can be noted, albeit on a much reduced level, in the data set for heptane/910/0.3, however the regression coefficient for this set was 0.9067 so it does not cause any analytical problems. The remaining flux results do not display any significant deviations from those expected.

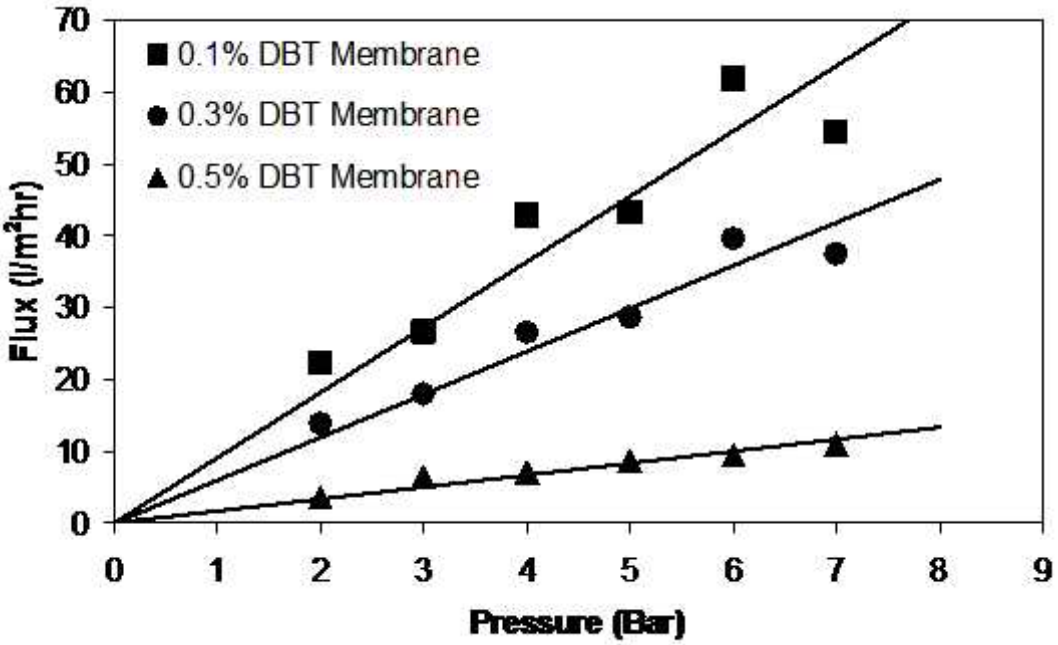

Figure 4.9 – Crossflow flux results for heptane solvent and 9,10-diphenylanthracene solute.

4.3.2.2. Rejection Results

The three tests using Iron (III) Acetylacetonate all demonstrate the logarithmic trend to a point but all the individual sets contain outlying points where the actual rejection result lies significantly different from the expected result. Of these deviations the most prominent was the 4 bar result for the 0.5% DBT membrane, where an apparent rejection of 49% was recorded when in truth the trend suggested a value of 25% be more appropriate for the conditions, see Figure 4.10. As this deviation is significantly outside the reproducibility extent confirmed in Section 3.4.2, it is thought to be an isolated case. Deviations such as this graphically display the inherent variation present within the experimental system, however any such deviations were shown up when considering the set as a whole meaning that multiple deviations, each one deviating proportionally to the last, would be required to produce a chart with the wrong characteristics.

Overall a few outlying points were to be expected with any experimental process and their presence does not invalidate the quality of the remaining data points.

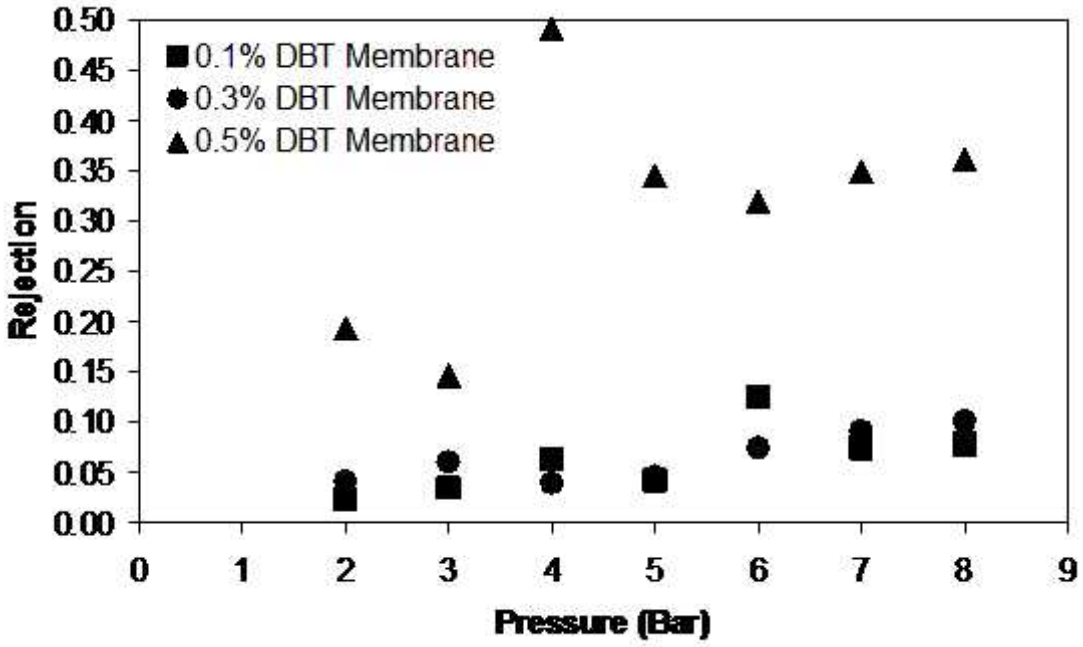

Figure 4.10 – Crossflow rejection results for heptane solvent and iron (III) acetylacetonate solute.

The results for the iron (III) naphthenate tests have produced two points of interest. First, the 0.5% DBT membrane set contains one deviated point at 4 bar, but when this was excluded, the remaining points form an almost perfect (PMCC = 0.9964) linear trend through the origin. Such a close approximation to linearity was strange considering the logarithmic trend that has been present in all the other sets so far discussed, but it simply means that the pressures used were not sufficiently high for the curved section to be pronounced as the lower section of a logarithmic curve appears linear.

4.3.3. Xylene Based Tests

4.3.3.1. Flux Results

The nine flux trends which use xylene as the solvent component all obey Darcy's law, with the possible exception of one. The results for the 0.3% DBT membrane using xylene solvent and I3A solute produced a PMCC value of only 0.609, see Figure 4.11. This anomaly seems to have arisen because of a slightly high result for the 5 bar test and a slightly low result for the 8 bar test, which was still inside the base deviation already shown. As when these were excluded from the remaining data points the

PMCC value increases to 0.871 which was more inline with the other runs in the set. In an ideal situation these two tests would have been redone, however if repeats for this type of minor deviation were undertaken the additional time this would have added to the project would have been prohibitive.

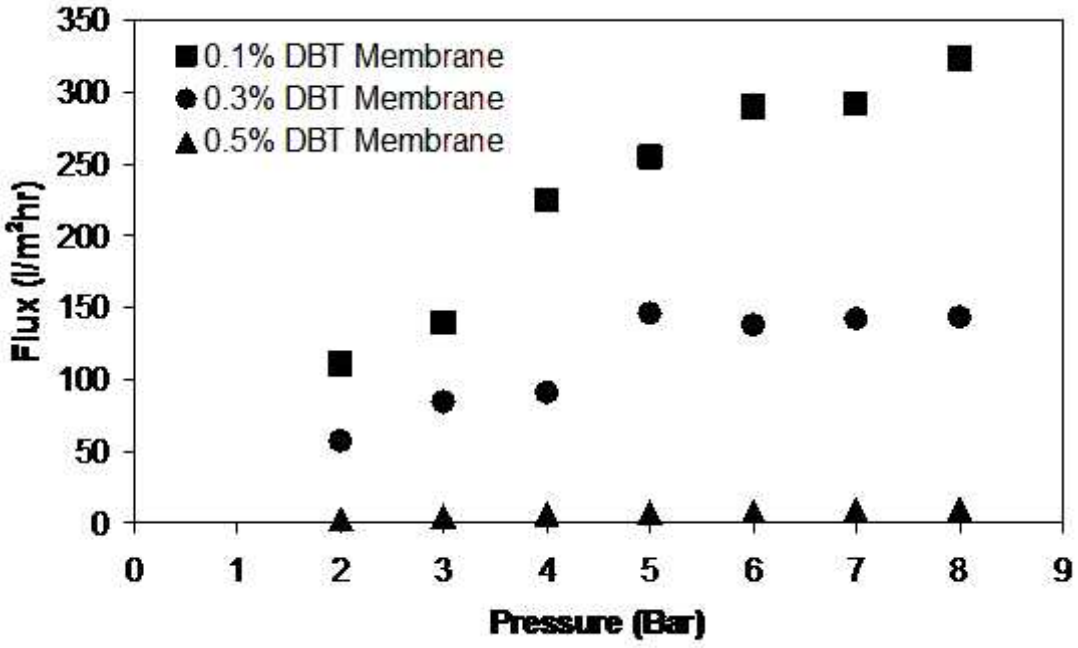

Figure 4.11 – Crossflow flux results for xylene solvent and iron (III) acetylacetonate solute.

4.3.3.2. Rejection Results

The three iron (III) acetylacetonate data sets can be approximated by the logarithmic trend. These results feature a few outliers with the most prominent being the 5 bar result for the 0.5% DBT membrane which appears to be about 15% lower than it should. The reasoning behind this was the same as for the heptane based deviation previously noted, but it does mean that such deviations were not just limited to a specific solvent.

The iron (III) naphthenate data sets were like the others in this group and show the expected trend shapes with some deviation on individual points, however an interesting effect occurred with the limits of each membrane grade see Figure 4.12.

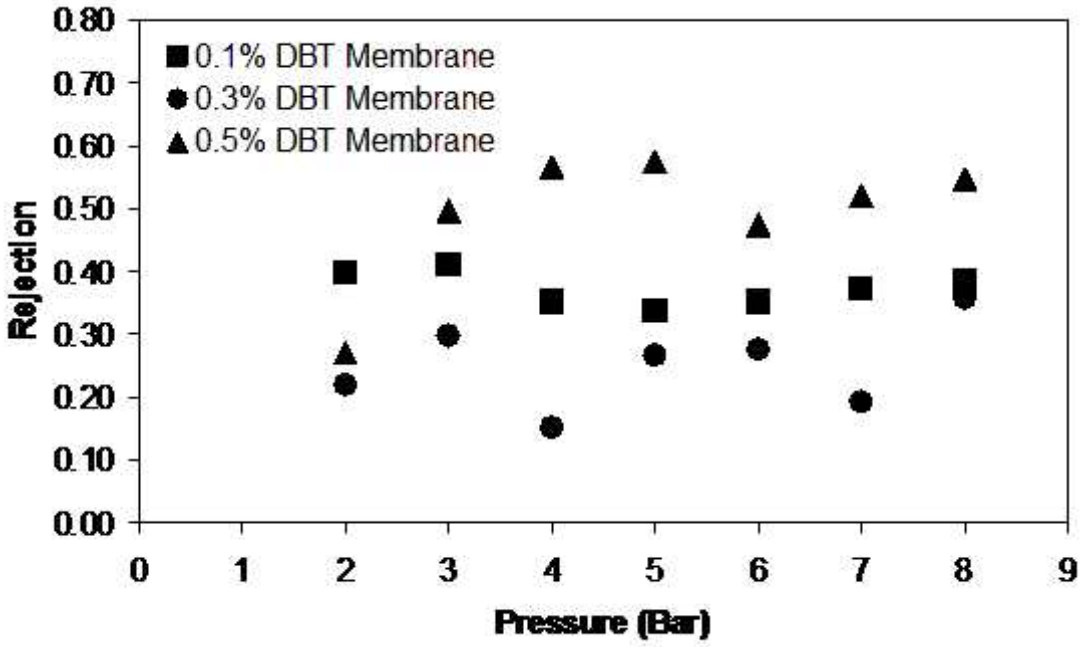

Figure 4.12 – Crossflow rejection results for xylene solvent and iron (III) naphthenate solute.

As can be seen from the chart the rejection results for the 0.1% DBT membrane were higher than those for the 0.3% DBT membrane across the entire range of pressures tested. This result was opposite to all the other experiments carried out and also different to the theory behind membrane manufacture. The theory was that higher membrane grades included more homogeneous catalyst during manufacture, which would result in relatively more crosslinking, an overall decrease in the size of the transport regions and ultimately produce a higher rejection. As this reverse trend has occurred in only one set it was considered to be an anomaly; however noted the trend is supported by some of the previously discussed polymer slab data. During the polymer swelling experiments (Section 3.1.2.4) it was found that no real dependency could be assigned between catalyst amount and swelling extent, and if swelling is not dependent on membrane grade the relative rejection extent need not follow the same trend as membrane grade. Additionally the membrane swelling data detailed in Section 3.5.3 supports this result for similar reasoning.

4.3.4. Octane Based Tests

4.3.4.1. Flux Results

The flux results for the octane based tests were generally good with only one point worth discussing in this section. The point in question was the 910/0.1/8 bar result, which can be seen in Figure 4.13. It can be seen that this point was around 50 l/m^2 hr greater than it should be. This point was an obvious anatomy in the data and simply should not be considered (or rather repeated if time constraints were slacker), however it has been mentioned as it was the single largest deviation from an expected point in the entire filtration data set. The reason for such a large discrepancy was unknown as the most likely reason (the membrane was not seated properly in the cell) was ruled out as the rejection extent coupled with this result was of the correct magnitude. All the other flux data points in this set were inline with the expected trend.

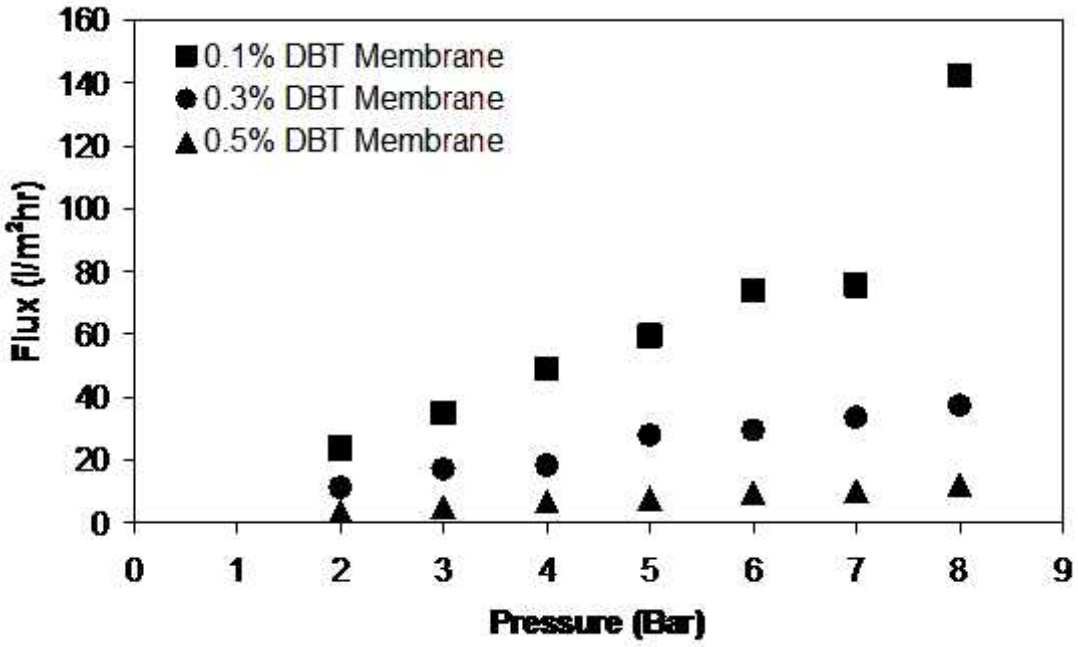

Figure 4.13 – Crossflow flux results for octane solvent and 9,10-diphenylanthracene solute.

4.3.4.2. Rejection Results

The rejection results for the octane based tests have not produced any new points, which have not already been covered in the discussion of the heptane and xylene tests.

4.3.5. Effect of Operational Parameters on Flux and Rejection

The effect different parameters have on the physical properties of the membranes produced has already been discussed, however the point of this section was to consider any additional implications these choices have on the flux and rejection properties of the tested membranes.

4.3.5.1. Effect of Solute on Flux and Rejection

The effect the choice of solute had on the flux of the 0.5% DBT membrane is considered here. The 0.1% DBT and 0.3% DBT membranes were not considered for the reasons outlined in Section 4.3.1. The first thing to note in Table 4.1 when considering the effect on flux rates of different solutes is the relative spread of data by solvent. For example a difference of 0.599 l m^{-2} hr^{-1} bar^{-1} was found between the largest and smallest heptane result, but a similar calculation for xylene produced a difference of only 0.176 l m^{-2} hr^{-1} bar^{-1}, octane's range falls between these two extremes. This difference was due to the relative extent of swelling and is covered in Section 4.3.5.2, but it does mean that any solute trend should be more evident in the heptane data than the other solvents due to the larger range present in this combination. Considering the heptane results the choice of solute seems to have a effect on flux rate through the membrane where the 910 solute retarded the flux rate the most and I3A solute elicited the largest flux.

A full discussion about the reasons for this order has been included in section 5.3.3, as it seemed more relevant to the overall trend analysis in that chapter. Briefly, the reason for this trend has been attributed to the relative approximation each solute molecule was to a sphere. This was due to the random arrangement of polymer chains in the matrix and the probability that a spherical object could randomly pass through the inter-polymer spaces with a higher likelihood than a highly non-spherical object.

As can be seen from Table 4.3 this solute order was almost the same for rejection as it was for flux. The 910 solute produces the lowest average rejection, next was I3A producing almost twice the rejection of 910, and I3N having the largest rejection of all. This result can again be linked to the size of the solute a molecule present, as 910 produces the lowest flux, the lowest rejection and was the smallest of the three solutes tested. This implies that whilst a large amount of 910 molecules must be passing through the membrane, they must also be close to the characteristic pore size of the membranes produced, blocking some of the passageways and lowering the overall flux. The larger solutes have higher rejections but also higher fluxes as the solvent was still able to make it through the membranes structure to a reduced extent. The choice of solute had an interesting effect on the performance of a chosen membrane but in real life it was unlikely that choice of solute will be a viable option, it was more likely to have to filter whatever had been produced by another unit operation, so solute choice whilst unrealistic was something to bear in mind for large scale operations.

4.3.5.2. Effect of Solvent on Flux and Rejection

From Table 4.1 it was able to be seen that for the nine constant solute/membrane combinations, two favour the heptane<xylene<octane combination for flux magnitude, where as another three favour xylene<octane<heptane and the final four demonstrate the order octane<heptane<xylene. So it initially seems for the range of solvents tested, this choice has no great bearing on the inherent flux dynamics. However if just the 0.5% DBT membrane results were considered (the data set with the most confidence) the order from smallest to largest flux was xylene<octane<heptane. This order was the most logical as it mirrors the already established swelling profile demonstrated in Section 3.1.2.2 and in the literature by Tarleton et al (2005, shown as Figure 2.10). The result means that the largest solvent flux was generated by the solvent which swells the polymer the most and conversely the lowest flux was generated by the solvent which swells the polymer the least. This result is in line with the findings of Dijkstra *et al* (2006) who noted as the membrane swells the permeability will increase as new, larger channels are formed in the matrix leading to higher solvent fluxes. Swelling based flux rates have also been found by Robinson et al (2004) for a similar experimental set up (detailed in Section 2.2.2)

Considering rejection, from Table 4.3 it can be seen that the highest rejections were obtained when using xylene solvent and the worst when using heptane (38.37% Vs.

20.35%) whilst octane falls in between the two (24.38%), but closer to the result for heptane. This order again directly correlates to the measured extent of polymer swelling which in turn relates it to the inherent solubility parameter of the material, i.e. the closer the solvent is to PDMS (in terms of solubility parameter) the greater the effect on both swelling and rejection. When the active layer swells, it increases in volume, but the mass of polymer chains must be the same, therefore the spaces between adjacent chains (transport regions) must increase to increase the overall volume. When this occurs, the apparent pore size of the membrane must increase as well. Heptane has been shown to swell the active layer the most so it was logical that it would be the worst solvent for rejection, the solute molecules can more easily pass through the enlarged matrix. The converse was also true as xylene, the solvent which swells the active layer the least, had a higher rejection for otherwise identical conditions as the matrix was more dense making solute transport less easy. Gevers *et al* (2006) have reported that non-polar solvents swell PDMS membranes to a greater extent than polar ones. This finding was inline with the work of Doig *et al* (1998) who noted that as the fraction of solvent in a swollen membrane increased, the membrane resistance for certain solutes decreased, leading to a lower total rejection.

4.3.5.3. Effect of Membrane Grade on Flux and Rejection

Reading Table 4.1 in rows highlights the nine constant solute/solvent combinations relevant for checking the effect of different membranes and as can be seen there was a high correlation between grade and flux. A strongly negative trend was inherent within these results with a higher grade producing a lower flux. On average the results for the 0.3% DBT membrane were about half (47.7%) that of the 0.1% DBT membrane and the 0.5% DBT membrane was about a fifth (18.0%) of the 0.3% DBT membrane. This correlation between membrane grade and flux had already been discussed in Sections 3.4 and 4.3 and does not need to be repeated here, save to say that these results add further weight to the previously drawn conclusions regarding this phenomenon.

As with flux the effect of membrane grade on rejection was also logical. Looking at the values in Table 4.3 it can be seen that the highest rejection was obtained when using the 0.5% DBT membrane, then the 0.3% DBT membrane and the lowest rejection was realised with the 0.1% DBT membrane. As it had already been shown the higher grade membranes were produced stiffer by the introduction of a larger amount of catalyst which had created more crosslink's between individual polymer chains and had led to a denser active layer. This means that the size of the transport regions of the membrane

grades decreases in the order of 0.1>0.3>0.5, so it was logical that rejection increases as well.

4.3.6. Review of Flux and Rejection

It has been shown that the choice of solute had an effect on the filtering characteristics of the membranes tested, for flux the variation was inline with the aspect ratio of the solute molecule and for rejection it was found that the larger solutes were rejected more than the smaller solutes, which means that a size exclusion mechanism must be at least partially evident in the transport mechanism. It has been found that both flux and rejection are affected by solvent type with the higher swelling solvents producing the dual effects of higher flux and lower rejection. The extent of this effect has also been shown to correlate with the difference in solubility parameter between membrane and solvent. Finally the effects of membrane grade were shown to include the expected dual phenomenon of higher rejection and lower flux when considering higher grades. This result was in line with the concept of increased crosslinking bonds being formed in higher grade membranes.

4.4. Solute Size Analysis

One of the primary aims of this work was to characterise the membranes produced by determining the effective pore size. The pore size determination is discussed in Chapter five along with the relevant model; however the separation trend discussion was included here as it was related to the experimental work presented in this chapter. By using the rejection data obtained from the crossflow filtration experiments it was possible to produce charts similar to Figure 1.1. These are included as Figures 4.12 and 4.13. From the data collected it was possible to create a vast number of different charts by varying the membrane, applied pressure and solvent displayed, however as all the charts were similar only one typical representative of each type was shown. Figure 4.14 displays the results for the 7 bar tests using the 0.1% DBT membrane and Figure 4.15 displays the results for the 7 bar tests using octane solvent. Determination of solute size has already been discussed in Section 3.3.2.

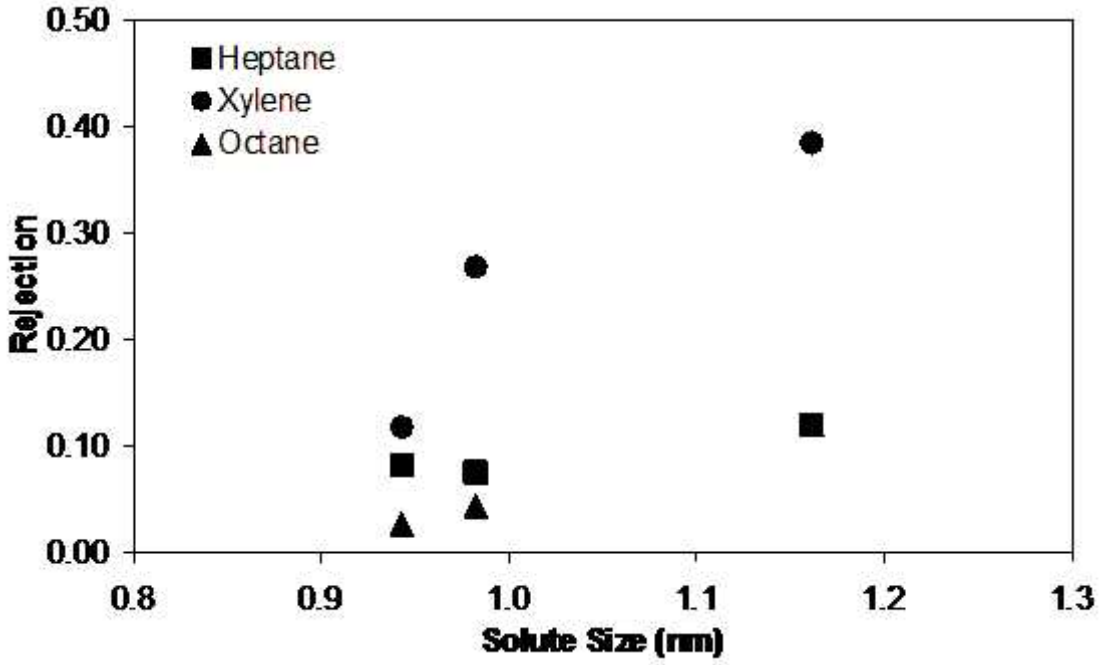

Figure 4.14 – Rejection against solute size – Solvent version / 7 bar.

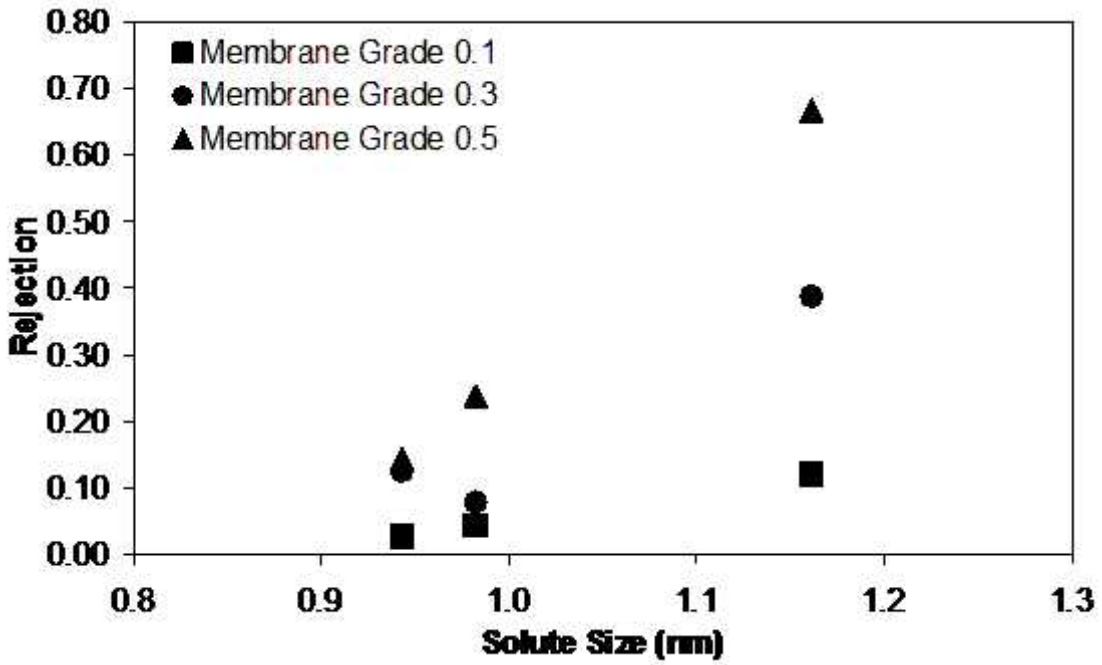

Figure 4.15 – Rejection against solute size – Membrane version / 7 bar.

Figure 4.14 shows, for the smaller solutes, the same solvent order as the swelling tests proved, i.e. as heptane and octane swell the polymer the most they would conversely reject the least and as xylene swells the membrane the least, it would cause rejection to be the largest. A similar phenomenon can be seen in Figure 4.15 where the

expected membrane grade trend was also apparent. The 0.1% DBT membrane rejects the least and the 0.5% DBT membrane rejects the most, in line with crosslinking extent. Overall, the correlation of the data to the expected trends is good, with only one point on each chart varying from the expected. This was most likely due to the small values obtained for those results. The MWCO of a membrane is the solute size which corresponds to 90% rejection (See Toh *et al*, 2007b) but as none of the experiments reached 90% rejection, the corresponding MWCO of the membranes tested can not be determined. This result was not important as determining the MWCO was not one of the main aims of this work, however with additional experimental work, specifically by testing larger solutes, this values could be determined. These findings reinforce the PDMS characterisation work of Chapter three, with agreement being found between solubility parameter and swelling extent and between the membrane grade and rejection.

4.5. Intermediate Conclusions

In this chapter the entirety of the membrane testing phase has been covered. In doing this, a new test cell had to be designed and produced, a testing methodology had to be devised and checked, and a significant experimental set had to be undertaken. In all, a total of 186 crossflow experiments (not including repeats) have been completed which represent the largest part of the experimental workload of this entire project. The results produced are logical and underlying filtration trends have been deduced. Both flux and rejection parameters have been shown to increase at higher pressures implying that the process was pressure driven, but the curvature in the rejection profiles means that an optimum operating point does exist. The benefit gained by increasing the operating pressure is not infinite. The dual effects of catalyst concentration were deduced with a higher concentration producing both higher rejection and lower flux. The converse was also true.

The flux relationship has been shown to obey Darcy's law and the rejection shows some correlation with a logarithmic curve. Overall the use of a linear trend to fit the flux data seems to be justified, all the experiments conducted obey this relationship and it can predict the membrane behaviour well. The prediction of rejection however has not been as straightforward. The general trend of rejection is that of a standard logarithmic curve which was found to describe the trend acceptably. The result that after an initial

linear section the rate of the curve decreases to form a plateau is indicative of membrane compaction. The variation between different rejection data sets was significantly greater than for the flux sets. Some of the tests have stayed in the initial linear section and some have stayed in the final plateau section. The underlying mechanics behind rejection are more complicated than the mechanics behind flux and seem to rely on more than a single parameter, with size exclusion and active layer swelling being primary candidates. Solving this mechanism was the purpose of Chapter five where several well known models were applied to the experimental results.

4.6. Nomenclature

J Solvent flux ($m^3\ m^{-2}\ s^{-1}$)

k Permeability coefficient ($m^2\ s^{-1}\ bar^{-1}$)

L Membrane thickness (m)

ΔP Trans-membrane pressure (bar)

μ Viscosity (Pa S)

4.7. References

Baker R.W., 2004, *Membrane Technology and Applications*, 2nd Edn. John Wiley & Sons, Chichester.

Bhanushali D., Kloos S., Kurth C., Bhattacharyya D., 2001. Performance of solvent resistant membranes for non aqueous systems: solvent permeation results and modelling, *J. Membrane Science*, **189**, 1-21.

Dijkstra M.F.J., Bach S., Ebert K., 2006. A transport model for organophilic nanofiltration. *J. Membrane Science*, **286**, 60-68.

Doig S.D., Boam A.T., Livingston A.G., Stuckey D.C., 1998. Mass transfer of hydrophobic solutes in solvent swollen silicone rubber membranes, *J. Membrane Science*, **154**, 127-140.

Gevers L.E.M., Meyen G., De Smet K., van de Velde P., Du Prez F., Vankelecom I.F.J., Jacobs P.A., 2006. Physico-chemical interpretation of the SRNF transport mechanism for solutes through dense silicone membranes, *J. Membrane Science*, **274**, 173-182.

Low J.S., 2004. A Study of Organic Solvents Nanofiltration, PhD thesis, Loughborough University.

Peeva L.G., Gibbins E., Luthra S.S., White L.S., Stateva R.P., Livingston A.G., 2004. Effect of concentration polerisation and osmotic pressure on flux in organic solvent nanofiltration, *J. Membrane Science*, **236**, 121-136.

Robinson J.P., 2004. The selective removal of components from gasoline using membrane technology, PhD thesis, Loughborough University

See Toh Y.H., Loh X.X., Li K., Bismarck A., Livingston A.G., 2007a. In search of a standard method for the characterisation of organic solvent nanofiltration membranes, *J. Membrane Science*, **291**, 120-125.

See-Toh Y.H., Ferreira F.C., Livingston A.G., 2007b. The influence of membrane formation parameters on the functional performance of organic solvent nanofiltration membranes. *J. Membrane Science*, **299**, 236-250.

Silva P., Han S., Livingston A.G., 2005. Solvent transport in organic solvent nanofiltration membranes, *J. Membrane Science*, **262**, 49-59.

Tarleton E.S., Robinson J.P., Low J.S., 2009. Nanofiltration: A technology for selective solute removal from fuels and solvents, *Chemical Engineering Research and Design*, **87**, 271-279.

Tarleton E.S., Robinson J.P., Smith S.J., Na J.J.W., 2005. New experimental measurments of solvent induced swelling in nanofiltration membranes, *J. Membrane Science*, **261**, 129-135.

Teixeira M.R., Rosa M.J., Nystrom M., 2005. The role of membrane charge on nanofiltration performance, *J. Membrane Science*, **265**, 160-166.

5. Transport Models and Discussion

Whenever a process is not fully understood, too expensive or too time consuming to optimise manually, models will be developed that attempt to predict the outcome of an experiment. In the current case that outcome is the flux-pressure and rejection-pressure relationships that exist between a specific membrane and the solution to be separated. These models are usually initially based upon experimental work, incorporating the experimental variables (such as trans-membrane pressure) and include at least one characterisation or fitting parameter. Ultimately all that would be required to model a new process would be to choose the correct value for the characterising parameters and the entire performance of a membrane would be known before even a single test had been run. In practice, skill and past experience are advantageous to choosing the appropriate values based on physical properties and, of course, some models simply fit better than others. The purpose of this chapter is to present the correlation between the experimental findings and the predictions from seven existing filtration models.

The models presented here have all been solved by the use of custom made Excel worksheets with embedded Visual Basic scripts. All the worksheets operate on the principle of minimising error, where error is defined as the sum of the absolute difference between the models predictions and the experimental result. A trial value was assigned to the fitting parameter and the predicted flux (or rejection) was calculated separately for each pressure. The difference between the predicted and experimental result was noted and summed over the entire pressure range tested. Then the trial value was altered and the total error was compared, with the value for the fitting parameter being chosen as the one which produces the smallest total error. For parameters which have a specific range, such as the reflection coefficient in the Speigler Kedem model which must be within the range $0 \rightarrow 1$, the worksheet systematically checks values within this range in steps of $1x10^{-3}$ to find the correct result. For parameters which are unbounded, the worksheets use graphical analysis to check for global minima before focusing in on the correct value – in all such cases accuracy to at least three significant figures was obtained. For multi-parameter models a looped macro was applied – the value of the first parameter was fixed and the best value for the second parameter found, then the value of the first parameter was step increased and the best value for the second parameter found again, and so on. When this process was completed the combination which corresponds to the lowest error was

chosen as the ‘correct’ values for the model. A similar process was also true for the solution of three parameter models.

5.1. Modelling Overview

One of the main topics of debate in the field of nanofiltration is the exact mechanism by which species are transmitted through the membrane, which can be thought of, in simplest terms, as the solution diffusion model versus pore flow model debate. For filtration processes that remove particulates in the ultrafiltration range or larger the pore flow model is generally valid, and for processes that operate at reverse osmosis sizes solution diffusion usually applies.

The division between the two models is not simply based on size as there is no definite size above which pore flow is valid and below which solution diffusion model is applicable, but instead an intermediate region exists, where pore flow is sometimes appropriate and other times solution diffusion is the correct choice. Which model is valid is dependent on the chemical species and filter media involved, specifically it is dependent on membrane form and membrane-solvent / membrane-solute interactions. As the operating range for nanofiltration falls squarely into this unclear region either model could be valid and so both models shall be outlined here. The following descriptions of the two models were adapted from Wijmans and Baker (1995).

Solution diffusion:

- Permeants dissolve in the membrane material.
- Permeants diffuse through the membrane material down a concentration gradient.
- Separation is achieved between different permeants because of differences in the amount of material that dissolves in the membrane and the rate at which the material diffuses through the membrane.

Pore flow:

- Permeants do not dissolve in the membrane material.
- Permeants are separated by pressure driven convective flow through pores.

- Separation is achieved between permeants because one of the permeants is excluded (filtered) from some of the pores in the membrane through which other permeants move.

The main difference between the two models is the definition of chemical potential gradient. For solution diffusion, pressure is assumed to be constant and the drive is provided solely by the concentration gradient. For pore flow, the concentration gradient is assumed to be constant and the drive is provided solely by the pressure gradient. This differences are highlighted in Figure 5.1.

Figure 5.1 – Conceptual differences between solution diffusion and pore flow. (Wijmans and Baker, 1995).

These two models have arisen due to the inherent difficulty in developing a transport model for non-aqueous nanofiltration with dense nanofiltration membranes. this endeavour has been complicated by the swelling of the membrane material by organic solvents, noted in Chapter three. As the membrane swells the permeability will increase as new, larger transport regions are formed in the matrix leading to higher solvent fluxes (Dijkstra *et al,* 2006). From a review of available literature the selection of the correct model seems to be arbitrary, as many authors simply apply several models to their experimental data and take the one which provides the best prediction. Both Yang *et al* (2001) and Han *et al* (2003) have published work stating that the pore flow model was more appropriate for their respective systems, but White (2002), Peeva *et al* (2004) and Bhanushali *et al* (2001) have all published articles in which the solution diffusion model was used to infer experimental results. From this review the most diligent practice seems to be to wait until at least preliminary experimental data has been recorded before deciding which model was best for any new application.

Yang *et al* (2001) described a series of experiments filtering dyes from a range of aqueous and organic solvents. The experiments were carried out using a dead end filtration cell operating at a pressure of 30 bar and total of six commercially available membranes were tested. It was reported that a neither viscosity nor surface tension of the solvent used explained the flux results obtained and therefore the transport mechanism cannot be based solely on viscous flow through pores. The work goes on to compare the manufacturers stated MWCO value to the experimental results and notes that the nominal values worked out for aqueous systems might not be valid for

organic systems and that the transport mechanisms may be different. The work concludes that the specific interactions between the solvent and membrane are important and must be considered for each process implying that a blanket transport property is impossible.

In a 2002 work by White, six different solutes were separated from toluene based solutions by the use of several different SRNF membranes. The solutes took the form of both branched and straight chain hydrocarbons with molecular weights ranging from 142 to 310. For each membrane it was found that rejection increased with increasing solute molecular weight. It was also noted that both flux and rejection were increased by reducing the initial feed concentration of solute. Although each membrane had a different value of MWCO it was noted that the relative order of transport of the different solutes was unchanged. This result was consistent with a solution diffusion mechanism governing the solute transport.

Bhanushali *et al* (2001) found similar results when testing the permeation of three different commercial membranes. In the study the flux rate of up to ten different polar and non-polar solvents was assessed by a series of batch dead end filtrations utilising compressed nitrogen as the driving force. The tests were conducted up to a pressure of 100 bar. It was noted that a good understanding of the specific polymer-solvent interactions was critical in the prediction of transport mechanisms. The data obtained from the hydrophobic membranes was generally good and successfully predicted by the SD model (R^2 = 0.89). The report concludes that for non-polar solvents the membrane must be correctly chosen as the relative permeation of hexane and methanol was reversed over the range of membranes tested.

It is acknowledged that there are many more transport models than the two explained here however the purpose of this section was to illustrate the difficulty of choosing the correct model rather than the actual models presented. Solution diffusion versus pore flow was chosen as it is the classic example of completely different models occurring from a simple difference in the base assumptions.

5.2. Application of Models to Data

From the experiments detailed in Chapter four, 27 sets of data were obtained (flux and rejection relationships from a matrix of three solvents, three solutes and three membranes). Seven well established models were applied to these sets in order to determine which models best predict the experimental findings. By this approach two of the main aims of this work were addressed – identification of transport mechanism and determination of effective pore size. The transport mechanism was determined by the application of the data collected from the crossflow experiments to the models presented in this chapter. The effective pore size was found by using a pore flow model (detailed in section 5.2.2) to establish the best fit for the parameter. The models chosen span a reasonable range of criterion; there were representatives of diffusive transport, convective transport and hybrid models, there were representatives of single, double and triple parameter models and there were representatives of older models (*ca.* 19th century) right up to recent additions (2009). Each model was discussed in detail in its individual section with comparisons between models saved for Section 5.3. For space concerns charts of each of the 27 experimental combinations have not been included for each model as many of the charts are similar. Any chart shown in this section can be assumed to be representative of the whole set unless specifically stated otherwise.

Each of the individual model sections follows the same progression. A description of how and by whom the model has previously been used by comes first. Then the equations used are stated, this part was important as during the research stage it was found that some of the models have no standardised form (i.e. they do not have a single defined form) and significant differences can be found in the equations of supposedly identical models. Finally the degree of correlation between the model and the experimental data was discussed, including an analysis of the sensitivity of the fitting parameters with regards to error where applicable. When discussing compiled data the standard procedure was to look for patterns or trends and as the results from these models exist as 27 experiments based on three parameters (solute, solvent and membrane), the trends can be discussed by keeping any two of the parameters constant and looking at the effect of the third parameter. This leads to six different ways of assessing trends in each data set, all of which will be considered within the relevant model's section but only the most prominent individual patterns will be noted here, as well as the overall fit. The transport mechanism discussion is included in Section 5.3 after each model has been assessed individually.

5.2.1. Convection Diffusion Model

Due to irregularities in the size of the inter-polymer transport regions within the random polymer matrix, a size distribution of transport regions must exist. When a solute is in a pore significantly larger than itself, transport can occur due to convection, but when a solute is in a transport region of a similar size this can not happen. In these cases diffusion takes over and is responsible for transport. The Convection Diffusion (CD) model tries to allow for both of these mechanisms by considering both convective and diffusive transport, hence the name. The CD model has been applied by Tarleton *et al* (2005)

The CD model can be used to interpret both the flux and rejection relationships, via equations (5.1) and (5.2).

$$J_s = \frac{k\Delta P}{x} \tag{5.1}$$

$$R = \frac{1-a}{1+\frac{(1-a)D_i}{k\Delta P}} \tag{5.2}$$

where J_s is solvent flux, x is membrane thickness, k is permeability coefficient, ΔP is trans-membrane pressure, R is rejection, D_i is diffusion coefficient and 'a' is fraction of solute undergoing viscous flow.

Equations (5,1) and (5.2) were taken from Robinson (2004). To solve the model, as with all the models presented here, the flux part was converged first. Convergence was done by finding a value of k which corresponds to the minimum error, the minimum deviation between the predicted and the recorded. The value of k was then used in Equation (5.2) with the values of a and D_i being determined. The value of a had to be within the range of 0~1 to ensure the rejection value stays positive. Figures 5.2 and 5.3 show the best fit of the CD model for the experimental set up using 9,10-diphenylanthracene solute, heptane solvent and 0.3% DBT membrane. The charts shown are typical of the output from this model.

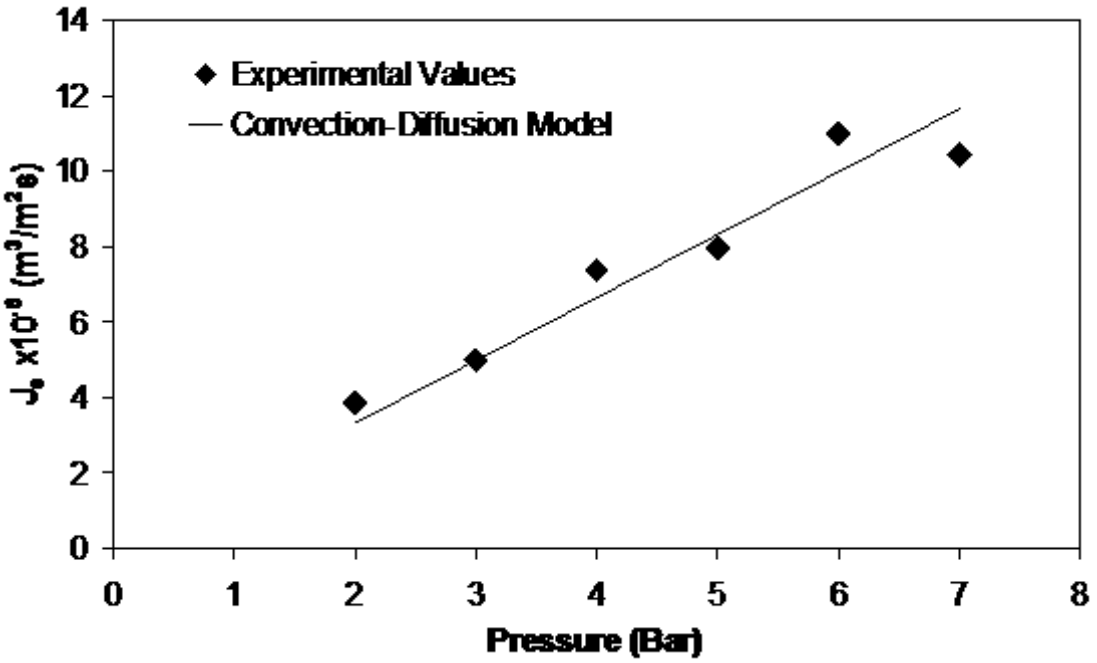

Figure 5.2 – Typical convection diffusion prediction vs. experimental data – flux version.

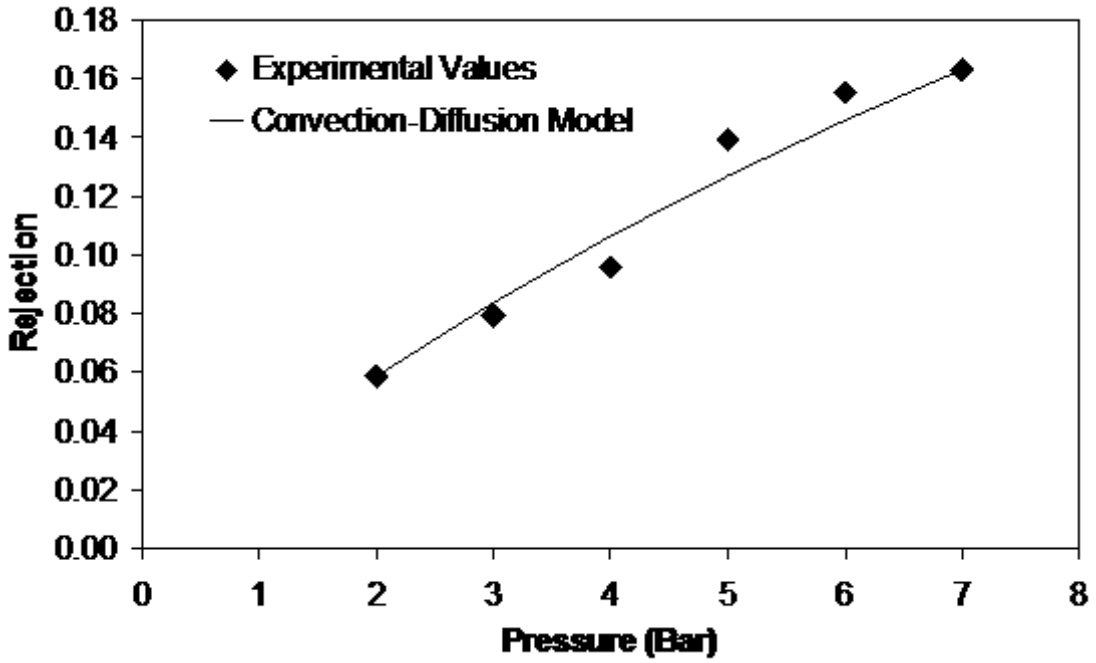

Figure 5.3 – Typical convection diffusion prediction vs. experimental data – flux version.

The CD model predicts a linear relationship for flux and a curved relationship for rejection, both of which exist in close proximity to the experimental data implying that

this model was adequate to predict this type of behaviour. The fit the model demonstrated between the predicted and experimental rejection produced the smallest total error of all the models tested and should be used to predict the characteristic in processes using these conditions – see Section 5.3.2 for a more in-depth discussion on this point.

This model uses a characterisation parameters for the flux and two fitting parameters for rejection, one of which must exist in the range of 0 to 1. There was a strong trend between the characterisation parameter *k* and membrane grade. For any constant solute and solvent combination, the value of *k* decreases by approximately an order of magnitude between each membrane from 0.1% DBT to 0.5% DBT. For example the tests using 910 solvent and octane solvent, recorded a value of *k* of 6.47×10^{-10} $m^2 s^{-1} Bar^{-1}$ for the 0.1% DBT membrane and a value of 8.28×10^{-11} $m^2 s^{-1} Bar^{-1}$ for the 0.5% DBT membrane. There was no prominent discernable trend between *k* and either solvent or solute, meaning that *k* for the experiments tested was only a function of filter media not the filtrate. However a similar argument can not be made for either D_i or *a* as there seems to be no correlation between these values and any of the parameters, solute, solvent or membrane grade. A more complete discussion of these points exists in Section 5.3.3.

5.2.2. Pore Flow Model

The Pore Flow (PF) model is not a singular defined set of equations but rather the generic name for a group of models which have the core principle that filtration occurs through rigid pores of a finite size. This concept was first proposed sometime during the 19th century (Wijmans and Baker, 1995). For example both the Speigler Kedem model described below and this model fall into the pore flow category, although Speigler Kedem also has convective components. As the model in this section does not have an official name (it is a modified extended Nernst-Planck equation) it has been designated the PF model for the purpose of this work. This designation should not be taken to imply that this model is more representative of the PF philosophy than others described here.

The pore flow model has been applied many times by authors such as See-Toh *et al* (2007), Silva and Livingston (2006), Ahmad *et al* (2004) and Szymczyk *et al* (2003). The PF model can be used to predict the rejection relationship only, the main equations for which can be seen as Equations (5.3) and (5.4). In addition to these two equations

there were eight other equations used in the model to calculate intermediate parameters, these have not been reproduced here but are available in See-Toh *et al (*2007).

$$R = 1 - \frac{\Phi_i \cdot K_{i,c}}{1 - \left(\left(1 - \Phi_i \cdot K_{i,c} \right) \cdot e^{-P_{i,e}} \right)} \tag{5.3}$$

where,

$$P_{i,e} = \left(\left(\frac{K_{i,c}}{K_{id} \cdot D_{i\infty}} \right) \cdot \left(\frac{r_p^2}{8\mu} \right) \right) \cdot \left(\frac{\Delta P}{J} \right) \tag{5.4}$$

where Φ_i is partition coefficient, $K_{i,c}$ is solute convective hindrance factor, $K_{i,d}$ is solute diffusive hindrance factor, $P_{i,e}$ is solute permeability, $D_{i,\infty}$ is diffusivity in dilute bulk solution, r_p is pore radius, and μ is viscosity.

This form of the model was taken from See-Toh *et al* (2007), where it has been derived from the extended Nernst-Planck equation, subject to the following assumptions.

- Parabolic fully developed solute flow exists within the transport region.
- Interactions between the solute and pore wall are completely steric.
- The effects of concentration polarisation are neglected.

This version of the pore flow model was different to the other models described, in that rather than predicting the rejection profile, this model aims to estimate the effective pore size. All of the terms in Equations (5.3) and (5.4) are either constants or solely calculated from constants except for r_p – the radius of the membrane pores. This outcome means that by choosing different values for r_p and checking the error between the predicted and measured rejection, the optimum value of r_p can be determined. The model was applied by first choosing a range and step interval of trial r_p values, with the default settings being: start at 5×10^{-11} m, end at 1×10^{-8} m and step size of 5×10^{-11} m. The program then checked each of the 200 trial values and produced a table of the relative error of each trial value. Error in this case is defined as the total difference between the experimental values for rejection and the corresponding prediction from the model, over all the pressures tested. The correct value of pore radius was then assumed to be the value which produced the lowest error, i.e. the value at which the model produced the best agreement with the experimental results. A typical error vs. pore radius graph is shown as Figure 5.4.

During the calculation of the optimum r_p an interesting trend was noted in the extent of error for different trial values of r_p, an example of which can be seen as Figure 5.4. The curve shown is for 9,10-diphenylanthracene solute, octane solvent and 0.1% DBT membrane, however the form was representative of all the analysis performed.

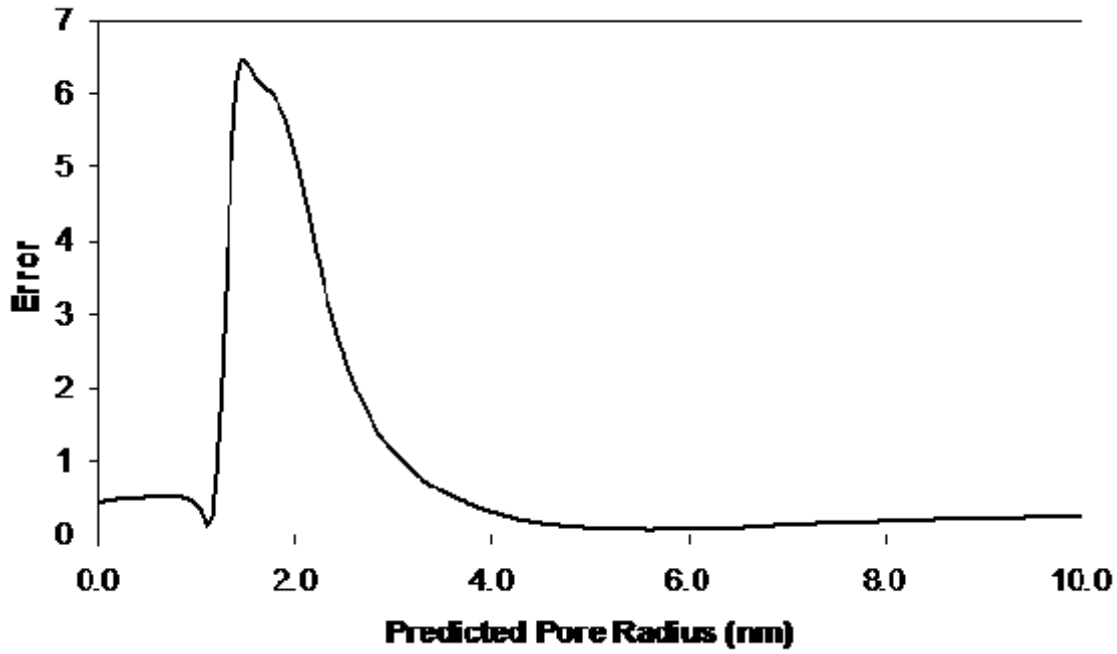

Figure 5.4 – Total error in relation to pore radius.

There are two noteworthy points in this graph; first a total error of zero was not possible, and second, there exists two minima. The former means that whatever value of pore radius was chosen the prediction will not be completely accurate, which was to be expected as natural variation in experimental data means that no fitted model will ever be 'completely' accurate. The latter means that both minima will need to be checked to verify which was most accurate.

For each of the 27 combinations (solute/solvent/membrane) a double minimum was noted, one near the size of the solute (Table 3.3) in question and one several times larger than the solute. From this it has been assumed that the minimum furthest from the solute size exists as a mathematical possibility only, and was in fact erroneous. This conclusion was drawn as it is unlikely that a pore 10 nm across (5 nm radius) would be able to filter out solutes less than 2 nm long. It is acknowledged that due to effects of charge difference and tortuosity a 10 nm pore could filter 2 nm solutes, however as these effects have not been proved to exist in this case, the most sensible

course of action is to assume the larger pore size is erroneous. The smaller pore size minimum has been adopted as the actual pore size for the membranes produced and will be the value given in the remainder of this section unless otherwise stated.

With the correct value for pore radius determined the pressure-rejection profile of the model was produced by using the experimental values for flux and pressure in Equation (5.4). A typical fit of this model is shown as Figure 5.5 which features data from the tests using iron (III) naphthenate as the solute, octane solvent and 0.3% DBT membrane as well as the model prediction. The chart shows a good fit of the correct shape which could be used with confidence to predict experimental data.

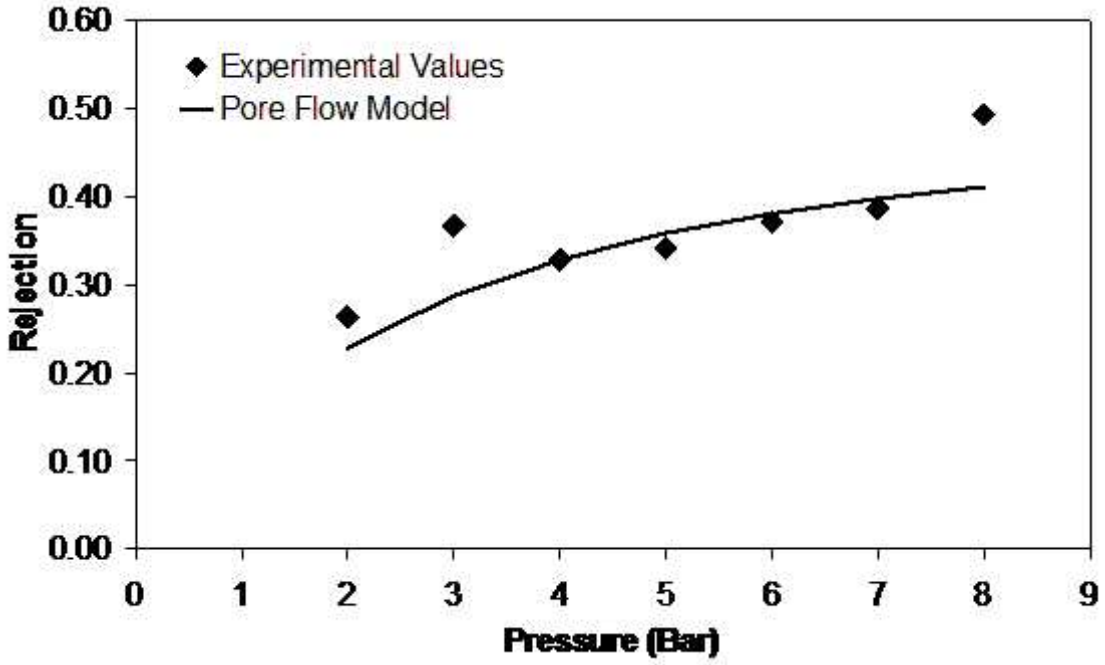

Figure 5.5 – Typical pore flow prediction vs. experimental data – rejection version.

With the model applied to every data set, trends within the results were checked for. Looking at the predicted pore radii, little to no pattern can be discerned between r_p and solute, with a minor trend between r_p and solvent type (see Figure 5.6). A strong trend also existed between membrane grade and predicted pore radius (See figure 5.7).

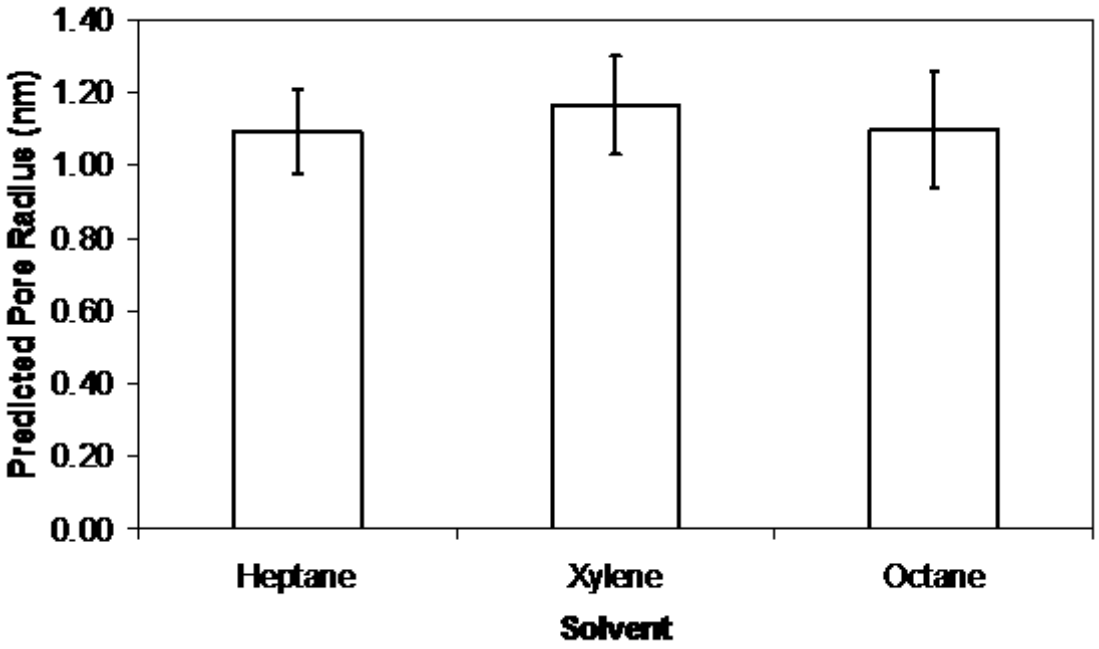

Figure 5.6 – The effect of solvent type on predicted pore radii.

Overall the predicted pore radius varies between 0.94 and 1.42 nm but if the limits of each solvent were considered, the xylene tests produced pore radius estimates of between 1.02 and 1.42 nm, the octane tests between 0.94 and 1.35 nm, and the heptane tests between 0.96 and 1.30 nm. The average pore radius can be related to the solubility parameter driving force (Table 3.2) which in turn can be related to the extent of swelling each solvent produces. From the work in Chapter three it was known that the order of effect from greatest to smallest was heptane (0.2 $MPa^{0.5}$ difference), octane (1.2 $MPa^{0.5}$ difference) and finally xylene (2.7 $MPa^{0.5}$ difference), and this same trend was noted in the predicted pores sizes, with heptane producing the smallest pore radius prediction and xylene the largest. This result means that the larger swelling solvents produce the smallest predicted pore sizes which can be explained by considering the effect of polymer swelling. The pore flow model assumes the presence of rigid pores so as the polymer swells these pores will be constricted by the expanding polymer reducing the pore diameter. This means that the effective pore size of the membrane is not a fixed value but will vary based on the solvent(s) used and the relative extent of swelling.

A second trend within this data was expected to exist between predicted pore size and membrane grade. This work has been based on the fact that the three membranes were different, with the grades higher in catalyst composition having a greater extent of crosslinking and logically a smaller pore radius. Figure 5.7 shows the average

predicted pore size for each of the membranes – that was the average of the nine experimental combinations featuring each membrane grade.

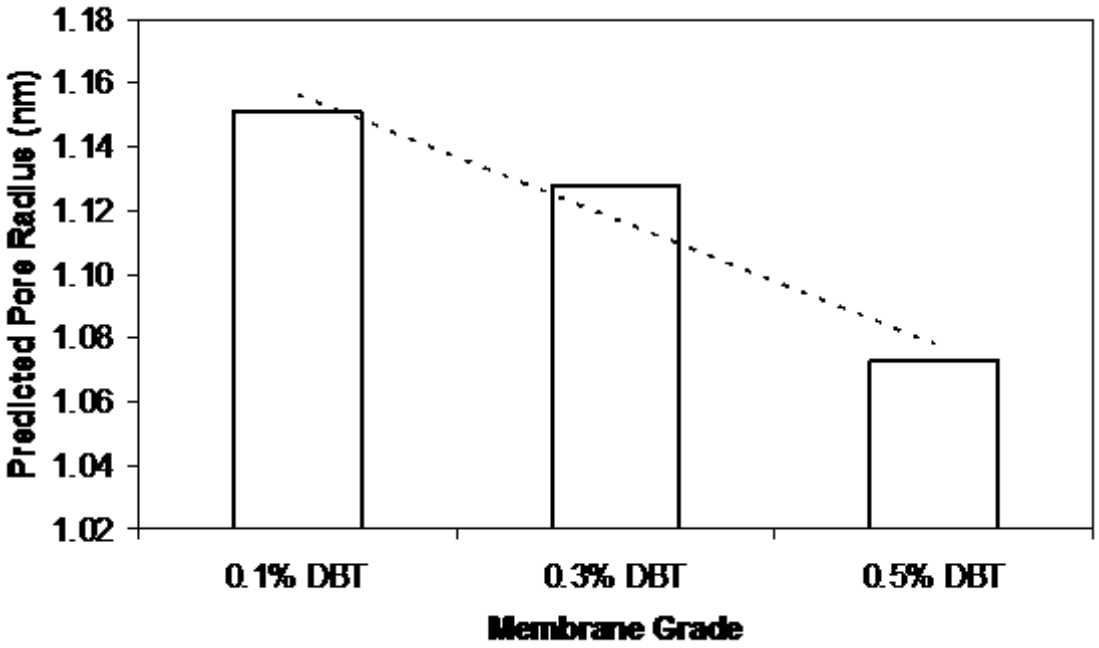

Figure 5.7 – The effect of membrane grade on predicted pore radii.

As well as demonstrating the expected logical trend between pore size and catalyst amount, the results in Figure 5.7 should be noted as an almost perfect linear trend exists (with an R^2 value of 0.9497). This result confirms that catalyst addition both had an effect on crosslinking, and that the effect was linear. The fact that such a clear cut relationship exist was reassuring however too much should not be read into this as the total change in pore radius was just less than a tenth of a nanometre over the range produced. The fact that the variance was this slight was backed up by the small but noticeable differences between the SEM images taken of the membranes, covered in Section 3.4.3.

The relationship between higher catalyst amounts and smaller pore size is supported by the crossflow filtration tests (Section 4.3) as it was found that for any constant set of parameters the 0.5% DBT membrane produced a higher rejection than the other grades – having a smaller effective pore size could be the reason for this. This trend is also supported by the Young's modulus discussion of Section 3.1.3. Generally, a material with smaller pores would be more resistant to deformation than a similar material with larger pores in its structure; however the specifics of this case would mean that a drop in predicted pore size of only 0.1 nm has caused a doubling of the

Young's modulus which seems to be quite a large effect for a relatively small change. Confirming this relationship was outside the scope of the work. Finally the link between predicted pore size and membrane grade is not supported by the membrane swelling work of Section 3.5.3. The effect of membrane grade on pore size was linear, where as the swelling effect was clearly not, meaning that the reason behind the swelling anomaly was not pore size related.

In conclusion, the PF model seems to be capable of predicting the experimental rejection curve to an adequate level. However this models best quality was in predicting effective pore size, which has been used to reinforce the conclusions made in both the swelling section (Section 3.5) and in the discussion of the SEM photographs taken (Section 3.4.3). Overall the pore flow model was considered to be one of the more useful models discussed in this chapter.

5.2.3. Pure Diffusion Model

As the name implies this model assumes that the solute moves throughout the membrane solely by diffusive transport i.e. the contributions to separation by any hydraulic mechanism are zero. The PD model can be used to predict both the flux and rejection relationships, the equations for which can be seen as Equations (5.5) and (5.6).

$$J_s = \frac{k\Delta P}{x} \tag{5.5}$$

$$R = \frac{1}{1 + \frac{D_i}{k \cdot \Delta P}} \tag{5.6}$$

This form of the model was taken from Robinson (2004). The flux equation (Equation (5.5)) was solved by finding a value of k which corresponds to the minimum error. This value of k was then used in Equation (5.6), with the value D_i being determined.

The PD model as the name suggests is a special case of the CD model where the fitting parameter a is zero and as such produces similar results to the already discussed model. The relative effects of each model are compared in Section 5.3.2. Figures 5.8 and 5.9 show the best fit of the PD model for the experimental set up using

iron (III) naphthenate solute, heptane solvent and 0.5% DBT membrane. The charts shown are typical of the output from this model.

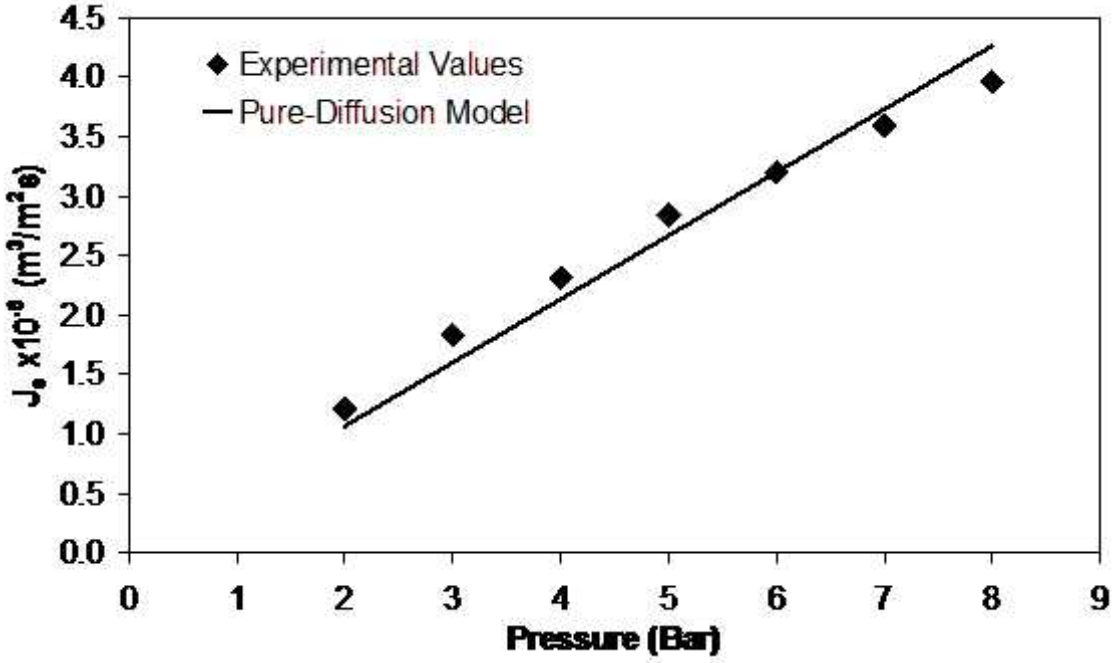

Figure 5.8 – Typical pure diffusion prediction vs. experimental data – flux version.

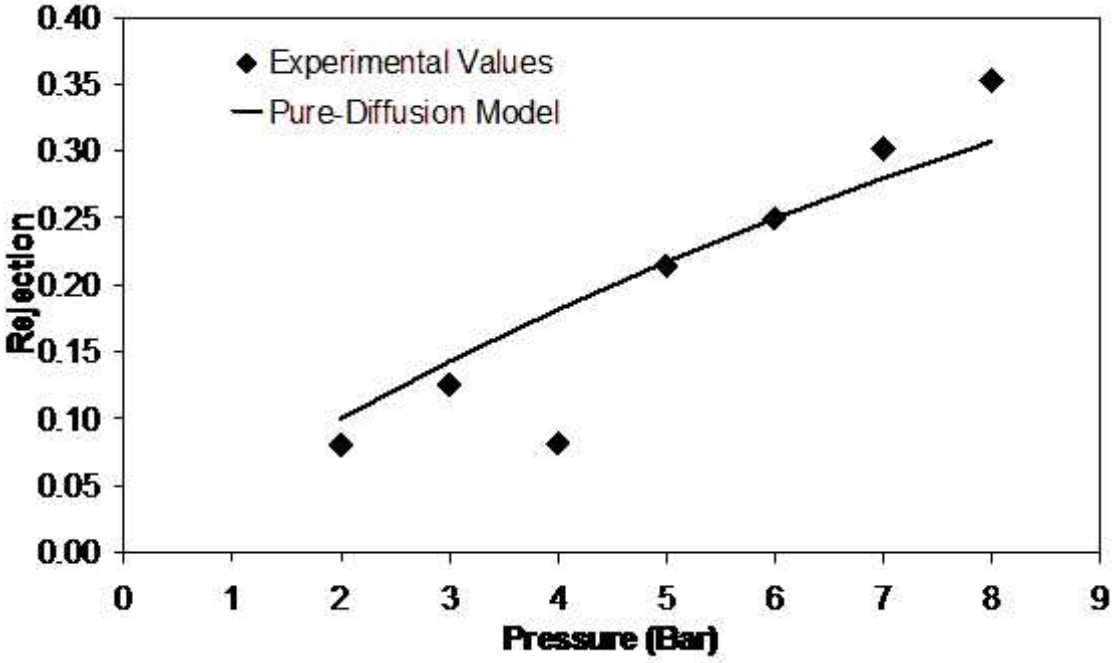

Figure 5.9 – Typical pure diffusion prediction vs. experimental data – rejection version.

The PD model contains only two variables, one characterisation parameter for both flux and rejection and a fitting parameter just used for the rejection stage. However as the characterisation parameter *k* was fixed during the flux part, the rejection equation was able to be thought of as a single parameter model for all practical purposes.

Both D_i and *k* show an inverse proportionality to membrane grade with larger values being determined for the 0.1% DBT membrane than the 0.3% DBT membrane, which produced larger values than the 0.5% DBT membrane. The magnitude of the values varies between 6.16×10^{-11} ~ 2.45×10^{-9} $m^2 s^{-1} Bar^{-1}$ for *k* and between 1.94×10^{-10} ~ 2.72×10^{-7} $m^2 s^{-1}$ for D_i. Neither parameter showed any defined proportionality with solvent or solute. Dependency between filter media and parameter size was a common trait amongst all the models presented here, the reasons for which are discussed in Section 5.3. Ultimately this model seemed to fit the rejection data best when the upper rejection limit was not very pronounced, with the best predictions being almost linear rather than curved.

In completion of this model, tables of error for different values of *k* and D_i were compiled and charts produced to check for any obvious trends or patterns. Unlike some of the other models, the charts produced showed only one trend for each of the parameters (rather than the multiple states which were able to be seen with the Speigler Kedem model, for example). Figures 5.10 and 5.11 show the shape of these trends for both *k* and D_i.

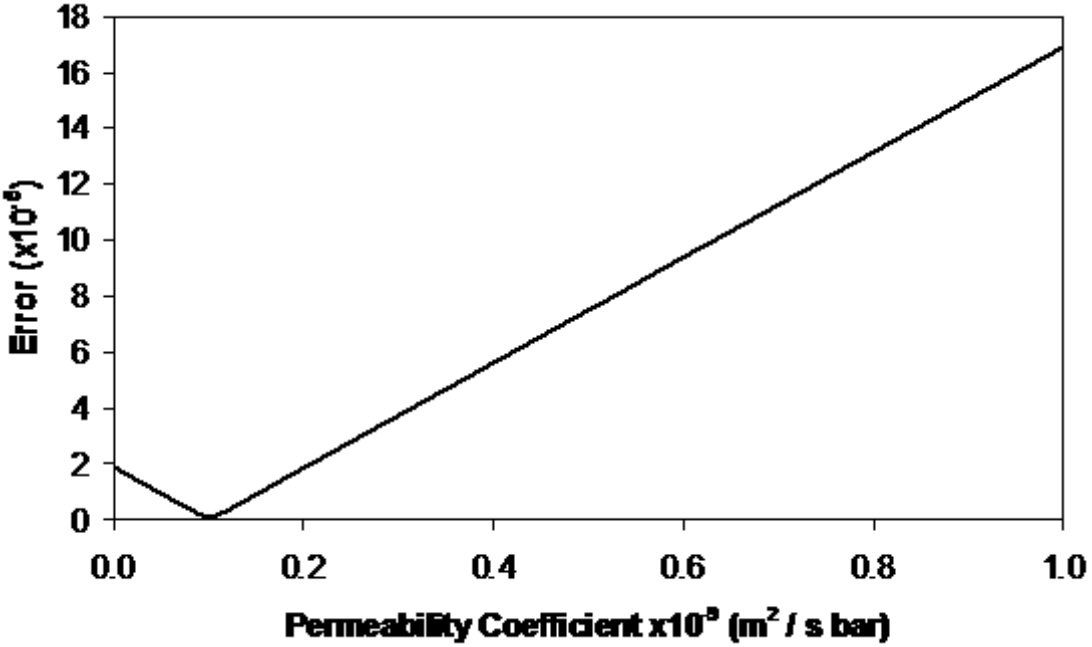

Figure 5.10 – Error trend produced by *k* for the pure diffusion model.

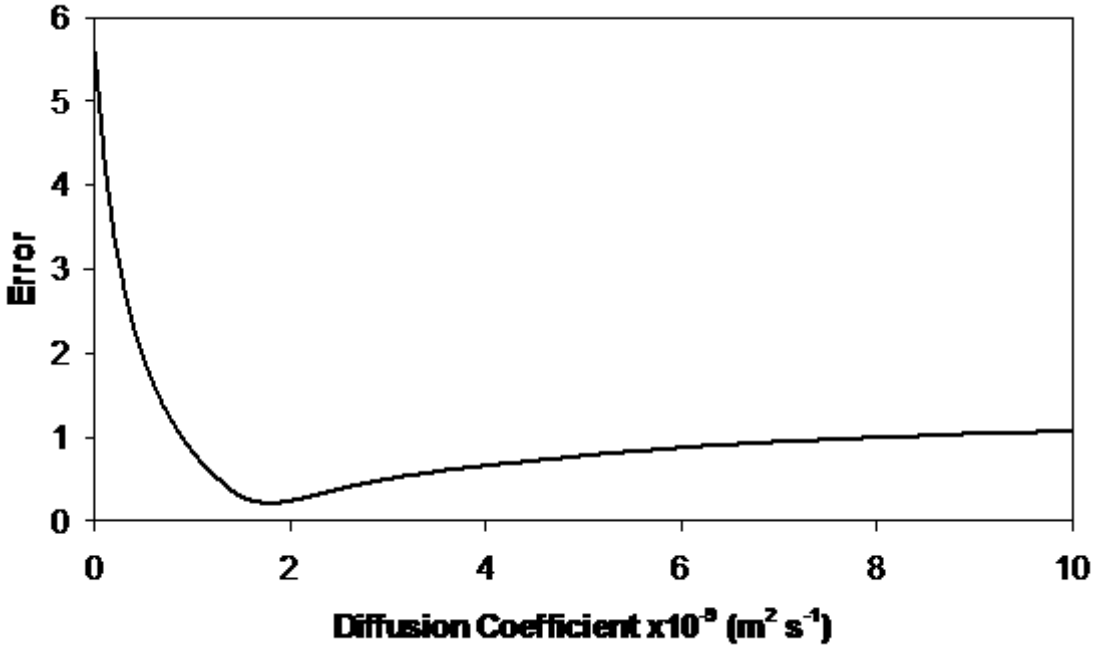

Figure 5.11 – Error trend produced by D_i for the pure diffusion model.

The main reason for checking the error trends for each experimentally defined parameter was that it ensured that the results obtained from the solved models were the global minima, i.e. the optimum solutions, rather than a local minimum, however

sometimes such a check unearths a hidden relationship between two models. Completion of Figures 5.10 and 5.11, in conjunction with Figures 5.14 and 5.15 below, highlighted one such relationship between the PD and SD models, which is discussed in Section 5.2.4.

5.2.4. Solution Diffusion Model

The solution diffusion (SD) model was first proposed in the 19th century (Wijmans and Baker, 1995) and was subsequently used by many authors including Robinson *et al* (2004), Dijkstra *et al* (2006), Silva and Livingston (2006) and Santos *et al* (2007). The main principles of this model were discussed in Section 5.1 but concisely this models assumes a constant pressure throughout the membrane equal to the pressure on the feed side, and separation occurs due to differences in the diffusivity rates and the rate at which initial dissolving takes place. The SD model can be used to predict both flux and rejection relationships, the equations for which can be seen as Equations (5.7), (5.8) and (5.9).

$$J_s = \frac{D_s K_s \cdot \alpha}{x} \tag{5.7}$$

$$R = \frac{D_s K_s \cdot \alpha}{D_i K_i + D_s K_s \cdot \alpha} \tag{5.8}$$

where,

$$\alpha = 1 - e^{\left(\frac{-V_s \cdot \Delta P}{R_g \cdot T}\right)} \tag{5.9}$$

where K_s is partition coefficient, V_s is solvent molar volume, R_g is universal gas constant and T is temperature.

This form of the model was taken from Robinson (2004), in which two assumptions were made; low solute concentration in feed and membrane separation was at steady state. The coupled parameter D_sK_s was altered to find the best fit for the flux part and this was then used in conjunction with D_iK_i in the rejection equation to determine the final fitting parameter for this model. Figures 5.12 and 5.13 show the typical fit of this model; data were from iron (III) acetylacetonate / xylene / 0.1% DBT membrane experiments.

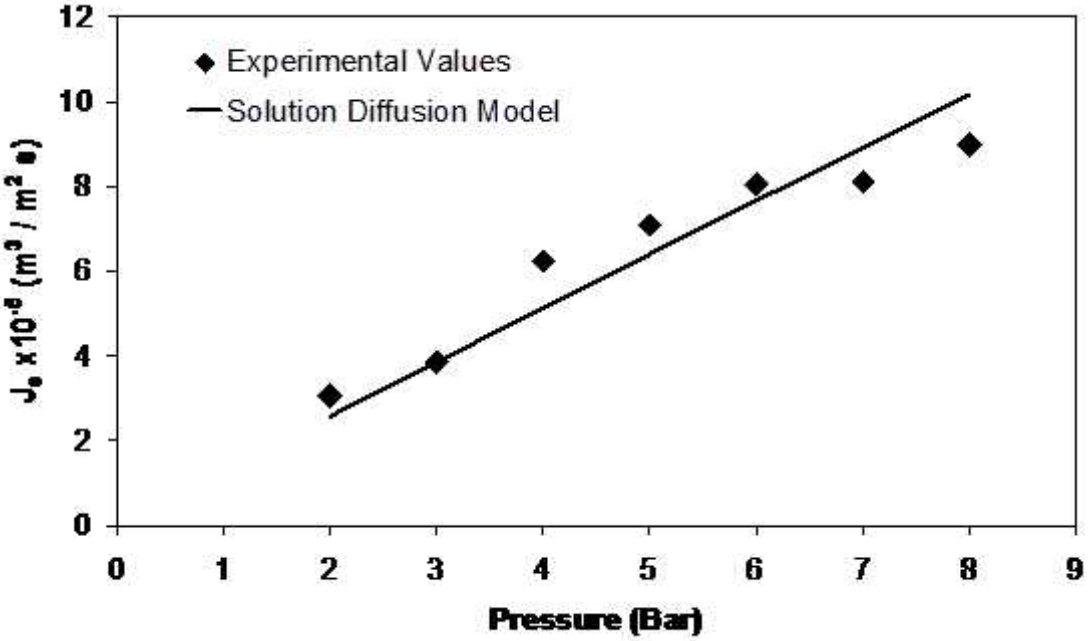

Figure 5.12 – Typical solution diffusion prediction vs. experimental data – flux version.

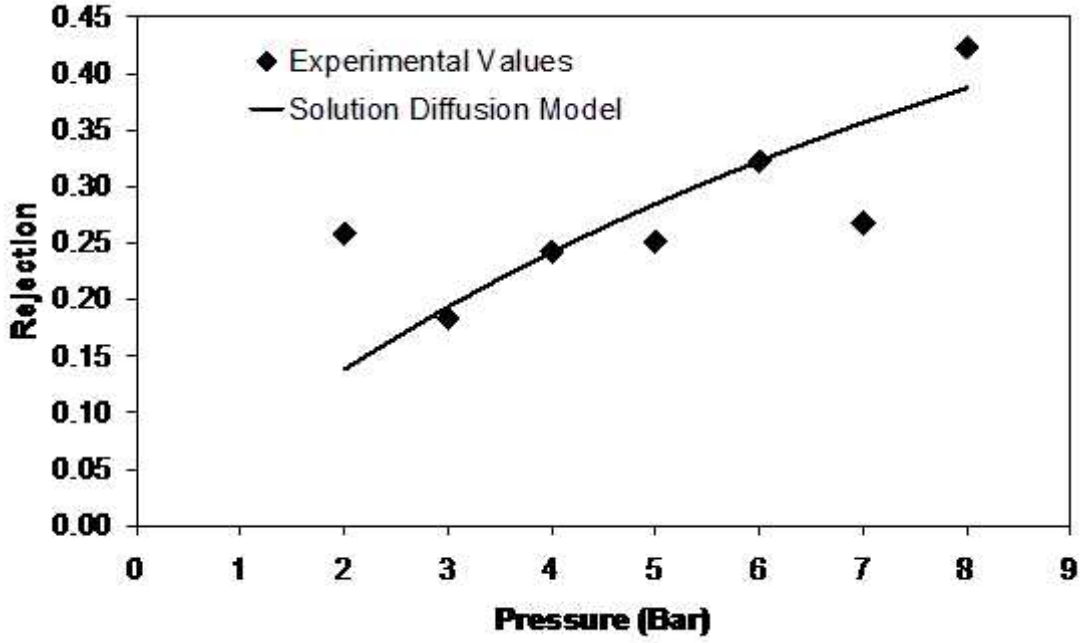

Figure 5.13 – Typical solution diffusion prediction vs. experimental data – rejection version.

The SD model predicts a linear relationship for flux and a curved fit for rejection, with an overall adequate fit to both the lower and higher range rejections. In completion of this model, tables of error for different values of D_sK_s and D_iK_i. were compiled and charts produced to check for any obvious trends or patterns. Unlike some of the other models, the charts produced showed only one trend for each of the parameters (rather than the multiple states which were produced by the Speigler Kedem model, for example). Figures 5.14 and 5.15 show the shape of these trends for both D_sK_s and D_iK_i.

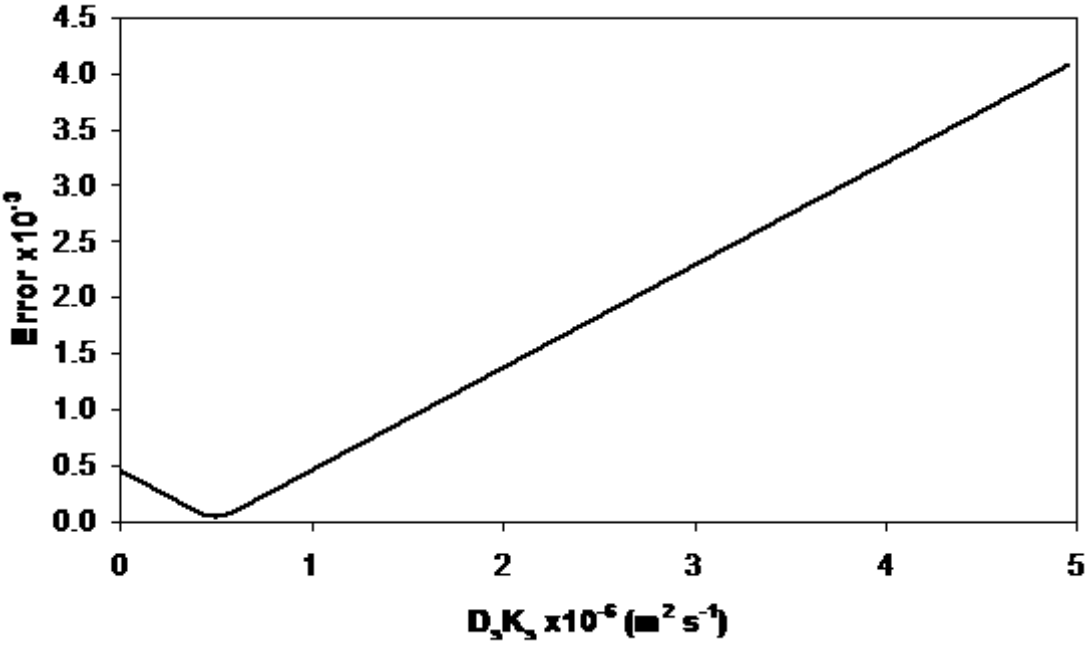

Figure 5.14 – Error trend produced by D_sK_s for the solution diffusion model.

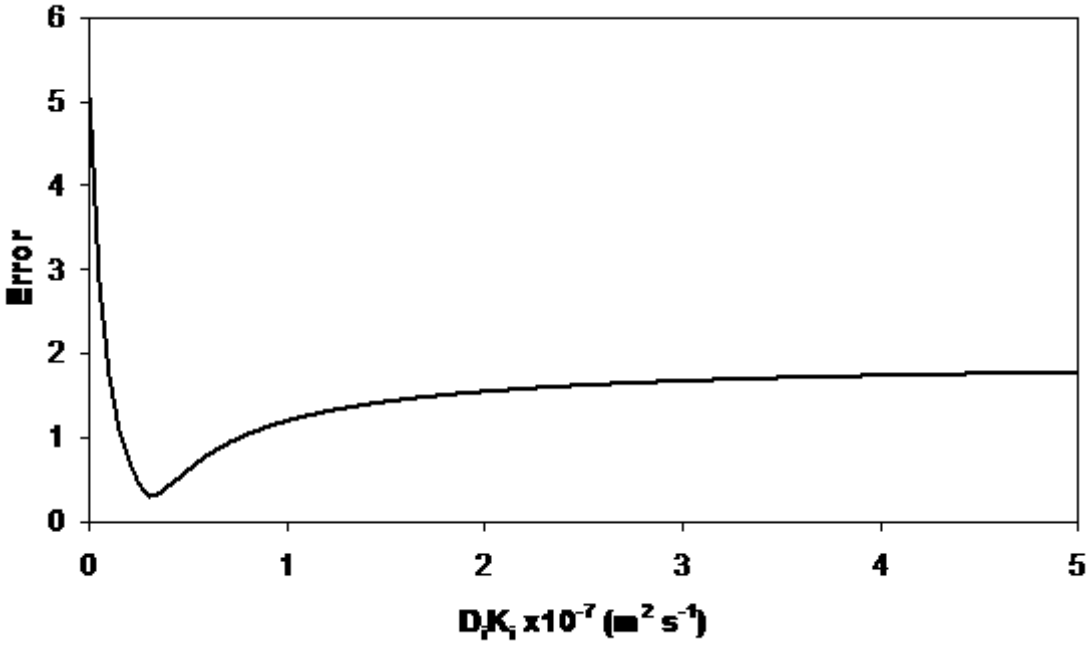

Figure 5.15 – Error trend produced by D_iK_i for the solution diffusion model.

The clarity of these error relationships has ensured that the solutions presented for the SD model were the global minimums and have helped to make this model, one of the easier models to solve – both trends have only one minimum across the entire range of the experimental parameters.

Figure 5.14 displays a mirror line through its minimum point where by the absolute gradient of the error before and after were identical in magnitude. This was due to Equation (5.7) which for error can be reduced to a linear fit. In the solution of the equation the only two terms that were allowed to alter between different tests of the same set were D_sK_s and ΔP, and the effect of pressure was allowed for in the error calculation so although it changes it had no bearing, making this a pseudo one term equation, and one term equations produce linear trends. Add to this the fact that any error must be positive (the magnitude rather than the absolute value of error was added to ensure that internal cancellation doesn't occur) means that instead of having a single straight line Figure 5.14 has a reflected line. Solution of the model in this way has produced a simple graphical solution to finding the correct value of D_sK_s.

The error trend for D_iK_i (Figure 5.15) by contrast shows the more common trend similar to the one produced for the pore flow model without the left most minimum (Figure 5.4), making the determination of the value of D_iK_i simple.

The shape of the error curves in the PD and SD charts were identical with the only difference being the axis limits. Such an exact pattern could not be due to coincidence and must indicate an underlying connection between the two models. In Figures 5.10 and 5.14 a minimum error exists between two linear sections with a mirror line at the minimum point. In Figures 5.11 and 5.15 the error drops sharply to a curved minimum before a gradual increase. The similarity between the two flux based charts was easy to explain however the similarity between the two rejection charts was not so straightforward. Both flux equations were in the form of flux was equal to some coupled term including pressure divided by membrane thickness. Just because the magnitude of the coupled term changes, the trend of the error line should not. The relationship behind the experimentally derived parameters for rejection was less straightforward but still exists. Compare the two Equations (5.6) and (5.8) and specifically the terms D_i and D_iK_i. Both of these terms were in the denominator of a fraction with an identical term in the numerator and forming the other additive half of the denominator – the fact one of these terms was one and the other was $D_sK_s\alpha$ effects the magnitude only, not the shape, and so it was able to be seen that the two equations have similarities. There was no functional difference between these forms of the PD and SD models, a practical difference does exist as the two models do not predict the exact same trends, nor are they based on the same theory. Further discussion on the similarities between models can be seen in Section 5.3.1. Overall this model provides an adequate prediction of the experimental data.

5.2.5. Solution Diffusion with Imperfections Model

The main problem with the standard solution diffusion model was that it does not take into account any effect caused by convective transport. In the case of SRNF as the membrane swells the bulk volume increases which will lead to the inception of convective transport. To include this effect the SDi model was created as early as 1967 by Sherwood *et al* (1967) and has become one of the main variants of the solution diffusion model. It had subsequently been used by Yaroshchuk (1995), Ebert *et al* (2006) and Dijkstra *et al* (2006). The SDi model was able to be used to predict both the flux and rejection relationships, the equations for which can be seen as Equations (5.10) and (5.11).

$$J_i = \frac{P_w}{l}\left(\Delta P - \Delta\Pi\right) + \frac{P_3}{l}\Delta P \tag{5.10}$$

$$R = \left[1 + \left(\frac{P_2}{P_w}\right) \cdot \left(\frac{1}{\Delta P - \Delta \Pi}\right) + \left(\frac{P_3}{P_w}\right) \cdot \left(\frac{\Delta P}{\Delta P - \Delta \Pi}\right)\right]^{-1} \qquad (5.11)$$

where P_w and P_3 are flux fitting parameters, P_2 is rejection fitting parameter, l is membrane depth and Π is osmotic pressure.

This form of the model was taken from Ho and Sirkar (1992). The solution of this model was different to the others already discussed in that Equation (5.10) had two fitting parameters (P_w and P_3) and the rejection equation (Equation (5.11)) had only one (P_2). The best values for the fitting parameters were chosen by minimising the error. Figures 5.16 and 5.17 show the fit of this model when applied to the tests featuring iron (III) naphthenate, octane and 0.3% DBT membrane.

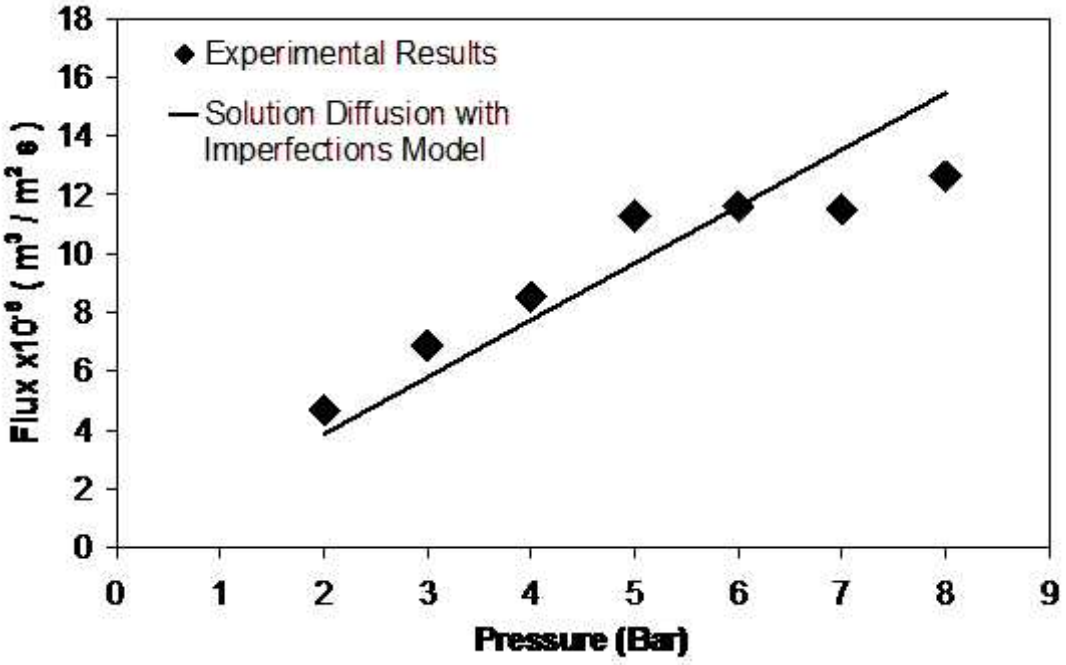

Figure 5.16 – Typical solution diffusion with imperfections prediction vs. experimental data – flux version.

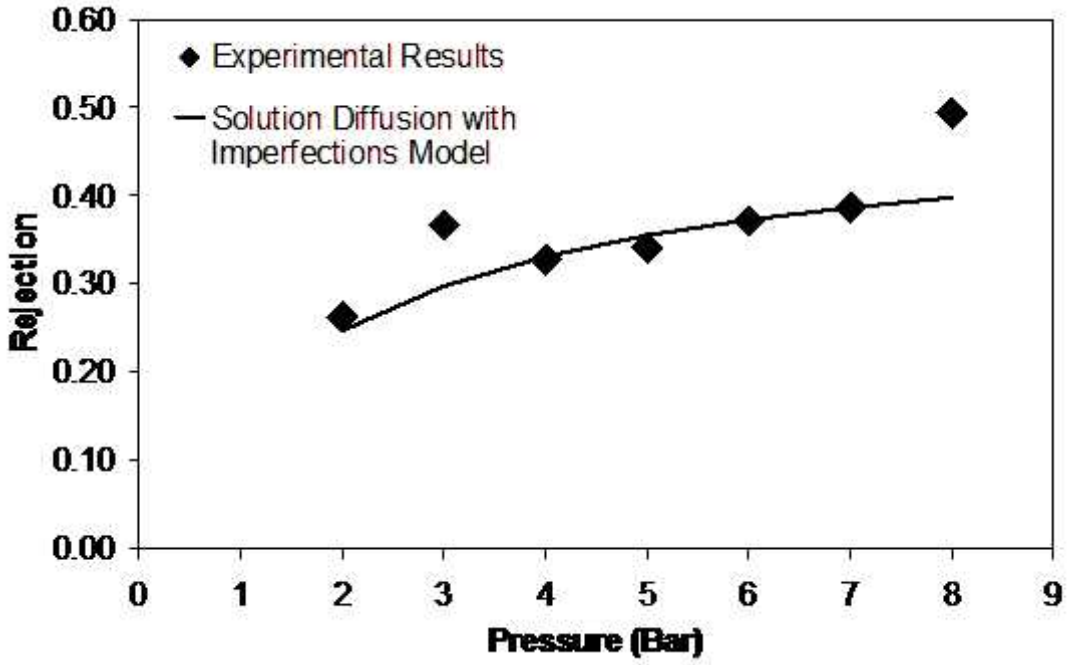

Figure 5.17 – Typical solution diffusion with imperfections prediction vs. experimental data – rejection version.

The model provides adequate prediction over the range of parameters tested, predicting a linear fit for the flux part and a curved fit for the rejection part. Discussions already stated for the CD, and SD models were just as valid here and shall not be repeated for brevity.

All three parameters show dependency on membrane grade and also show little to no association with either solute or solvent. In each case this dependency was inversely proportional with the lower catalyst amount membranes producing the highest values of P_w, P_3 and P_2. This outcome is logical as can be seen from Equation (5.10) since the lower grade membranes produce the largest flux values and both P_w and P_3 exist on the top of the equation. Another noteworthy point from this data was that in every case tested the optimum values of P_w and P_3 were always within 1% of each other; however the exact value varies from test to test. For example the iron (III) napthenate/xylele/0.5% DBT membrane test produced values of 3192 l $m^{-2}hr^{-1}Bar^{-1}$ (P_w) and 3211 l $m^{-2}hr^{-1}Bar^{-1}$ (P_3) where as the iron (III) acetylacetonate/xylene/0.1% DBT membrane produced values of 121945 l $m^{-2}hr^{-1}Bar^{-1}$ (P_w) and 122012 l $m^{-2}hr^{-1}Bar^{-1}$ (P_3). It was believed that this was the case for the work presented here because of the small value of osmotic pressure. The value of osmotic pressure throughout this work varies based on the exact strength of solution and the solute involved, but in any case the value was small, in the region of 10^{-3} bar, and could be neglected when considering

the minimum pressure tested was 2 bar. The value of osmotic pressure was relatively small as all the solutions tested in this work were around 30 ppm and considered to be dilute. When $\Delta\Pi$ is small Equation (5.10) reduces to a simpler form, where only the combined value of P matters. The computer program scripted had therefore produced similar values for the two parameters, only differing because of the very small interference of osmotic pressure. If this model was applied to simulate a more concentrated solution, the effect of osmotic pressure would be more relevant and it is expected in that case that the two parameters would not necessarily be the same.

5.2.6. Speigler Kedem Model

The Speigler Kedem (SK) model is a special case of the Keden Katchalsky (KK) model and as such a brief description of the KK model is required here.

The KK model was derived from first principles and uses irreversible thermodynamic laws as a basis for the prediction of separation. It relates the volume flux of a membrane to the solvent flux passing through it by using the reflection coefficient, solute permeability and pure water permeability in the same medium. The KK model only works for cases where the concentration of the permeate is close to the concentration of the retentate (Wang *et al*, 1997) and so has limited applicability.

The SK model is a modification of the KK model derived to handle cases that the standard KK cannot, i.e. in situations where large separations occur, resulting in a large difference in the concentrations of the retentate and permeate streams. The SK model uses the same parameters as the original model except that it uses the local solute permeability integrated across the entire depth of the membrane to give a more complete picture of the gradients involved (Wang *et al,* 1997). This model has been subsequently covered by Geens (2006). The SK model has been used to predict the rejection relationship, the equations for which can be seen as Equations (5.12) and (5.13). This form of the model has been taken from Robinson *et al* (2004).

$$R = \frac{(1-F)\cdot\sigma}{1-\sigma\cdot F} \tag{5.12}$$

Where,

$$F = e^{\left(\frac{-J_v(1-\sigma)}{P_s}\right)} \tag{5.13}$$

As this model only calculates rejection there was no fitting parameter to be brought forward from the flux part. The fitting parameters were σ and P_s, and both have to be

solved in the rejection equation with the former existing within the range 0~1 to keep the ultimate rejection positive.

The prediction of the SK model for an experimental set up using iron (III) naphthenate, heptane and 0.5% DBT membrane is shown as Figure 5.18.

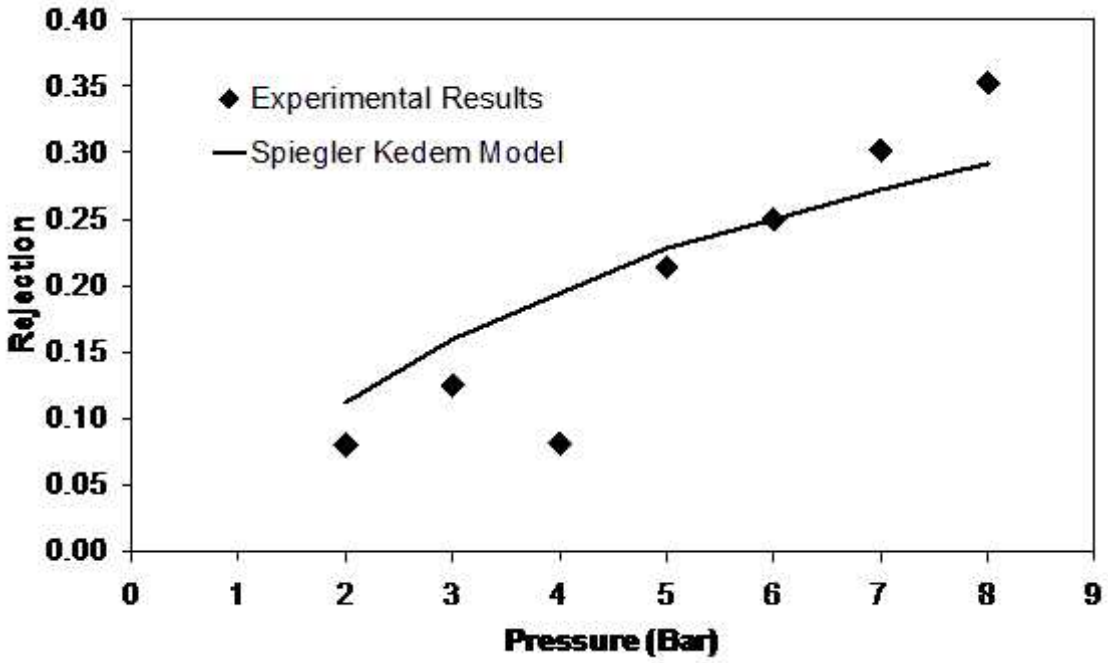

Figure 5.18 – Typical Speigler Kedem prediction vs. experimental data – rejection version.

Like all the other models a curved fit for rejection was predicted. Overall the SK model was one of the better models, meaning that the predictions were close to the experimental data, and by absolute error it was the second best model for the rejection prediction, see Section 5.3.2 for a discussion of this point.

As this model has two experimentally derived parameters for rejection, a different approach was required to determine these values. As σ has a definite range (σ must exist between 0 and 1) its value was fixed and then the optimum value of P_s determined. The value of σ was then sequentially increased over its entire range with the optimum value of P_s determined at each stage. In this way the overall minimum error was able to be deduced rather than the local minimum, any iterative process has the potential to discover.

By completing the process tabulated values of the total error for every potential value of reflection coefficient (σ) were obtained and proved to produce a result worthy of note. When the data were plotted the variance of error with change in σ produced one of two different shaped trends for any specific experimental set, examples of which can be seen as figures 5.19 and 5.20. Both figures were from experimental sets utilising 9,10-diphenylanthracene and octane but figure 5.19 was produced from the 0.3% DBT membrane results and figure 5.20 was produced from the 0.5% DBT membrane results.

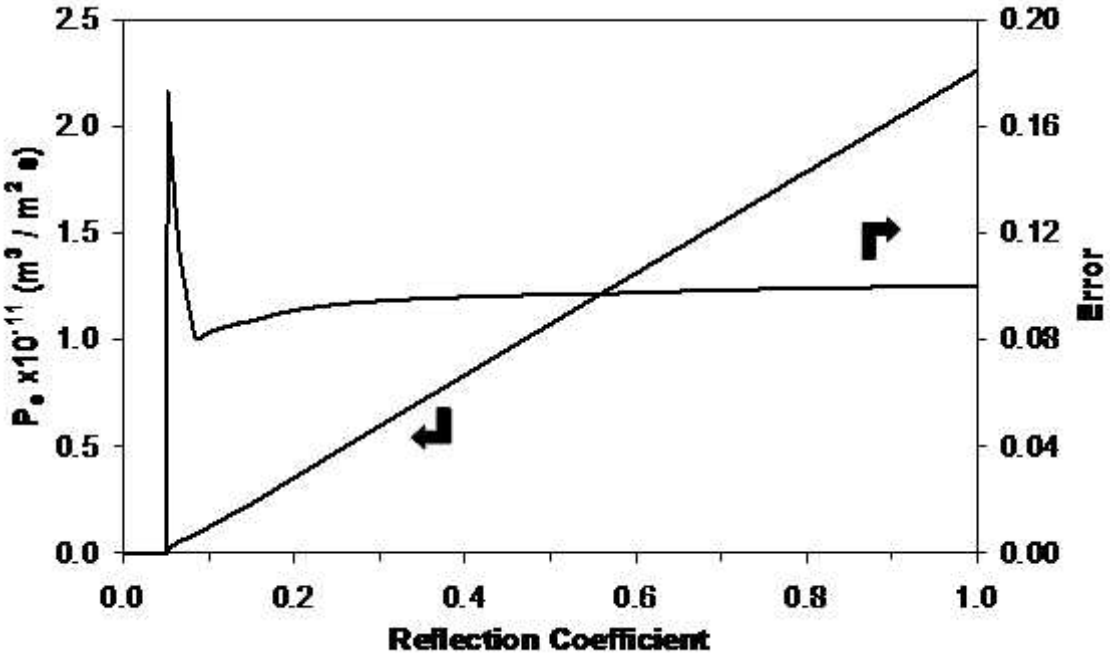

Figure 5.19 – Type I error trend in Spiegler Kedem model.

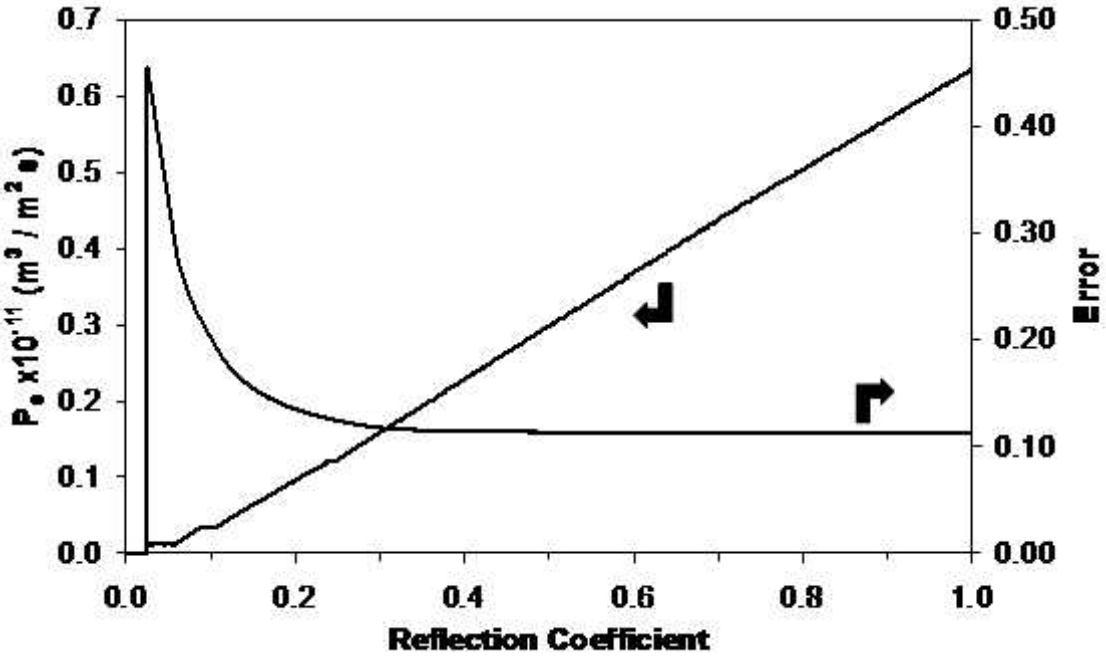

Figure 5.20 – Type II error trend in Spiegler Kedem model.

The two error trends have both similarities and differences. In both cases at small values of σ the noted error tends to zero, however this result was a false positive and such results should not be considered correct. The reason behind these erroneous predictions was that they correspond to situations where P_s was close to zero – in the figures it looks like P_s was zero but in reality a difference of the order of 10^{-10} l $m^{-2}hr^{-1}$ exists. As P_s tends to zero the value of F from Equation (5.13) tends to infinity and this causes the denominator of Equation (5.12) to tend to zero, causing the error. Therefore the sharp decline of the error noted at small values of σ was a quirk of the model and although it should be remembered, it was not crucial to the solution of the model.

The differences between the two error types were more important. In Type I the initial error drop was sharp and followed by a minimum after which increasing the value of σ increases the total error, leading the obvious solution being the minimum point. In Type II the initial error drop still exists but it was of a lower gradient and with increasing σ come decreasing error leading to the obvious solution that the minimum error should occur with maximum σ. In actuality solution of Type II situations usually returns values of σ of 0.98 and above (rather than automatically choosing σ =1 as the solution) as a very shallow minimum exists at the extremity of the trend making the largest values of σ marginally bigger than the preceding points. In addition to this point the result σ=1 returns the same error as when P_s tends to zero, also for the same reasons already stated.

It is unclear why two types of error exist; by number alone Type II is rarer than Type I with only 7 of the total 27 possible demonstrating this behaviour, but the predictions arising from each type seem to be just as valid as each other. The Type II occurrences cover all the solutes and membrane grades used, but not solvents, with no xylene based tests amongst this group, however due to the relatively small sample size this could just be due to simple probability. The Type II experiments also hinder dependency analysis (see Section 5.3.3) by hiding the definite trends which occur within the Type I's. Overall both types of error trend were valid as they both produce an accurate prediction of the experimental data, just with the Type I's being easier to analyse.

5.2.7. van der Bruggen Model

This model was the most recent of all the models covered in this chapter, being published in 2009 in the paper Darvishmanesh *et al* (2009). In the literature the model had not been given a name, but for ease of discussion it is referred to here as the van der Bruggen (VDB) model.

The VDB model is described as a semi-empirical modification to the solution diffusion with imperfections (SDi) model. The paper states that solvent permeability is dependent on viscosity and two constants based on dielectric constant and surface tension. The VDB model can be used to predict the flux relationship only, the equation for a hydrophobic membrane, such as PDMS can be seen as Equation (5.14).

$$J_v = \frac{a_0 \cdot \alpha}{\mu \cdot e^{(1-\beta)}}\left(\Delta P - \Delta\Pi\right) + \frac{b_0}{\mu \cdot e^{(1-\beta)}}\Delta P \qquad (5.14)$$

Where, α is dielectric constants ratio between the solvent used and hexane, and β is the ratio between the surface tension of PDMS and the solvent used. This model calculates flux only and was solved by finding values for the two fitting parameters a_0 and b_0. Figure 5.21 shows the typical fit of this model, for the data set using iron (III) naphthenate, heptane and 0.3% DBT membrane.

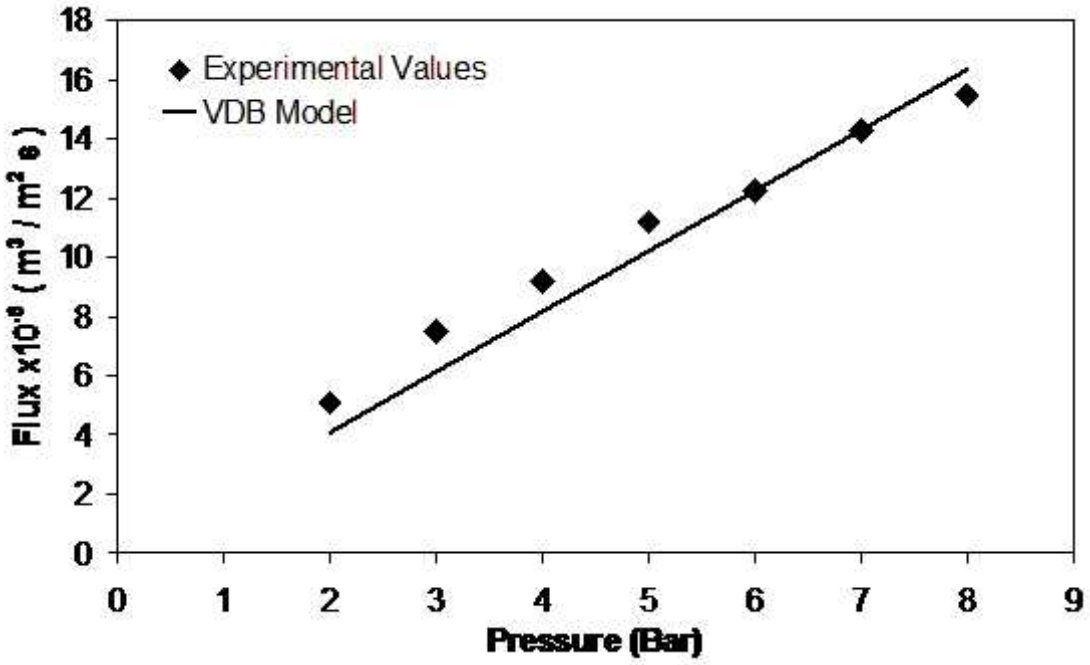

Figure 5.21 – Typical VDB model prediction vs. experimental data – flux version.

This model provides a linear fit of the flux data providing an adequate fit of the data. The use of two fitting parameters for flux was a strange concept compared to the other models and one which seemed largely unnecessary for the solvents used in this study. When solved the value of the two parameters were almost identical (a_0 is *ca.* 95~100% of the value of b_0) for all the tests using heptane or xylene, and for octane an 80% relationship exists. The fact that the parameters can be different for a different solvent appears to validate their inclusion but it still seems that with a bit more refinement the terms could have been coupled, as a single parameter model is easier to use than a additive two parameter model. Due to the problems with this model most of the critical discussion occurs in the next section (Section 5.3.1) rather than here.

5.3. Comparison of Models

5.3.1. Model Analysis

The seven models discussed in the previous section cover a wide range of underlying theory each striving to predict the filtration properties based on their own definition of separation, and so it was expected that common ground between the different models would be limited. However during this section the shear amount of similarities

discovered, especially in the error trends between supposedly opposed models has made a review of the underlying mathematics between each model a necessity. The pore flow model was, by principle, different to the other models. It was used to infer the characteristic pore size where the other models were used to predict performance therefore the form of this model was not considered here, merely the outcome from it.

The first point is about redundancy. In numerous models there exists a constant and an experimentally derived parameter in a cancellable relationship. This was best explained by way of an example – see Equation (5.1). In this case flux was calculated by using the fitting parameter *k* and the membrane thickness *x*, however this could be reduced to a single parameter, say *K* such that $K = \frac{k}{x}$, without changing the overall effect or applicability of the model – where *K* was just another constant. The inclusion of the membrane thickness was an attempt to make it easy to substitute in one filter media for another and then just update the models prediction to gain the new filtration properties, but this only works if *K* does indeed equal $\frac{k}{x}$, for every filter media discovered. For this to be true it would require the efficiency of every filter media that was, say 2 mm thick, to be the same regardless of the materials of construction, or the feed solution, which was unlikely to be true as it had been found that every dependent parameter was affect by membrane type – Section 5.3.3. So if $K = \frac{k}{x}$ is not universal truth, then by changing the media both *x* and *k* would have to be altered to model the new set up and if both terms have to change they might as well be replaced by the single parameter *K*. This same argument can be made multiple times for different terms throughout the models featured.

Anywhere a constant and a fitting parameter exist they might as well get replaced by a single altered fitting parameter as the benefits outweigh the downsides. An advantage of this proposal is that less literature data would be required, for example there would be no need to look up dielectric constants or surface tensions, which are difficult to obtain, and in the worst case non-existent for new processes, meaning that extra laboratory work would be required to determine these ultimately unnecessary constants. The only disadvantage to this change, would be that the new parameters would not be directly comparable with the old parameters, but this would only ever be an issue when considering two identical processes so the occurrences of this would be rare. Overall the ease of use increases immensely by cancelling these terms, at the

cost that some of the theoretical grounding is lost, however as the theory applied wasn't universal anyway this loss is not really that important.

A reduction in this way makes the flux Equations (5.10) and (5.14) (VDB and SDi models) identical and if osmotic pressure was small enough to be neglected it also makes them identical to the flux Equations (5.1) and (5.5) (CD and PD models), demonstrating the common approaches between the models. In total five models that predict flux were considered, four of those predict flux to be equal to some multiple of pressure (Darcy's law), with the fifth (SD) stating that flux was equal to a multiple of a fraction which uses the exponential of pressure rather than direct pressure. This makes it appear that there was two different ways of calculating flux however if the exponential pressure term, α (Equation (5.9)) was calculated it defines a trend identical to pressure alone except for the magnitude, so these are functionally identical. This means that flux is simply proportional to applied pressure and the question of why anything more complicated than Darcy's law exists for calculating flux should be raised.

The osmotic pressure issue, although it didn't apply in this case (test solutions were too dilute) it is feasible that it would be relevant to other processes so this addition, if it works, is still probably prudent. Besides this slight concession the reason why so many forms exist seems to be that different people have tried to invent grand models with superfluous complexity to justify their preferred separation scheme, when the simple model was all that was required.

An underlying pattern between the different approaches to predicting rejection was harder to locate than it was for flux; all the models predict a curved relationship reaching a limit with increasing pressure but the terms exist within multiple line fractions which makes isolation less straightforward. Already discussed, the link between the rejection parts of the CD, PD and SD models and the link between the error trends of the SD and PF models shows that these models were linked but as could be seen from Section 5.3.2 there was little to choose between the models in terms of predictions.

Of all the models discussed here, the VDB model has the most redundancy and potential for simplification within its form. This could be due to the fact that it was the most recent model covered and has not yet reached its final form but in its current version a lot can be altered. By simplification, it has already been shown that the model reduces to be identical to all the other flux predicting models, but further to this the

model uses both viscosity and surface tension in the same denominator which was redundant.

There is a well documented relationship between surface tension and viscosity. The earliest record that could be found of this link was by Pelofsky (1966), where it states that the relationship shown by Equation (5.15) was valid for 33 different liquid systems, both organic and inorganic.

$$\ln \alpha = \ln A + \frac{B}{\eta} \tag{5.15}$$

This work references other papers from as far back as 1932 postulating on the relationship between these two properties so this link had been well established but these paper were not obtainable. Later work (Schonhorn, 1967) has since refined Equation (5.15) to cope with the discrepancy that although surface tension can be zero, viscosity can't, but the same direct link still remains. Therefore it is unclear why the VDB model uses both these property terms as one could have been substituted for the other, making the model less demanding on the amount of pre-required information.

The analysis of the models has highlighted the common traits between supposedly different models; this was to be expected as the different models must have some similarities if they are meant to produce similar trends or predictions. The discussion on extent of comparisons between the different approaches is continued throughout the next two sections.

5.3.2. Error Analysis

With each model covered separately it would be prudent to compare similarities and discuss differences to assess which model(s) was the best. The purpose of this section was to assess these points as well as evaluate the models themselves to find out how functionally different they really were from each other as well as to satisfy one of the aims of this work.

Each model, for each of the experimental data sets produced an amount of error, i.e. no model fitted the data precisely due to the natural variation in experimental data. Some sets produced smaller errors than others but the error always existed to some

extent. Error, in this case, is defined as the absolute difference between the model prediction and the experimental value. The sum total of the error recorded across all of the 27 experimental combinations was termed 'total error'. Table 5.1 was constructed in an attempt to determine the best model for this work, defined as the model with lowest total error.

Model	Parameter	Total Error	Average Set Error	S.D. of Error
CD	Flux (m^3/m^2s)	$2.66x10^{-4}$	$9.86x10^{-6}$	$1.21x10^{-5}$
PD	Flux (m^3/m^2s)	$2.66x10^{-4}$	$9.86x10^{-6}$	$1.21x10^{-5}$
SD	Flux (m^3/m^2s)	$2.40x10^{-4}$	$8.90x10^{-6}$	$1.20x10^{-5}$
SDi	Flux (m^3/m^2s)	$2.66x10^{-4}$	$9.86x10^{-6}$	$1.21x10^{-5}$
VDB	Flux (m^3/m^2s)	$2.66x10^{-4}$	$9.86x10^{-6}$	$1.21x10^{-5}$
CD	Rejection	5.45	0.20	0.19
PF	Rejection	7.43	0.27	0.21
PD	Rejection	7.41	0.27	0.21
SD	Rejection	7.91	0.29	0.22
SDi	Rejection	7.39	0.27	0.27
SK	Rejection	5.67	0.21	0.19

Table 5.1 – Overview of error by model.

The first thing to bear in mind from Table 5.1 is that the flux error and the rejection error are different by definition. As error was the difference between the experimental and predicted it had the same units as the base parameters, specifically flux error had units of m^3/m^2s and rejection error was dimensionless. Due to this the two error types cannot be directly compared. The second point is that the standard deviation was of a similar size (if not larger) to the average set error, this was due to the fact that both of these values reflect results from the entire range of data, covering every solvent, solute and membrane grade. The deviation was high in this case as it was covering variables which in the strictest sense were not considered to be the same so a high deviation was logical with no common ground (This summation combined heptane and xylene tests for example). This column was included to show the consistency between the models. Finally, the fact that the rejection values were lower than the flux values has no meaning as there is no basis for comparison between the two types, they were

included here in one table to save space but should be thought of as two separate tables for discussion purposes.

Comparison of relative error was a good way of determining which model was more suited to this operation and also a good way of determining the underlying mechanisms at work. The CD and PD models were identical for flux and so gave an identical value for flux error, however for rejection the PD model produced an error of 7.412 whilst the CD model produced the better value of 5.458. An explanation can be found by returning to the assumptions inherently made in each model. The CD model takes into account contributions from both convection effects in large transport regions and diffusion effects in small transport regions. The PD model assumes that the separation by any hydraulic mechanism is zero, i.e. only diffusive transport effects apply. As the CD model better predicts the behaviour of the given system this implies that the contribution from convective transport cannot be neglected, which means that some transport regions must exist within the produced membranes which are large enough for convection to occur.

Considering the flux section there were two immediately apparent details; the SD model's error was less than the other models (around 90% of the others) and those other models total were all within 7.34×10^{-8} $m^3 m^{-2} s^{-1}$ of each other (due to rounding all four models show the same value in Table 5.1). The fact that four of the models produced such similar totals cannot be just coincidence and was likely to be due to the mathematics of how the predictions were made. Each of the models in question provides a simple linear fit of the data with both pressure and the fitting parameter on the numerator – in the case of CD and PD, the equations were identical. With such similar methods it was inevitable that the results will be similar, however the shear scale of the agreement was still surprising. Now compare this to the flux equation for the SD model, it still included the pressure term and fitting parameter in the numerator, but the pressure was expressed as part of an exponential. This change had produced a modestly better fit to the data lowering the total error and subsequently the average set error meaning that the SD model is more valid for the experimental set up tested. Overall the SD model (Equation (5.7)) seems to be the best one to use for predicting the flux of solvent through the membranes produced during this work.

Applying a similar train of thought to the rejection section of Table 5.1, two models were clearly better at fitting the data than the rest, namely CD and SK. The spread of fit in the rejection section was greater than the flux section with the best models having

around 70% of the error of the worst fitting models. A similar correlation between the magnitudes of the values in the same row existed here as it did in the flux part of the table. An explanation of why the CD and SK models were the best for predicting rejection was again able to be found by considering the mathematics involved. The PF model is a one parameter model, having only r_p as a settable parameter. SD and PD both have two parameters for the rejection part, but one of them was fixed during the solution of the flux section, so they can be thought of as one parameter models for rejection. The SDi model has three parameters for rejection but two of them were fixed during the solution of the flux section, so it can also be thought of as one parameter models for rejection. Compare this to the CD and SK models, both of which have two discrete parameters for the rejection part, neither of which was set in the flux solution so they were likely to predict the data the best, as having two parameters to alter will invariably produce a closer approximation than one.

In form the CD and SK models are similar; both are multi-level fractions that include fitting parameters in both the numerator and denominator. The fact that the two models were similar in form was not surprising as they were models which allow both convective and diffusive mechanisms to occur. The models differ in the variables that were used in their solution; the CD model uses the standard pressure term seen in many of the other models, whereas the SK model uses the exponential of flux within itself rather than pressure. As all other models so far covered predict a linear relationship between flux and pressure, on the face of it, this switch was not important, as it simply means that the magnitude of the relevant fitting parameter (permeability coefficient) was one constant rather than another. However, in reality this change has had an effect on the data obtained, for although the pressure term used in the models was an absolute (the test was conducted at 2 bar for example) the flux obtained was not an absolute. Theoretically for a fixed pressure, a fixed flux should have existed, but in practise natural variation in the experimental data existed which in turn introduced an error into the fundamental assumptions of the SK model. This was the reason why the CD model produces a better (lower error) fit of the data – it does not have to compensate for this extra variance.

Just because the CD model produces a smaller error does not necessarily make it more valid, as validity was not solely measured by (lack of) error. The SK model attempts to include real data (the value of flux including within it the inherent error) into the model to give it more of a practical bearing, rather than using the assumed pressure term without this inherent error (although all effort was taken to set the

pressure to say 2 bar, there will be some discrepancy in reality which was not compensated for in the model). The SK model therefore includes this 'background' error and although the attempt to include this was commendable, ultimately the model suffers for it. A model which is not technically valid but actually predicts the process is always better than a model that is technically valid but provides a poor prediction, from a practical standpoint.

So as far as this experimental set up was concerned the SD model should be used to predict flux and CD model used to predict rejection. This outcome would require, in its current configuration, completing the flux part of CD to determine the parameter k, which was ultimately unnecessary as the flux was already being provided by SD. To save this, a coupled term could be proposed i.e. let $D_i/k = \beta$ and then the model would work as a two parameter model for rejection without the need for the flux part to be solved. The proposed modification can be seen in Equations (5.16) and (5.17).

Equation (5.2) becomes

$$R = \frac{1-a}{1+\frac{(1-a)\beta}{\Delta P}} \tag{5.16}$$

where,

$$\beta = \frac{D_i}{k} \tag{5.17}$$

This change works as both the values of D_i and k are experimentally derived constants and the ratio of two constants is still just another constant. The only downside to this proposed method was that the individual values of D_i and k are not known, making it more difficult to compare with literary values for these parameters. This is not a major inconvenience as unless another author had previously published work detailing the exact set up, filter media and solution you intend to use the values will be incompatible anyway. Ultimately if the parameters chosen accurately model the actual situation it does not matter if they vary from literary values.

Overall the error analysis has identified which models predict the experimental results the best. The SD model was found to be the best model for flux and the CD model was found to be the best for rejection. As both of these models describe diffusive transport it is clear that the contributions from diffusion cannot be ignored. However the CD model

also includes a convection element so diffusion alone does not account for the results observed (otherwise SD would have been the most appropriate model for both flux and rejection). In truth it is believed that the actual transport mechanism employed a combination of both diffusive and convective processes, but with the diffusive component being more critical than the convective component.

5.3.3. Dependency Analysis

Each of the models had been found to be somewhat dependent on a certain experimental parameter be it membrane selection, solvent or solute. This means that the magnitude of the fitting parameters varies in sequence with one of the experimental parameters. To confirm this, a table was constructed for each model detailing the output for each of the 27 experimental combinations. The table was then ordered by the magnitude of the first fitting parameter and the experimental parameters checked to see if groupings of like terms existed.

For example Table 5.2 shows the part of the data for the PD model ordered based on the magnitude of the parameter *k.* In this form it can be seen that the smallest values for *k* correspond to the tests using the 0.5% DBT membrane, the largest values of *k* are found from the tests using 0.1% DBT membrane with the 0.3% DBT membrane providing values for *k* within these two extremes. A similar argument cannot be made for either solute or solvent, so the parameter *k* is deemed to only be dependent on membrane grade. The procedure was repeated for each fitting parameter of each model. Table 5.3 shows the dependencies found.

Solute	Solvent	Membrane (% DBT)	k ($m^2s^{-1}Bar^{-1}$)
Iron (III) Naphthenate	Xylene	0.5	$6.16x10^{-11}$
9,10-Diphenylanthracene	Xylene	0.5	$6.41x10^{-11}$
Iron (III) Naphthenate	Octane	0.5	$7.05x10^{-11}$
Iron (III) Acetylacetonate	Xylene	0.5	$7.09x10^{-11}$
Iron (III) Acetylacetonate	Octane	0.5	$7.21x10^{-11}$
9,10-Diphenylanthracene	Octane	0.5	$8.45x10^{-11}$
9,10-Diphenylanthracene	Heptane	0.5	$8.87x10^{-11}$
Iron (III) Naphthenate	Heptane	0.5	$9.92x10^{-11}$
Iron (III) Acetylacetonate	Heptane	0.5	$1.18x10^{-10}$

9,10-Diphenylanthracene	Octane	0.3	2.48×10^{-10}
9,10-Diphenylanthracene	Heptane	0.3	3.08×10^{-10}
Iron (III) Naphthenate	Octane	0.3	3.58×10^{-10}
Iron (III) Naphthenate	Heptane	0.3	3.78×10^{-10}
9,10-Diphenylanthracene	Xylene	0.3	4.33×10^{-10}
Iron (III) Naphthenate	Xylene	0.3	4.39×10^{-10}
9,10-Diphenylanthracene	Heptane	0.1	4.69×10^{-10}
9,10-Diphenylanthracene	Xylene	0.1	5.28×10^{-10}
Iron (III) Acetylacetonate	Octane	0.3	5.87×10^{-10}
9,10-Diphenylanthracene	Octane	0.1	6.47×10^{-10}
Iron (III) Naphthenate	Heptane	0.1	1.00×10^{-9}
Iron (III) Naphthenate	Xylene	0.1	1.03×10^{-9}
Iron (III) Acetylacetonate	Heptane	0.3	1.16×10^{-9}
Iron (III) Naphthenate	Octane	0.1	1.17×10^{-9}
Iron (III) Acetylacetonate	Xylene	0.3	1.17×10^{-9}
Iron (III) Acetylacetonate	Octane	0.1	1.57×10^{-9}
Iron (III) Acetylacetonate	Heptane	0.1	2.25×10^{-9}
Iron (III) Acetylacetonate	Xylene	0.1	2.45×10^{-9}

Table 5.2 – PD model dependency table.

Model	Fitting Parameter 1	Fitting Parameter 2	Fitting Parameter 3
CD = f (k , a , D_i)	$k = f$ (M_{IP})	$a = f$ (N)	$D_i = f$ (N)
PF = f (r_p)	$r_p = f$ (M_{IP} , S)	–	–
PD = f (k , D_i)	$k = f$ (M_{IP})	$D_i = f$ (M_{IP})	–
SD = f (D_sK_s , D_iK_i)	$D_sK_s = f$ (M_{IP})	$D_iK_i = f$ (M_{IP})	–
SDi = f (P_w , P_3 , P_2)	$P_w = f$ (M_{IP})	$P_3 = f$ (M_{IP})	$P_2 = f$ (M_{IP})
SK = f (σ , P_s)	$\sigma = f$ (M_P , S_x)	$P_s = f$ (N)	–
VDB = f (a_0 , b_0)	$a_0 = f$ (M_{IP} , V_{CT} , S_{CT})	$b_0 = f$ (M_{IP} , V_{CT} , S_{CT})	–

Table 5.3 – Model dependency summary.

The definitions for Table 5.3 are as follows; *M* indicates that the parameter was dependent on membrane grade, *S* indicates dependency on solute, with *V* standing for solvent dependency and *N* being no dependency for any of the above. For the subscripts *P* and *IP* represent proportional and inversely proportional respectively. *X* means that the noted dependency was valid for the xylene based tests only, and *CT* means constant test – the dependency was noted only whilst the other two settings were constant.

Dependence was determined by tabulating the 27 experimental runs, ordering them by each fitting parameter in turn and then looking for patterns within the main. For example with the CD model when the table was sorted by values of *k*, the smallest *k* values belonged to the 0.5% DBT membrane tests, the largest values corresponded to the 0.1% DBT membrane tests and the 0.3% DBT membrane grades existed in-between these extremes. Whenever this situation was found, with a definite pattern, it was deemed to be a dependant parameter and recorded in Table 5.3.

During the checking of each parameter a second kind of trend was found, which only presented itself in the analysis of one model (VDB) and has been termed constant test dependence. When the data table was ordered first by membrane grade, then solute,

and finally solvent, if a relative pattern emerged it was deemed to be constant test dependence. This dependence was best described by an example – when looking at solvent differences for constant solute and membrane, the smallest values of a_0 was obtained for heptane, then octane and xylene the largest. The individual solute/membrane does not matter so long as they were constant. If the list was ordered for a_0 the values were scattered, but within each set they were ordered and this was unlikely to be a coincidence as it extends over the entire data range. A similar discussion was able to be made for the solutes with the order from largest to smallest being, iron (III) acetylacetonate, iron (III) naphthenate then 9,10-diphenylanthracene.

Table 5.3 shows the fourteen fitting parameters across the seven models and of those nine were inversely proportional to membrane grade. Table 5.3 actually details fifteen parameters but as the parameter *k* was identical for CD and PD (the flux equations were identical) this repetition should not be included in this discussion. This means that the filter media must have a great effect on the filtration performance of any setup, and much greater than the effect of either solute or solvent. The inversely proportional relationship between membrane grade and flux was logical as the higher grades consist of a denser polymer which will impede flow, so the fitting parameters will be largest with the lowest membrane grade.

The parameter σ in the SK model was the only term found to have direct (i.e. not inverse) proportionality to membrane grade. As discussed in Section 5.2.6 the term σ was a restricted term, capable of existing only within the range zero to one, and due to the effect noted in Figure 5.20 some of the σ terms simply migrate to one (or close) and stay there. This noted dependency of σ was more visible if these outlying points (type II errors) were excluded from the discussion. The reason for this different trend can be found in the formula used to calculate rejection, the term σ exists four times, twice in both the numerator and denominator and the interaction of these alters the orientation, but this was a trivial matter as the overall dependency on membrane grade was more important. The σ term of the SK model also hosts another partial dependency. σ was smallest when considering 9,10-diphenylanthracene solute, largest when considering iron (III) acetylacetonate solute and iron (III) naphthenate solute residing in-between, but all of this was only true for xylene based tests, no similar trend was found in either the heptane or octane based experimental work.

Four of the terms showed no dependence for membrane grade, solute or solvent, and as such must exist solely to improve the predictions of the model without a physical

grounding. One of these cases was the pore radius term in the pore flow model. The lack of dependence in this case was not thought to be because of a lack of physical grounding but rather a result of the computation process and the fact that this model was different from the rest presented here, in that this model was used to calculate membrane pore size rather than performance predictions.

Within the terms that show dependence the same order occurred each time from largest to smallest, i.e. for membrane grade the order was 0.1% DBT / 0.3% DBT / 0.5% DBT; for solvent the order was xylene / octane / heptane and for solutes the order was iron (III) acetylacetonate / iron (III) naphthenate / 9,10-diphenylanthracene. The purpose of this part is to discuss reasons why this order series exists.

When the experimental data was ordered there was a definite cut off between the 0.5% DBT membrane and the remaining two – all the 0.5% DBT membrane tests were found to exist at one extreme. However this was not the case between the 0.3% DBT and 0.1% DBT membranes, as one or two of the 0.3% DBT membrane tests usually resided in the final third of the table, and one or two of the 0.1% DBT membrane tests resided in the middle third of the table. This effect of the definite cut off point between the 0.5% DBT membrane and the others and the blurred line between the 0.3% DBT and the 0.1% DBT membrane was similar to the swelling extent recorded in the membrane samples (see Figure 3.24), where the 0.1% DBT and 0.3% DBT membranes swelled a comparable amount and the 0.5% DBT membrane swelled an order of magnitude more. This result serves to add more weight to the unexpected swelling results already discussed.

Explaining the specific order of the solutes and solvents was more complicated than explaining the order of the membrane grades as an underlying basis of structure was not as apparent. The basis within the membrane grade was catalyst amount, the logical choice as this was the only variable employed during their manufacture. The solvents and solutes were not manufactured from the same materials using the same process so their individual bases have to arise from some measurable physical property. To determine which property was appropriate in each case, data was obtained and a correlation between the order deduced through modelling and the magnitude of the property was checked. This data has already been discussed in Section 3.4, Tables 3.2 and 3.3 detail the parameters for the solute and solvent respectively that follows the required trends.

The most logical trend which could be found to explain the solutes order was aspect ratio of the molecule. Table 3.3 contains the values for a theoretical minimum cylinder size needed to contain a single molecule of the solute. These values were obtained by using ChemDraw V12 Pro, and were previously applied and discussed in Section 4.3.5.1. A new facet was discovered when checking the aspect ratio (the diameter divided by the length) as a decreasing trend of the same order as the solute trend was found.

The aspect ratio should be an important parameter when considering the filtration efficiency. For any randomly aligned filter media, from the random chain arrangement in the PDMS matrix right up to and beyond the macro filaments found in a standard depth filter, the separation occurs due to the retentate particles (or molecules) becoming held up in the mazelike passageways (transport regions or pores) of the filter media. In a random matrix there will be some transport regions larger than others, some more branched than others and some which will be dead ends (either the transport region will end or the diameter will reduce to a size smaller than the particle making it for all intents and purposes closed). Therefore the path of any single particle will vary greatly and only because of large initial particle amount and the laws of probability do some make it through. Added to this, the effect of solute shape was important – shape in this case meaning any physical orientation of molecules to produce a defined structure and similar shapes means any two different shapes having of identical volumes. For any similar shape the best one to make it through a random matrix is a sphere as it has the largest volume for the smallest projected size. A long thin cylinder of the same total volume to the sphere would be held up more than a sphere, as although the cylinder will be able to theoretically fit in smaller transport regions the mathematical probability of this occurring is less and when it does occur the cylinder is more likely to get stuck as it can't cope with the tortuosity of the matrix. So the aspect ratio of the solute molecule has a direct bearing on the ultimate filtration efficiency. It is acknowledged that the ratio between a cylinders length and diameter is not the same as defining a sphere but the approximation was close enough for the purposes of this discussion. The aspect ratio decreasing from largest to smallest mirrors the predicted trend from the modelling work and was a logical reason for this.

The expected trend within the solvents was both easier to rationalise and harder to confirm. Table 3.2 details three parameters, any of which or all could be the reason for the specific order already determined. The solvent trend was noted during completion of the VDB model which utilises both the surface tension and viscosity of the solvent in

order to make the prediction, so checking these physical properties was sensible. Both these properties were similar (Section 5.2.7– VDB model, for the discussion on this point) and both predict the correct solvent order, so either could be the reason for this trend.

As the solvents in question have proved to swell the membranes used to a significant extent a check on the solubility parameter, the main physical property responsible for this effect, was required. On their own the solubility parameters do not follow the same trend of xylene – octane – heptane as predicted, but the important factor was not the magnitude of the parameter but rather the driving force it generates. When the absolute difference between the solubility parameters of the solvent and PDMS (15.5 $MPa^{0.5}$) were taken, the expected solvent order was noted. As it currently stands it was impossible to tell which of the three potential factors, or any combination, the cause of this order is, and all that can be said for definite was that the order exists.

Overall this analysis has shown a clear dependency on filter media as each model has been affected by this parameter. An off shoot from this was the underlying order that has been found in the three main parameters, of which explanations for two were deduced and logical options presented for the third. This section has provided a greater understanding of the interconnectivity between the seemingly disparate models.

5.4. Intermediate Conclusions

Seven models were applied to the filtration data producing a rather limited range of success, i.e. each model predicted almost identical trends leaving little to choose between them in terms of applicability. On sheer weight of error, the solution diffusion model was found to best predict the available flux data, with the convection diffusion model being the best on the rejection data, however as Table 5.1 shows the difference between best and worst model was not very significant. Initially it was hoped that the work presented in this chapter would be able to answer the question of whether the pore flow or solution diffusion regime was in effect within the membranes produced, however as the study continued this was not to be the case. Although the best fits for flux and rejection were models from the SD camp the shear closeness of the predictions produced by the pore flow based models makes it seem that this result was not definite, and on another set of similar data the result might have been reversed.

Apart from the PF model which was used to deduce the theoretical effective pore size of the active layer all the models predicted a positive linear relationship between flux and applied pressure (i.e. the models obey Darcy's law), with an exponential to a limit curved fit for rejection and applied pressure. Similar linear and curved plots were predicted by every model, which mirror the trends observed in the experimental data. The fact that similar trends were obtained from supposedly antipodean theories suggests that they were not as different as they first seemed.

The more models that were considered and the more terms that were cancelled and reduced, the more it became obvious that the definite division placed between the two opposing theories was in fact more of a grey area. This statement can be explained best by returning to the base differences detailed in Section 5.1. Comparing the first points, in the SD model the permeants dissolve in the membrane material then diffuse through the structure whereas in the PF model the permeants do not dissolve but rather move through tiny pores which are already present in the material. These two statements seem to be mutually exclusive however the statement 'the permeants move through the transport regions' can be applied to both models meaning that the differences are more terminology related than physical.
The second points are not mutually exclusive; the permeants can diffuse (SD) and undergo convective pressure based flow (PF) at the same time. Diffusion and convection are both passive processes for any given species, and it would be impossible to prevent one type of transportation whenever the other type exists. Wherever there is diffusion, there will be a pressure gradient, even if it is just the head of liquid, which will cause bulk convection. Wherever there is convection, diffusion of individual molecules will occur which is especially true at low overall velocities such as which occur within the membrane matrix. So it is perfectly feasible that these second points both occur and so a choice between them is not required.
The third points seem to be different ways of describing the same concept. The SD model states that separation is caused by differences in diffusion extents where as the PF model describes a size exclusion principle. Diffusion is a size dependent process, with smaller species typically having faster diffusion rates and the larger solutes dissolve less as there are fewer transport regions within the surface of the polymer matrix that their size will allow them to enter.

So in conclusion, the correct choice of SD or PF for the experimental set up detailed in this thesis is not straightforward, as either could feasibility exist. The SD model has

been shown to best describe the experimental flux data with the CD model providing the best predictions of rejection; however the difference between the best and worse fitting models was so small making experience in the field more important than the individual models themselves when choosing the correct membrane for a new process

5.5. Nomenclature

A	Experimentally derived constant (-)
a	Fraction of solute undergoing viscous flow (-)
a_0	Specific diffusivity (kg m^{-3} bar^{-1})
B	Experimentally derived constant (-)
b_0	Specific permeability (kg m^{-3} bar^{-1})
D_i	Diffusion coefficient (m^2 s^{-1})
$D_{i,\infty}$	Diffusivity in dilute bulk solution (cm^2 s^{-1})
J	Solvent flux (l m^{-2} h^{-1})
J_i	Solvent flux (l m^{-2} h^{-1})
J_s	Solvent flux (m^3 m^{-2} s^{-1})
J_v	Solvent flux (SK Model) (m^3 m^{-2} s^{-1})
	or Solvent flux (VDB Model) (l m^{-2} h^{-1})
K	Solute hindrance factor (-)
	or partition coefficient (-)
k	Permeability coefficient (m^2 s^{-1} bar^{-1})
l	Membrane depth (m)
M	Membrane (-)
N	No dependency (-)
P_2	Rejection fitting parameter (l m^{-3} h^{-1})
P_3	Flux fitting parameter (l m^{-3} h^{-1} bar^{-1})
$P_{i,e}$	Solute permeability (mol m^{-2} s^{-1})
P_s	Rejection fitting parameter (m^2 s^{-1})
P_w	Flux fitting parameter (l m^{-3} h^{-1} bar^{-1})
R	Rejection (-)
R_g	Universal gas constant (m^3 bar mol^{-1} K^{-1})
r_p	Pore radius (m)
S	Solute (-)
T	Temperature (K)

V	Solvent (-)
V_s	Molar volume (m^3 mol^{-1})
x	Membrane depth (m)
α	Ratio of dielectric constant (-)
	or Surface tension (N m^{-1})
β	Ratio of surface tension (-)
ΔP	Trans-membrane pressure (bar)
$\Delta \Pi$	Osmotic pressure (bar)
μ	Viscosity (PaS)
η	Viscosity (PaS)
σ	Reflection coefficient (-)
Φ_i	Partition coefficient (-)

Subscripts

CT	Constant term
IP	Inversely proportional
P	Proportional
X	Xylene
c	Concentration
	or Convective
d	Diffusion
	or Diffusive
i	Solute
s	Solvent

5.6. References

Ahmad A.L., Ooi B.S., Mohammad A.W., Choudhury J.P., 2004. Composite nanofiltration polyamide membrane: A study on the diamine ratio and its performance evaluation. *Industrial and Engineering Chemistry Research*, **43**, 8074-8082.

Bhanushali D., Kloos S., Kurth C., Bhattacharyya D., 2001. Performance of solvent resistant mambranes for non aqueous systems: solvent permeation results and modelling, *J. Membrane Science*, **189**, 1-21.

Darvishmanesh S., Degreve J., van der Bruggen B., 2009, Comparison of pressure driven transport of ethanol/n-hexane mixtures through dense and microporous membranes, *Chemical Engineering Science*, **64**, 3914-3927.

Dijkstra M.F.J., Bach S., Ebert K., 2006. A transport model for organophilic nanofiltration. *J. Membrane Science*, **286**, 60-68.

Ebert K., Koll J., Dijkstra M.F.J., Eggers M., 2006. Fundamental studies on the performance of a hydrophobic solvent stable membrane in non-aqueous solutions, *J.Membrane Science*, **285**, 75-80.

Geens J., 2006. Mechanisms and modelling of nanofiltration in organic media. PhD thesis, Katholieke Universiteit Leuven.

Han S.J., Luthra S.S, Peeva L., Yang X.J., Livingston A.G., 2003. Insights into the transport of toluene and phenol through organic solvent nanofiltration membranes, *Separation Science and Technology*, **38**, 1899-1923.

Ho W.S.W., Sirkar K.K., 1992, *Membrane handbook*. Van Nostrand Reinhold, New York.

Peeva L.G., Gibbins E., Luthra S.S., White L.S., Stateva R.P., Livingston A.G., 2004. Effect of concentration polerisation and osmotic pressure on flux in organic solvent nanofiltration, *J. Membrane Science*, **236**, 121-136.

Pelofsky A.H., 1966. Surface tension – viscosity relation for liquids, *J. Chemical and Engineering Data*, **11**, 394-397.

Robinson J.P., Tarleton E.S., Millington C.R., Nijmeijer A., 2004. Solvent flux through dense polymeric nanofiltration membranes, *J. Membrane Science*, **230**, 29-37.

Robinson J.P., 2004 The selective removal of components from gasoline using membrane technology, PhD Thesis, Loughborough University

Santos J.L.C., Hidalgo A.M., Oliveira R., Velizarov S., Crespo J.G., 2007, Analysis of solvent flux through nanofiltration membranes by mechanistic, chemometric and hybrid modelling, *J. Membrane Science*, **300**, 191-204.

Schonhorn H., 1967. Surface tension – viscosity relationship for liquids, *J. Chemical and Engineering Data,* **12**, 524-525.

See-Toh Y.H., Ferreira F.C., Livingston A.G., 2007. The influence of membrane formation parameters on the functional performance of organic solvent nanofiltration membranes. *J. Membrane Science*, **299**, 236-250.

Sherwood T.K., Brian P.L.T., Fisher R.E., 1967, Desalination by reverse osmosis, *Industrial and Engineering Chemistry Fundamentals*, **6**, 2-12.

Silva P., Livingston A.G., 2006. Effect of solute concentration and mass transfer limitations on transport in organic solvent nanofiltration — partially rejected solute, *J. Membrane Science*, **280**, 889–898

Szymczyk A., Labbez C., Fievet P., Vidonne A., Foissy A., Pagetti J., 2003. Contribution of convection, diffusion and migration to electrolytr transport through nanofiltration membranes. *Advances in Colloid and Interface Science*, **103**, 77-94.

Tarleton E.S., Robinson J.P., Smith S.J., Na J.J.W., 2005. New experimental measurments of solvent induced swelling in nanofiltration membranes, *J. Membrane Science*, **261**, 129-135.

Wang X.L., Tsuru T., Nakao S.I., Kimura S., 1997. The electrostatic and steric-hindrance model for the transport of charged solutes through nanofiltration membranes, *J. Membrane Science*, **135**, 19-32.

White L.S., 2002, Transport properties of a polyimide solvent resistant nanofiltration membrane, *J. Membrane Science*, **203**, 191-202.

Wijmans J.G., Baker R.W., 1995. The solution-diffusion model: a review, *J. Membrane Science*, **107**, 1-21.

Yang X.J., Livingston A.G., Freitas dos Santos L., 2001. Experimental observations of nanofiltration with organic solvents, *J. Membrane Science*, **190**, 45-55.

Yaroshchuk A.E., 1995. Solution-diffusion-imperfection model revised, *J. Membrane Science*, **101**, 83-87.

6. Overall Conclusions

The main conclusions from this thesis are presented here. Each of the 4 initial aims have been addressed in the following manner throughout the course of this work producing a greater understanding in the field of membrane separations.

Production of composite membrane.

The use of a homogeneous catalyst to initiate the crosslinking reaction required to form the active layer of a composite nanofiltration membrane has been demonstrated to be a viable manufacturing method. Catalyst derived PDMS has been proved to be comparable to other forms of PDMS in terms of both its mechanical and separation properties. The in-house produced membranes were shown to perform comparably with industrially produced membranes in terms of both solvent flux and solute rejection.

With regards to filtration performance, a positive linear trend has been deduced between trans-membrane pressure and total solvent flux through these membranes, i.e. they obey Darcy's law. It was valid for every solute/solvent combination tested and has been found to be independent of polymer swelling. The rejection trend deduced approximates a logarithmic curve in shape; linear at low trans-membrane pressures but at a threshold maximum level it plateaus; meaning that the increase in rejection for a unit increase in pressure decreases. This result has been attributed to membrane compaction and means that, unlike for flux, there was a limit to the rejection which was able to be achieved. Similar trends can be found in literature confirming that the produced membranes behave in a similar fashion to commercial membranes.

Characterisation of PDMS.

In addition to the filtration performance characterisation already mentioned, a main theme through this work was polymer swelling and a significant amount of experimentation has been completed in order to characterise the mechanics behind it. Polymer swelling has been found to be greatest when using solvents of a similar solubility parameter to PDMS; this was true for both tests conducted on polymer slabs and for tests conducted on composite membranes. Fundamental thermodynamics was postulated as the reason for this result since materials with similar solubility parameters each gain enough free energy from the other to enable mixing to spontaneously occur, which in turn causes the polymer matrix to expand and swell. The increase of transport

region size was the most prominent effect of polymer swelling, reducing the overall rejection extent, whilst increasing relative flux.

The effect of catalyst concentration has been considered by producing five different polymer grades and three different membrane grades (different compositional arrangements). By increasing the catalyst amount it has been found that a stiffer (higher Young's modulus) polymer matrix was formed indicating that the addition of extra catalyst leads to an increase in the extent of inter-polymer chain crosslinking. This addition also affects the extent of swelling, the extent of compression and the flux and rejection characteristics of the composites. The maximum swelling and compression results were obtained when testing the largest catalyst amount membranes meaning that this type was the easiest to deform whilst being used. For multiple identical arrangements it has been shown that increasing the membrane grade has the dual effect of increasing rejection and lowering flux.

In general it was found that flux could usually be maximised at the cost of sacrificing separation efficiency. This trade off could be increased in one of three ways: A) Increasing operating pressure once membrane compaction effects had become significant; B) Using a lower catalyst grade membrane; C) Using a better swelling solvent (i.e. one with a solubility parameter close to that of PDMS). The converse, increasing separation efficiency by sacrificing overall flux, was also found to be true.

Identification of transport mechanism.

To complete this aim the filtration data produced was compared to the predictions from 7 existing filtration models, the applicability of each model was then discussed with specific regard given to error analysis and parameters dependency. The transport properties of the produced membranes were found to be best described using the solution diffusion model for flux predictions and the convection diffusion model for predictions regarding rejection. Overall it was found that of the seven models applied; all were in close agreement with little to set one out from the others, making experience in the field more important than the individual models themselves when choosing the correct membrane for a new process.

Determination of effective pore size.

The effective pore size of the membranes was predicted analytically by using a modified form of the Nerst-Planck equation. It was found that by controlling the amount of catalyst it was possible to affect the characteristic pore size thereby tailoring the

separation properties of this type of membrane to suit a specific application. The amount of catalyst present has an effect on the predicted pore size, producing an average range of 1.07 ~ 1.15 nm over the different membranes tested (0.1 ~ 0.5 wt% catalyst). Membrane swelling has also been shown to have an effect on effective pore size with heptane, the best swelling solvent, corresponding to the largest pore size and xylene, the worst swelling solvent, corresponding to the smallest pore size, which implies a pore like structure exists within the membrane. Increasing the trans-membrane pressure (up to the threshold limit) and using a higher grade membrane were two ways of increasing the separation efficiency of the process.

In conclusion several different factors have been found to be essentially aspects of the same trend. The separation efficiency of a membrane has been shown to be dependent on swelling, applied pressure, catalyst amount, solvent and solute used. In its simplest definition the extent of rejection is based on how many solute molecules can pass through the membrane, which is dependent on the size of the transport regions (including pores). Swelling and the associated solvent choice will increase the relative size of the transport regions, as when a membrane swells the same amount of mass now occupies a larger volume, which causes convective transport to be more prominent. Applied pressure and catalyst amount will reduce the size of transport regions: applied pressure will restrict swelling and cause membrane compaction whilst catalyst amount will alter the extent of crosslinking effectively splitting transport regions into smaller discrete sectors. These reductions cause diffusive transport to be more prominent. So the overall separation efficiency is the net result of both convective and diffusive transport with the relative extent of each process being determined by the physical parameters noted above.

7. Future Work

Throughout the completion of this project several different aspects worthy of further investigation have presented themselves, which had to be left for a variety of reasons usually time or cost based. The purpose of this section was to present these alternatives in such a way that they could form the basis of future projects.

Due to time constraints the crossflow filtration experiments could only be completed using three solvents and three solutes. Therefore, the first avenue for future work would be to conduct comparable experiments using an increased range of either solutes, solvents or both. The results obtained from using ethanol solvent would be interesting as it has been shown that polymer swelling is almost zero, so this variation would provide a good insight into the limits of the effect of polymer swelling. Similarly, by using solutes which are larger than the maximum size of 1.6 nm used in this work, the value of MWCO could be determined to fully characterise the produced membranes. This extension could be incorporated into any of the ideas below as a way of becoming familiar with the procedures and methodology described herein.

A new test cell was created during the course of this thesis. It has the potential be operated with or without an internal spacer present immediately above the membrane surface. By this addition the new cell was able to operate with the same hold up volume as the previous cell or the same total clearance. All the work presented here was conducted with the spacer present (i.e. same total clearance) so a potential avenue for future work would be to run the same experimental conditions three times; once in the ‘old’ cell, once in the ‘new’ cell with spacer present and once in the ‘new’ cell without the spacer. This would confirm whether or not the specific layout of the separation module was important, potentially leading to new operating procedures.

During the swelling with fixed pressure tests (Section 3.5.5) it was noted that directly applied pressure had the effect of reducing the swelling of the membrane by 50~60%. These restricted membranes will have different filtration properties to membranes that were allowed to swell normally and investigating the differences between permeation rates at different applied pressures would be an interesting and novel avenue for research. To achieve this restriction, a new test cell would have to be designed which is currently thought to centre around a pair of porous plates which would be clamped around the membrane to restrict swelling but still allow the solvent to permeate. Due to

this configuration, a crossflow state could not be generated so the tests would have to be pure solvent permeation (without solutes) only however the data generated would be intriguing. By this method it would be determined whether polymer based membranes need to swell to filter ‘correctly’ or if the swelling is a true hindrance.

The solution of the modelling section produced three lists one for each of the parameters of the experiment; membrane grade, solute and solvent. These lists were formed when it was noted that sorting the 27 experimental sets by size of experimentally derived fitting parameter always produced the same order. The orders were for membrane grade, 0.1% DBT / 0.3% DBT / 0.5% DBT, for solute, iron (III) acetylacetonate / iron (III) naphthenate / 9,10-diphenylanthracene, and for solvent, xylene / octane / heptane. The order of the membrane grade was due to the amount of catalyst used in the manufacture process, the order of the solute was thought to be due to the extent the individual molecules were spherical in nature, but the reasoning behind the order of the solvents was unknown, with the primary candidates being either surface tension, viscosity or solubility parameter driving force. An interesting study could be conducted to determine the cause of this certain order in the solvents tested and to confirm the causes of the orders in the other two parameters. This extension would take the project out of the nanofiltration area and into more general chemistry.